Environmental Science and Technology VII

Edited by

Ivy Hou

Environmental Science and Technology VII

Selected, peer reviewed papers from the
2016 7th International Conference on Environmental Science and Technology
(ICEST 2016)
June 10-12, 2016, Barcelona, Spain

Edited by

Ivy Hou

IACSIT PRESS
www.iacsitp.com

International Association of Computer Science & Information Technology Press
Singapore Office
#07-42, BLK 708
Jurong West
Street 71, Singapore
E-mail: pub@iacsit.org, press@iacsit.org
Web: http://www.iacsitp.com

Volume 94 of
International Proceedings of Chemical, Biological & Environmental Engineering
ISSN 2010-4618

ISBN 978-981-09-9846-2

Full text available online at http://www.ipcbee.com

***Distributed** worldwide by*

International Association of Computer Science & Information Technology Press
Singapore Office
#07-42, BLK 708
Jurong West
Street 71, Singapore
E-mail: pub@iacsit.org, press@iacsit.org
Web: http://www.iacsitp.com

And in the Hong Kong by
Hong Kong Office
Unit B on 15th Floor
EU YAN SANG Tower
Nos.11/15
Chatham Road South
Kowloon, Hong Kong

PREFACE

Dear Distinguished Delegates and Guests,

The Organizing Committee warmly welcomes our distinguished delegates and guests to the 2016 7th International Conference on Environmental Science and Technology (ICEST 2016) held during June 10-12 in Barcelona, Spain.

ICEST 2016 is sponsored by Asia-Pacific Chemical, Biological & Environmental Engineering Society (APCBEES), and supported by APCBEES Members and scholars from universities all round the world. If you have attended a conference sponsored by APCBEES before, you are aware that the conferences together report the results of research efforts in a broad range of Environmental Science and Technology and related areas. These conferences are aimed at discussing with all of you the wide range of problems encountered in present and future high technologies. ICEST 2016 is organized to gather members of our international community scientists so that researchers from around the world can present their leading-edge work, expanding our community's knowledge and insight into the significant challenges currently being addressed in that research. The conference Program Committee is itself quite diverse and truly international, with membership from the Americas, Europe, Asia, Africa and Oceania.

This proceeding records the fully refereed papers presented at the conference. The main conference themes and tracks are Environmental Science and Technology. The main goal of these events is to provide international scientific forums for exchange of new ideas in a number of fields that interact in-depth through discussions with their peers from around the world. Both inward research; core areas of Environmental Science and Technology and outward research; multi-disciplinary, inter-disciplinary, and applications will be covered during these events.

The conference has solicited and gathered technical research submissions related to all aspects of major conference themes and tracks. All the submitted papers in the proceeding have been peer reviewed by the reviewers drawn from the scientific committee, external reviewers and editorial board depending on the subject matter of the paper. Reviewing and initial selection were undertaken electronically. After the rigorous peer-review process, the submitted papers were selected on the basis of originality, significance, and clarity for the purpose of the conference. The selected papers and additional late-breaking contributions to be presented as lectures will make an exciting technical program. The conference program is extremely rich, featuring high-impact presentations.

The high quality of the program – guaranteed by the presence of an unparalleled number of internationally recognized top experts – can be assessed when reading the contents of the program. The conference will therefore be a unique event, where attendees will be

able to appreciate the latest results in their field of expertise, and to acquire additional knowledge in other fields. The program has been structured to favor interactions among attendees coming from many diverse horizons, scientifically, geographically, from academia and from industry. Included in this will to favor interactions are social events at prestigious sites.

We would like to thank the program chairs, organization staff, and the members of the program committees for their work. Thanks also go to Editor Ms. Ivy Hou Asia-Pacific Chemical, Biological & Environmental Engineering Society, for her wonderful editorial service to this proceeding.

We are grateful to all those who have contributed to the success of ICEST 2016. We hope that all participants and other interested readers benefit scientifically from the proceedings and also find it stimulating in the process. Finally, we would like to wish you success in your technical presentations and social networking.

We hope you have a unique, rewarding and enjoyable week at ICEST 2016 in Barcelona, Spain.

With our warmest regards,

The Organizing Committees
June 10-12, 2016
Barcelona, Spain

Organizing Committees

Conference General Co-Chairs

Prof. Bogdan Zygmunt, Faculty of Chemistry, Gdansk University of Technology, Poland

Program Co-Chairs

Prof. Solomon W. Leung, Idaho State University, USAAssoc

Prof. Ryusuke Hashimura, Sojo University, Japan

Technical Committee

Prof. Solomon W. Leung, Idaho State University, USA

Prof. Jen-Jeng Chen, Tajen University, Taiwan

Prof. Kadir AYDIN, Automotive Engineering Department, Turkey

Prof. Kevin Liu, Ming Chi University of Technology, Taiwan

Prof. Saif Al-Bahry, Sultan Qaboos University, Oman

Prof. Ibrahim Y. Mahmoud, University of Nizwa, Oman

Prof. Chin-Chen Chang, National United University, Taiwan

Prof. Dr. V. RAMADAS, Raja Doraisingam Govt. Arts College, India

Prof. Turhan Koyuncu, University of Adiyaman, Turkey

Prof. Selda Tekin Özan, Department of Biology, Isparta-Turkey

Prof. Geetesh Goga, Punjab Technical University, India

Prof. Wei-Zhen Jane LU, City University of Hong Kong

Assoc.Prof. Ryusuke Hashimura, Sojo University, Japan

Dr. M. M. S. Mohammed, Agricultural Research Center, Egypt

Dr. Mahesh, Kishorchandra Dalal, Shri J.J.T.University, India

Dr. Abdullah Esmaeili, National Iranian Oil Company (NIOC), Iran

Dr. Praveen Dahiya, Amity University, India

Table of Contents

International Proceedings of Chemical, Biological and Environmental Engineering
Volume 94 of IPCBEE (2016)
DOI: 10.7763/IPCBEE. 2016. V94. 1

Accuracy Assessment of Tropical Rainfall Measuring Mission (TRMM) Satellite Product over Tianshan Mountainous, Northwest of China

Chauncheng Zhao[1, 2], Shuxia Yao[1+], Jun Liu[1], Zhiguo Ren[1], Wenjiao Da[1]

[1] Lanzhou City university, Lanzhou Gansu 730000, People's Republic of China

[2] State Key Laboratory of Cryospheric Science, cold and Arid Regions Environmental and Engineering Research Institute, Chinese Academy of Sciences, Lanzhou Gansu 730000, People's Republic of China

Abstract. Precipitation is one of meteorological elements difficult to accurately observation measurement. Due to the large spatial and temporal variability, the reliability of areal precipitation is limited by the stations observation. The advancements in remote sensing techniques have provided precipitation data at higher spatial resolutions than was available from station measurements in mountainous regions. However, satellites-based products are subject to different types of errors such as inherent measurement and retrieval errors, and sampling uncertainty. As critical inputs of ecological and hydrological models, assessment the satellites-based products applied in mountainous become a critical role. We employed the correlation analysis to assess the accuracy of TRMM products using annual, seasonal and monthly data from 1998 to 2013. The results are shown that the TRMM products are good performance in wet regions and wet seasons in the Tianshan mountainous. The distribution of precipitation of TRMM products is depicted consistency with observations in wet season also.

Keywords: Climate Change, Precipitation, Correlation Analysis, Tianshan Mountainous

1. Introduction

As one important part of the hydrological cycle, precipitation is critical in understanding the hydrologic balance and the complex interactions among the small- and large-scale components [1]. Traditionally, rain guage observations are only direct source that is obtained through direct measurements before 1970's. Because of accessibility and financial limitations, the distribution of observation stations is not available, particularly in oceanic, remote, or developing regions [2, 3]. Spatial precipitation represents one of the main inputs to hydrologic, climatologic, and agricultural studies. However, the feature of spatial coverage is lack in situ observations which are usually too sparsely distributed to capture the spatial distribution [4, 5]. In general, observation measurements yield relatively accurate point measurements of precipitation, there are a number of well-known effect sources such as orographic, wind, precision instruments, which can strongly influence measurement accuracy, and defect of spatial representation [6, 7].

With the advent of meteorological satellites in the 1970s, the use of satellite measurements of precipitation in hydrologic and meteorological predictions has increased significantly in the past few decades [8, 9]. Satellite measurement of precipitation has been evident since its early days: the data are inexpensive, provide a complete area coverage, are available in real-time, provide very high temporal and spatial resolution [6-10]. A large number of precipitation products based on satellite, e.g. Global Precipitation and Climatology Project (GPCP) precipitation product, Global Satellite Mapping of Precipitation, Climate Prediction Center Merged Analysis of Precipitation are available with different spatial and temporal widely used in many research fields [11-14].

[+] Corresponding author. Tel.: + 86 931 496 7160; fax: +86 931 496 7345.
E-mail address: yaoshuxia@163.com.

Each instrument has advantages and shortcomings; none of them seems to completely perform satisfying the research needs [15]. Station observations could provide the long time series record, high accuracy in situ. However, there are suffered from various problems, limited in mountainous and oceanic and poor representation in spatial. Due to indirect, satellites remote senses are limited to retrieval algorithm, subjected to different error such as biases and random errors that are caused by the sampling frequency, while it provided high spatial and temporal resolution, homogeneous distribution. The precise areal precipitation is greatly affected the accurate of simulations for hydrologic and ecological modeling. Therefore, there is a pressing need for assessment and examining by comparison with satellite data and observation data in order to better understand the precipitation processes, and to improve the retrieval algorithms and accuracy of data [16, 17]. To address this, we compared the data of TRMM-3B43 based on satellite with observations and assessed the accuracy from 1998 to 2013 in Tianshan mountainous, northwest of China.

2. Materials and methods

2.1. Study area

The present study focuses on Tianshan mountainous, located in the northwest of China a typical arid and semi-arid region. It is stretched from west to east, divided Xinjiang into two parts, i.e. Southern Xinjiang and Northern Xinjiang [18]. Due to far away from the ocean, precipitation is the main source of surface and ground water, farm irrigation, industry water, and so on. Due to intercept by mountainous and Plateau, southwest monsoon from the Indian Ocean and southeast monsoon from Pacific Ocean are rarely reached. The major vapor resource over TianShan mountainous is originated from the west wind current, minor resource is originated from the dry and cold current from the Arctic Ocean. Because of west-east-oriented mountainous, the characteristic of precipitation distribution presents more in the north than in the south, more in the west than in the east, more in the mountainous area than in the plain. The distribution of precipitation is scarce and unevenly, with average annual mean of 180 mm, in the north at 220 mm and that of the south of only 70 mm in Tianshan mountainous. Eighty percent of annual precipitation occurs during the rainy period from May to September. Maximum precipitation falls in Ili valley facing west, where the mean annual precipitation is >600 mm. As a result, Tianshan mountainous is become a wet island in arid area of northwest of China.

2.2. Data collection

The Tropical Rainfall Measuring Mission (TRMM) is a joint US-Japan program to monitor tropical and subtropical rainfall, launched in November 1997 and has provided precipitation estimates since January 1998. A range of products from TRMM are generated by the NASA Goddard Space Flight Centre and released for free application via several websites. These products provided series of hourly, daily and monthly precipitation at spatial resolution of 0.25° for the 50°N – S areas, have been widely used many applications with evaluating better performance [18]. One of products is the TRMM 3B43 monthly is used in this study. This product is combined of data from the TMI, PR, and VIRS with SSM/I, IR, and rain guage. The newly version (Version 7) was released on public websites on May 22 (2012). Compared to the previous version, several improvements (additional satellite data, uniform data reprocessing and calibration scheme) were implemented in the Version 7 products [19]. The annual precipitation data were also generated by accumulating all 12 monthly data.

Because of the complex topography, the station is very sparse and unreasonable distribution in Tianshan mountainous. The monthly precipitation are collected for 64 stations which provided by the National Climatic Centre of China, the China Meteorological Administration in Tianshan mountainous period from 1998 to 2013 (Fig. 1). The quality of product is firmly controlled and homogeneity tests are also performed before its release (Ding et al., 2007). There are 32 stations distributed below 1000 m, 26 station distributed from 1000 to 2000m, and no station distributed over 4000 m.

2.3. Methods

In order to ensure consistency of assessing, the cells of TRMM 3B43 products have been selected which neighbored station. The assessment was made over 16-year between 1998 and 2013 for annual and monthly

time series. The error and correlation statistics were calculated to assess the accuracy between station observations and TRMM 3B43 products.

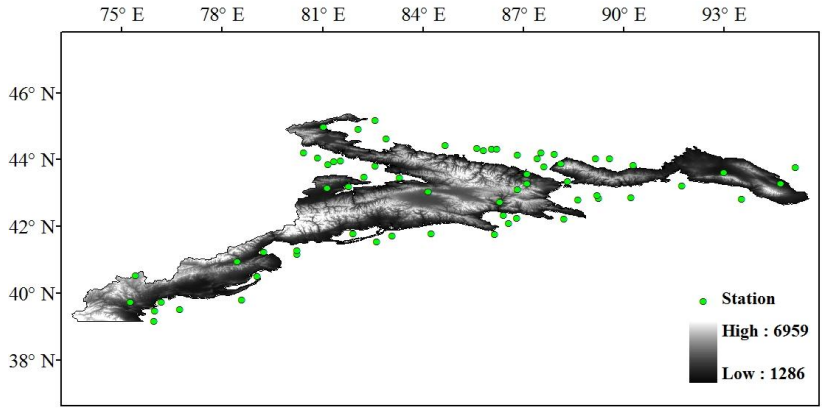

Fig. 1: Locations of precipitation stations in Tianshan mountainous.

One widely used method is employed to assess the differences between station observations and TRMM 3B43 products. The correlation analysis was calculated in annual and monthly as following:

$$r = \frac{\Sigma_{i=1}^{n}\left(P_{obs} - \overline{P_{obs}}\right)\left(P_{sat} - \overline{P_{sat}}\right)}{\sqrt{\Sigma_{i=1}^{n}\left(P_{obs} - \overline{P_{obs}}\right)^{2}\Sigma_{i=1}^{n}\left(P_{sat} - \overline{P_{sat}}\right)^{2}}} \quad (1)$$

where P_{obs} is the value of station observation, $\overline{P_{obs}}$ is the average of station observation, P_{sat} is the value of TRMM 3B43 products and $\overline{P_{sat}}$ is the average of TRMM 3B43 products for time series. The larger the correlation coefficient, the smaller the error is, and the distribution of scatter plots are more concentration in regression line.

3. Results and discussion

3.1. Annual

The distribution of annual average precipitation of TRMM 3B43 V7 products and observations are shown the statistically consistent, especially in western and eastern of Tianshan mountainous (Fig. 2. a,b). They are portrayed characteristic of south much less north of Tianshan mountainous. But, there is a significant difference in the middle of Tianshan mountainous. In east part of Ili River Valley, Daxigou and Xiaoqizi, the precipitation of observations are significantly higher than TRMM 3B43 V7 products. The pattern of coefficient is shown statistically significant across much of Tianshan mountainous area, above 0.5 except individual stations (Fig. 2. c). The value of coefficient is greater in the south than in the north, greater in the west than in the east of Tianshan mountainous. The value of coefficient is high which stations are above 2000 m, while correlation is increasing with elevation rising which stations are below 2000 m.

3.2. Seasonal

3.2.1. Spring

The distribution of seasonal precipitation is difference significantly, about accounting for 20% the annual precipitation arrives in spring over Tianshan mountainous. The correlation of *r* is calculated between the TRMM products and observations shown as Fig. 3(include March, April and May). The spatial distribution of *r* provided a more complete picture that the value is higher in north than in south in mid Tianshan, higher in east than in west. In the mid and east part of Tianshan mountainous, the value of *r* is higher than 0.9 that indicated a good performance between the TRMM products and observations. In the three months of spring, the value of *r* does not change in mid part of north that portrayed a more consistent picture, while different of value of *r* is obviously in mid part of south and west part of east of Tianshan mountainous where close the desert. As time goes on, the value of r is increases.

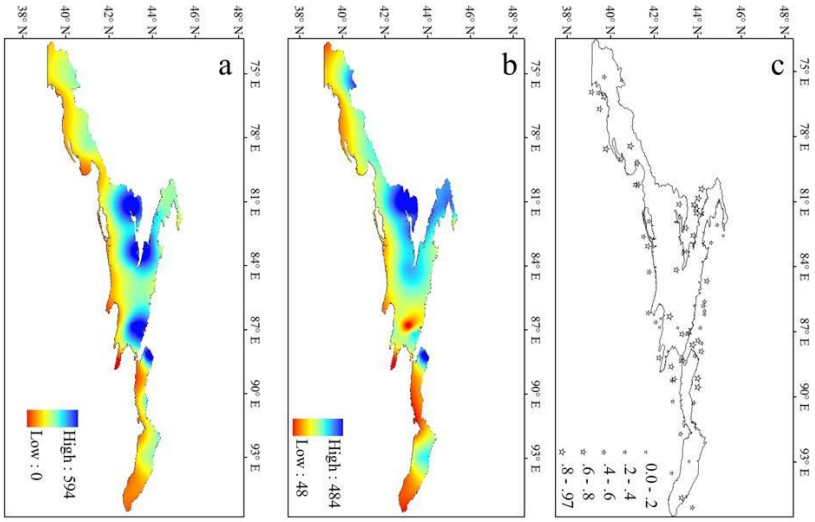

Fig. 2: The distribution of precipitation and coefficient of observations and TRMM products (a: distribution of observations, b: distribution of TRMM products, the coefficient of observations and TRMM products).

3.2.2. Summer

Summer is one of main period of precipitation in Tianshan mountainous, the total precipitation of summer is account for 40% of annual precipitation. The correlation of *r* is calculated between the TRMM products and observations shown as Fig. 4(include June, July and August). In July, the value of *r* is higher than other two months while precipitation is the highest of annual precipitation. Overall, the spatial distribution of *r* is similar to spring, the value of *r* is high that indicated the good performance between the TRMM products and observations in whole Tianshan mountainous. In June, the value of *r* is lower than other two months in the Ili valley where the amount of precipitation is high. In August, the value of *r* is decrease than other two months.

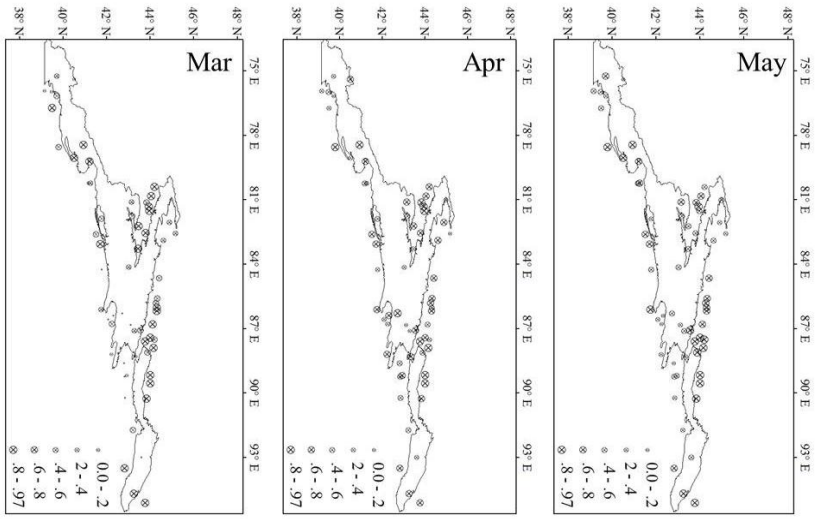

Fig. 3: The coefficient of precipitation and coefficient of observations and TRMM products in spring (a:Mar, b: Apr, c: May).

3.2.3. Fall

Fall is also one of main period of precipitation in Tianshan mountainous, the total precipitation of fall is account for 35% of annual precipitation. The correlation of *r* is calculated between the TRMM products and observations shown as Fig. 5(include September, October and November). Overall, compared with the summer, the value of *r* is decreased which the stations are in low mountainous, but the spatial distribution is very consistent that indicated the good performance between the TRMM products and observations in whole

Tianshan mountainous. In September, the variability of *r* is obvious in south slope of mid of Tianshang mountainous where nearby the desert. In October, the variability is obvious in south slope of west of Tianshan mountainous. In November, the variability is obvious in south slope of east of Tianshan mountainous where is locate the edge of westerlies.

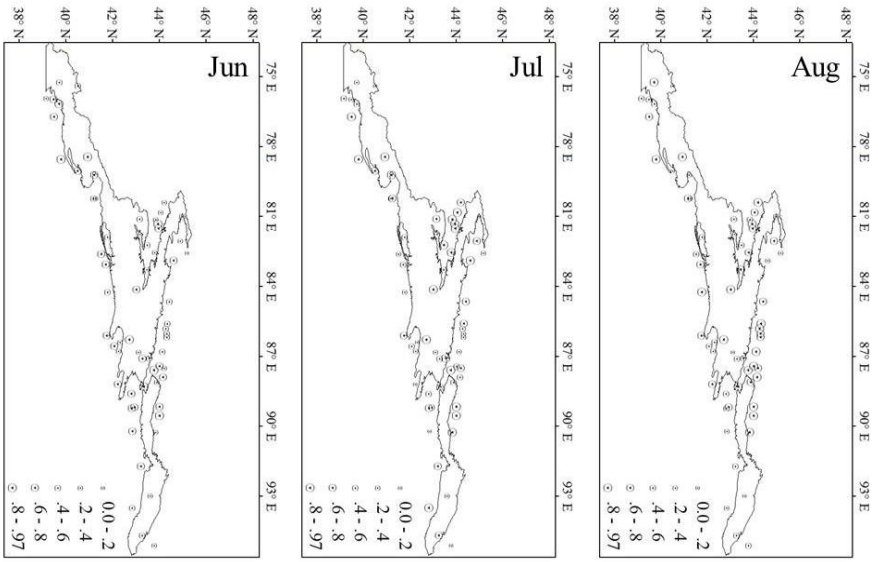

Fig. 4: The coefficient of precipitation and coefficient of observations and TRMM products in summer (a:Jun, b: Jul, c: Aug).

3.2.4. Winter

In all seasons, the precipitation of winter in least in annual, whereas only 5% the annual precipitation. Because of the low temperature, the precipitation is solid as snow in Tianshan mountainous. Additionally, the measurement of solid precipitation is affect by wind very large, the accuracy of observation is also greatly affected. The correlation of *r* is calculated between the TRMM products and observations shown as Fig. 6(include December, January and February). The value of *r* is higher in south than in north, higher in low mountainous than high mountainous. Overall, the value of *r* is decrease with time goes on. The variability of value *r* is change small in Ili valley while the significantly change in Wenqian, Bole and jinhe in December. The variability is obvious in south slope of east of Tianshan mountainous in January and February.

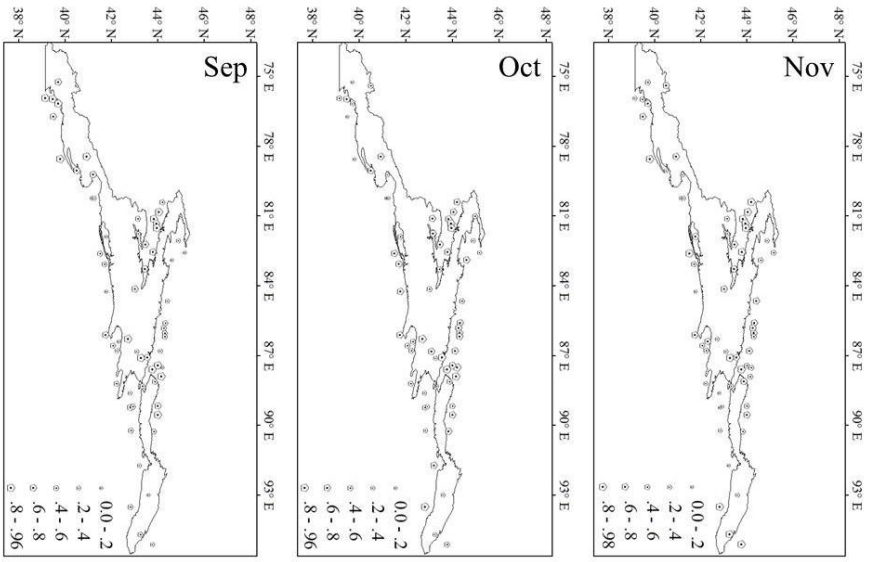

Fig. 5: The coefficient of precipitation and coefficient of observations and TRMM products in Fall (a: Sep, b:Oct, c: Nov).

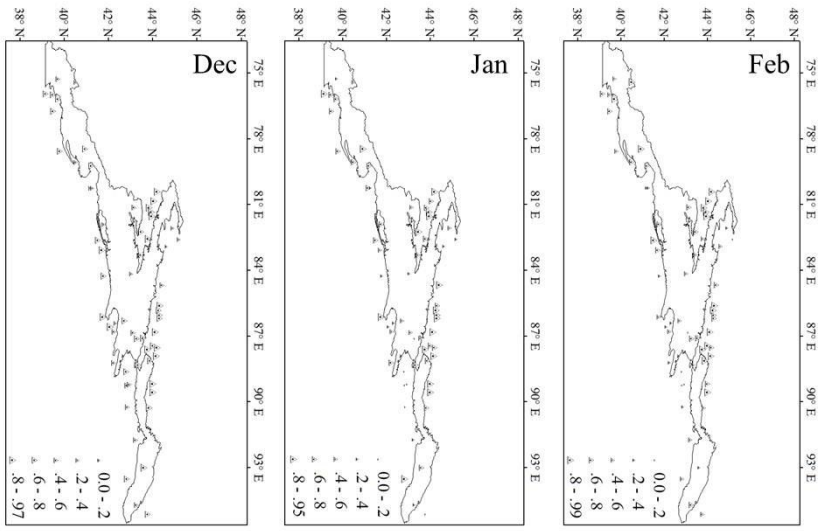

Fig. 6: The coefficient of precipitation and coefficient of observations and TRMM products in winter (a: Dec, b: Jan, c: Feb).

4. Conclusions

The comparison between TRMM products of satellite remote sensing and observations shows good agreement over Tainshan mountainous area but rather poor agreement in some region. The results show that the TRMM products and observations are performed better for wet climate regions and wet seasons whether in the high mountainous or low mountainous. But, the value of r is depicted that there has obviously difference in dry season. In high mountainous, the TRMM products and observations are good consistent while exist obviously difference in low mountainous.

Due to west wind current as the major vapor resource, and intercept by mountainous and Plateau, and affected by local water cycle, precipitation distribution is significantly different between north and south of Tainshan mountainous. Compared TRMM products and observations, the precipitation distribution of TRMM products is good agreement with observations. Thus, as the important driving data in the distributed hydrological model, accuracy of the simulation is directly affect by the accuracy of precipitation data. In large-scale hydrology studies, the TRMM products should have a broader application.

5. Acknowledgements

The authors are grateful to the anonymous reviewers for their very useful suggestions and comments. This study was supported by major national science research program (973 program) (No. 2013CBA01806), the National Natural Science Foundation of China (41361013, 31300388, 41271078), and Lanzhou City University PhD Research Fund (LZCU-BS2013-09, LZCU-BS2013-12).

6. References

[1] R. F. Adler, G. J. Huffman, and A. Chang, et al., "The version-2 global precipitation climatology project (GPCP) monthly precipitation analysis (1979-present)". *Journal of hydrometeorology*, 2003, 4(6):1147-1167.

[2] S. M. Vicente Serrano, S. Sánchez, and J. M. Cuadrat, "Comparative analysis of interpolation methods in the middle Ebro Valley (Spain): application to annual precipitation and temperature". *Climate Research*, 2003, 24(2):161-180.

[3] R. Mehrotra and A. Sharma, "A semi-parametric model for stochastic generation of multi-site daily rainfall exhibiting low-frequency variability". *Journal of Hydrology*, 2007, 335(1):180-193.

[4] X. Zhang and R. Srinivasan, "GIS-based spatial precipitation estimation using next generation radar and raingauge data". *Environmental Modelling & Software*, 2010, 25(12):1781-1788.

[5] E. Habib, A. T. Haile, and Y. Tian, et al., "Evaluation of the high-resolution CMORPH satellite rainfall product using dense rain gauge observations and radar-based estimates". *Journal of Hydrometeorology*, 2012, 13(6):1784-1798.

[6] Z. D. Adeyewa, and K. Nakamura, "Validation of TRMM radar rainfall data over major climatic regions in Africa". *Journal of Applied Meteorology*, 2003, 42(2):331-347.

[7] D. B. Michelson, "Systematic correction of precipitation gauge observations using analyzed meteorological variables". *Journal of hydrology*, 2004, 290(3):161-177.

[8] E. E. Ebert, J. E. Janowiak, and C. Kidd, "Comparison of near-real-time precipitation estimates from satellite observations and numerical models". *Bulletin of the American Meteorological Society*, 2007, 88(1): 47-64.

[9] A. Aghakouchak, E. Habib, and A. Bárdossy, "A comparison of three remotely sensed rainfall ensemble generators". *Atmospheric Research*, 2010, 98(2):387-399.

[10] E. Symeonakis, R. Bonifa ço, and N.Drake, "A comparison of rainfall estimation techniques for sub-Saharan Africa". *International Journal of Applied Earth Observation and Geoinformation*, 2009, 11(1):15-26.

[11] P. Xie, J. E. Janowiak, and P. A. Arkin, et al., "GPCP pentad precipitation analyses: an experimental data set based on gauge observations and satellite estimates". *Journal of Climate*, 2003, 16(13):2197-2214.

[12] T. Kubota, S. Shige, and H. Hashizume, et al., "Global precipitation map using satellite-borne microwave radiometers by the GSMaP Project: Production and validation". *Geoscience and Remote Sensing, IEEE Transactions on*, 2007, 45(7):2259-2275.

[13] C. Kidd, and G. Huffman. "Global precipitation measurement". *Meteorological Applications*, 2011, 18(3):334-353.

[14] F. J. Tapiador, F. J. Turk, and W. Petersen, et al., "Global precipitation measurement: Methods, datasets and applications". *Atmospheric Research*, 2012, 104:70-97.

[15] E. Todini, "A Bayesian technique for conditioning radar precipitation estimates to rain-gauge measurements". *Hydrology and Earth System Sciences*, 2001, 5(2):187-199.

[16] P. Crochet, T. Jóhannesson, and T. Jónsson, et al., "Estimating the Spatial Distribution of Precipitation in Iceland Using a Linear Model of Orographic Precipitation", *Journal of Hydrometeorology*, 2007, 8(6):1285-1306.

[17] O. P. Prat and A. P. Barros, "Assessing satellite-based precipitation estimates in the Southern Appalachian mountains using rain gauges and TRMM PR", *Advances in Geosciences*, 2010, 25:143-153.

[18] X. H. Li, Q. Zhang, and C. Y. Xu, "Suitability of the TRMM satellite rainfalls in driving a distributed hydrological model for water balance computations in Xinjiang catchment, Poyang lake basin". *Journal of Hydrology*, 2012, 426:28-38.

[19] Z. Duan, and W. G. M. Bastiaanssen. "First results from Version 7 TRMM 3B43 precipitation product in combination with a new downscaling–calibration procedure". *Remote Sensing of Environment*, 2013, 131:1-13.

International Proceedings of Chemical, Biological and Environmental Engineering
Volume 94 of IPCBEE (2016)
DOI: 10.7763/IPCBEE. 2016. V94. 2

Effect and Mechanism of Microorganism for Oil Degradation Enhanced by Magnetic Field

Ren Zhijun[+], Zhu Linan, Zhang Zhongxiang and Liu Qian

School of Aerospace and Civil Engineering, Harbin Engineering University, Harbin 150001, China

Abstract: One strain was isolated from activated sludge of oily wastewater biochemical treatment and named Acinetobacter sp B11 according to the determination of morphology, physiological, biochemical tests and 16S rDNA sequence analysis. In present research, magnetic field was used in oil biodegradation process to improve the degradation efficiency of microorganism for oil pollution and the effect and mechanism of oil-degrading bacteria (strain Acinetobacter sp B11) with magnetic field were conducted. The results showed that oil removal efficiency was 11.9% higher when magnetic field (25mT) was added in biodegradation process. Lower intensity of magnetic field could promote microbial growth and improve microbial enzyme activity and the results had showed that microbial logarithmic phase was shortened and the enzyme activity of bacteria increased by 27.4% at lower magnetic strength (25mT).

Keywords: Oil Degradation Bacteria, Magnetic Field, Microbial Activity, Microbial Growth.

1. Introduction

As an emerging technology, magnetic field had attracted more and more attentions in the field of water and wastewater treatment in recent years [1-3]. The magnetic field had been used in biodegradation process for pollutant removal and some studies showed that magnetic field could affect the growth of microbe. Nakamura et al [4] found that the cell number of Bacillus subtilis MI113 in an inhomogeneous (5.2-6.1T) magnetic field was about twofold higher than that of the reference (7T) in the stationary phase. Liu et al [5] studied the effect of steady magnetic force on the growth of Lentius edodes and concluded that magnetic field improved the biological efficiency by speeding up the formation and division of fungus' original medium. Zheng et al [6] studied the effects of electromagnetic field on Spirulina growth and found that lower magnetic field intensity(0～40kA/m) had a positive effect on Spirulina growth and it was most significant when the magnetic field intensity was 24 kA/m. Rutkowska et al [7] observed that magnetic field at induction of 7mT generated by permanent magnets was a factor improving p-nitroaniline biodegradation by microorganisms inhabiting activated sludge.

On the other hand, magnetic field could affect the biodegradation ability of microbes. It made the activity of catalase, peroxidase and three kinds of phosphatase increase in different degrees and the magnetic field effect could continue for a long time. Koneracka et al [8] found that the bioactivity could be maintained more than 90% if the proteins and enzymes were immobilized on magnetic particle surface. Studies of Li et al [9] showed that the activity of catalase increased by 48.6% after the enzyme liquid treated by 100mT. Celik et al [10] found that moderate intensity of the magnetic field (below 5mT) increased the activity of superoxide dismutase and catalase more than 20% and the increases of magnetic field exposure times did not cause linear increases in enzyme activities. Sui et al [11] compared the different magnetic field intensity in improving the efficiency of urban wastewater biodegradation with the contrastive system and found that the

[+] Corresponding author. Tel.: + 85 451 82519210; fax: +86 451 82519141
E-mail address: renzhijun2003@126.com

activated sludge system enhanced by additional magnetic field (1500 Gs) increased the removal rate of COD, NH_3-N and PO_4^{3-}P by 1.3%, 0.2% and 10.0%.

The process for magnetic field on biodegradation for pollutant removal was complicated. The aim of this work was to determine the effect of magnetic field (generated by permanent magnets) on the bacteria oil biodegradation ability and the mechanism of magnetic field on oil degradation bacteria was also investigated. Although the bacteria from a specific zone of Daqing oil wasterwater treatment were tested in the work, it was a reference and preparation for similar research on oily waste-water by biological process.

2. Methods

2.1. Bacteria isolation and cultivation

One strain was isolated from Daqing oilfield wastewater biochemical treatment plant. The test of microbial physiology and biochemistry was conducted and the results showed that the colony of strain was round with the diameter of 1~2mm. The surface of colony was smooth, moist, neat-edged and the central uplift slightly with yellow teeth. The strain was in the pattern of short rod, blunt at the two sides, usually in the form of single or paired and no spores. The results of physiological and biochemical identification showed that strain was catalase positive, oxidase negative, gram negative without growth factors.

Genetic sequence was conducted by SANGON biotech and compared with sequence homology in NCBI (National Center for Biotechnology Information) and the ribosomal database (http://rdp.cme.msu.edu/index.jsp). The result of 16S rDNA was also carried on sequence homology comparison by Blast in GenBank. Comparison showed that the results were similar to the genetic sequences of *Acinetobacter*, and the similarity reached 99.6% (FJ494703).

With the determination of morphology, physiological and biochemical tests and 16S rDNA sequence analysis, the strain was identified as *Acinetobacter* and named *Acinetobacter sp* B11.

2.2. Preparation of oily wastewater

The preparation process of oily wastewater was following: a certain amount of crude oil and Tween-80 was mixed according to the proportion of 1:5. The water heated to 35℃and was gradually poured into above mix solution. The emulsified liquid was transferred to a separatory funnel for around 30min.The emulsified oil solution released from the bottom of the separatory funnel and the upper oil was also removed in order to obtain the stable oily wastewater.

2.3. Biodegradation experiment

In order to prepare the bacterial suspension, the single colonies taken from the agarslant culture medium was inoculated to beef extract peptone medium and placed in a thermostatic shaker with 200r/min for 24h at 30℃. Then the bacterial suspension was diluted to OD600 value for 0.8. The 5mL above bacteria suspension was collected into a 150mL conical flask with 50mL liquid oil medium, which was placed in the thermostatic shaker with 100r/min and 30℃for 7 days.

The oil concentration was determined by ultraviolet spectrophotometer with referring to the method of Determination of oil - UV Spectrophotometry of 93-1994 SL.

A circular ferrite permanent magnet purchased from Changzhou was as the magnetic field generating device. The diameter and thickness of magnet were 70mm and 10mm, respectively. The magnetic field intensity was measured by Teslameter. Experimental setup for the biodegradation process is shown in Fig. 1.

Fig. 1: Experimental setup for the biodegradation process

For a good linear relationship between the concentration of bacterial suspension and the absorbance, the absorbance at a wavelength of 600nm (OD600) was used to characterize the biomass.

With reference to “Identification Manual of Common Bacterial System” and "Berger Bacterial Identification Manual" (Eighth Edition), morphological observation and physiological and biochemical characteristics experiment were carried on for isolated petroleum degrading bacteria with high efficiency, the preliminary result was genus. At the same time, through the sequence analysis of 16S rDNA, the species of strains were further identified.

Dehydrogenase activity was conducted in present research and was determinated according to the reduction method of chloride three TTC (2, 3, 5-Triphenyl Tetrazolium Chloride, TTC).

In order to better understand the effect of strain *Acinetobacter sp* B11 for oil removal, gas chromatography coupled with electron impact ionization tandem mass spectrometry was used to analyze the residual oil composition. Operating conditions of GC-MS: a capillary column of HP-5MS (60 m ×250μm×0.25μm);Carrier gas: He; The GC oven temperatures were: held at 45 ℃ for 3 min, ramped at 10 ℃/min to 320 ℃, with a final hold at 10 min. Constant voltage no shunt; The injector and detector temperatures were the same set at 280 ℃. Scanning: 40-400amv; Electron energy: 70ev; Helium was used as the carrier gas at a flow rate of 1.2mL/min. Ion source temperature: 200 ℃; transmission line temperature: 250 ℃.

3. Results and Discussion

3.1. Effects of magnetic field on oil-degrading bacteria for oil removal

The effect of magnetic field on microorganism biodegradation performance had an important relationship with the magnetic field intensities [12]. The strain *Acinetobacter sp* B11 were inoculated in the culture medium. The liquid petroleum oil concentration was around 200mg/L, temperature was controlled at 30℃and the magnetic field of 0, 18, 25, 30, 35, 43 and 60mT were also added respectively. The performance of strain *Acinetobacter sp* B11 at different magnetic field intensity was studied and the result was shown in Fig. 2.

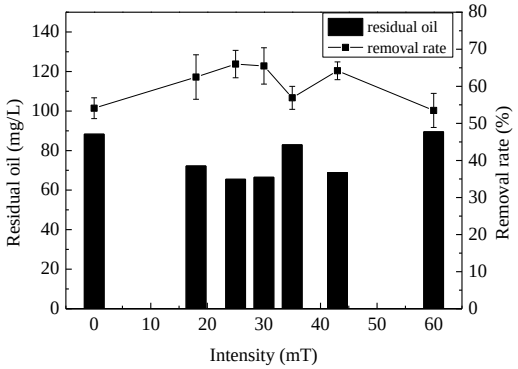

Fig. 2: Effect of different magnetic field intensity on oil degradation

In Fig. 2, the result showed magnetic field intensities had different effects on strain *Acinetobacter sp* B11 for oil degradation. When there was no external magnetic field, the concentration of the residual oil was

88.3mg/L and oil degradation rate was 54.1%. With the magnetic field intensity increased, oil removal rate also increased. When the magnetic field intensity reached 25mT, oil removal rate of strain *Acinetobacter sp* B11 reached a maximum value of 66% and the oil removal rate increased by 11.9% compared with the situation without magnetic field. As the magnetic field intensity was over 30mT, the performance of strain *Acinetobacter sp* B11 on oil degradation was not stable. The external magnetic field had few effects on the microbial oil degradation when magnetic field intensity reached 35mT and 60mT. This result was similar with Jia [13], who studied the magnetic field enhancement effect of the biodegradation ratio of COD and found that the biodegradation ratio went up first as the magnetic field intensity increased to 20mT, and then decreased sharply with further increased.

3.2. Effect of the magnetic field on the growth of oil-degrading bacteria

The impact on microbial growth with magnetic field was multifarious, and different magnetic field strength may have different impacts on microbes in different growth periods. The effect of magnetic field on microbial growth was conducted. The strain *Acinetobacter sp* B11 had been transferred from beef extract peptone medium to the oil liquid medium in the condition of 30℃ and 100r/min shaking culture with the magnetic field from 0 to 60mT. The growth of oil-degrading bacteria in liquid petroleum medium was shown in Fig. 3.

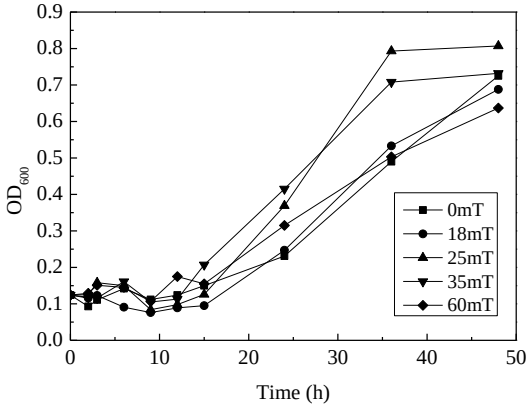

Fig. 3: Effect of magnetic field on the growth of oil-degrading bacteria

In Fig. 3, with different magnetic field strength, there was a large difference for oil-degrading bacteria of *Acinetobacter sp* B11 to adopt oily wastewater. At the beginning of 15 hours, no matter whether the external magnetic field was added or not, the lag phase of strains was no significant change. In the logarithmic phase, the slope of the curve became greater for the external magnetic field, which indicated the microbial growth rate increasing. Especially with the magnetic field of 25mT, the microbial growth was the fastest, the period of logarithm was the shortest, and biomass of strains firstly reached the maximum biomass.

In this context, results from Fig. 3 suggested that low-level magnetic field tended to benefit the bacterial growth compared without magnetic field. Probably due to the proper strength of the magnetic field could change the generation time of microorganism. This result was same with Cheng [14], who found that generation time of bradyrhizobium with magnetization treatment was shorter than the control strain. Zheng et al [6] also found that the magnetic field had an effect on microbial growth mainly in the logarithmic phase, and when the magnetic field intensity was 25mT, the promoting effect on strain growth was the most obvious.

3.3. Effect of the magnetic field on the microbial activity of oil-degrading bacteria

Acinetobacter sp B11 strain was inoculated in the culture medium with liquid petroleum oil at the magnetic field of 0, 18, 25, 30, 35, 43 and 60mT. Under the condition of 30℃ and 100r/min in the shaking culture, the dehydrogenase activity of bacteria liquid were determined and the results were shown in Fig. 4.

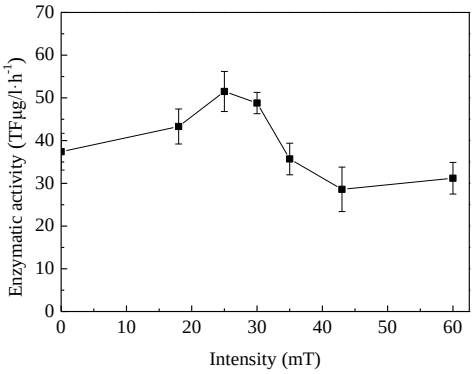

Fig. 4: Effect of the magnetic field on the microbial activity

In Fig. 4, the magnetic field had a promoting effect on the microbial enzyme activity when the magnetic field intensity was between 18-30mT. When the magnetic field intensity was 25mT, the promoting effect was the strongest, the microbial enzyme activity was 51.5 TFμg/L·h^{-1} and the activity was increased by 27.4% compared with no magnetic field. When the magnetic field intensity was more than 35mT, the magnetic field had an inhibitory effect on the enzyme activity, which tended to be stable and did not drop.

The active center of the enzyme contains iron, manganese, zinc, copper and other paramagnetic metalions has an enzyme molecule with certain magnetic moment of the side chains. Orientation distribution will change with the Lorenz force generated by the magnetic field, which results in the effect on the conformation and activity of enzyme [15]. The conformational change of enzyme molecular can be better fit with the substrate, producing the formation of the enzyme substrate complex, in general this process is very fast, but when the substrate diffusion limitation exists, the magnetic field can promote the rapid formation of complexes [16]. From the changes of enzyme activity, the magnetic field can promote the adsorption and utilization of microorganisms on organic matter and improve the degradation effect of organic matter. However, mechanisms that completely explain how magnetic fields may initiate changes in biological systems have not yet been elucidated [17].

4. Conclusion

The performance and mechanism of magnetic field on oil-degrading bacteria (*Acinetobacter sp* B11) for oil removal was conducted. The result showed that lower magnetic field intensity not only had a positive effect on the oil degradation efficiency, especially for short chains alkane degradation, but also had the most significant effect on the activity of enzymes. When the magnetic field intensity was 25mT, the oil removal rate of microorganisms increased by 11.9% and the enzyme activity of bacteria increased by 27.4% compared with no magnetic field.

5. Acknowledgments

This work was supported by the National Natural Science Foundation of China (No. 51209053) and Open Project of State Key Laboratory of Urban Water Resource and Environment，Harbin Institute of Technology (No.QA201619).

6. References

[1] S. Hattori, M. Watanabe, and T.Endo, et al. 2001. Effects of an external magnetic field on the sedimentation of activated sludge. *World Journal of Microbiology and Biotechnology*. 17(3): 279-285.

[2] Tomska A, Janosz-Rajczyk M. 2004. The effect of magnetic field on wastewater treatment with activated sludge method. *Environment Protection Engineering*. 4: 155-160.

[3] Tomska A, Wolny L. 2008. Enhancement of biological wastewater treatment by magnetic field exposure. Desalination. 222(1): 368-373.

[4] Nakamura K, Okuno K, Ano T, et al. 1997. Effect of high magnetic field on the growth of Bacillus subtilis measured in a newly developed superconducting magnet biosystem. *Bioelectrochemistry and bioenergetics*. 43(1): 123-128.

[5] Zuoxi L, Enju L, Hua Z. 1997. Effect of magnetic field on the growth of Lentinus edodes. J*ournal of Northeast Forestry University (China)*. 2:87-89.

[6] Zheng, B.S., Guo, S.Y., You, S .2007. Effects of Magnetic Treatment on Biomass and EPS of Spirulina. Food Science. (1):94-98.

[7] Rutkowska-Narozniak, A., 1997.An application of static magnetic field to intensify the biodegradation of pollutions in wastewater (in Polish). Praca doktorska, Wydział Inzynierii S´rodowiska, Politechnika Warszawska, Warszawa.

[8] Koneracká M, Kopčanský P, AntalíK M, et al. 1999. Immobilization of proteins and enzymes to fine magnetic particles. *Journal of Magnetism & Magnetic Materials*. 201(1-3):427–430.

[9] Li, Q,B., Yin, C.L., Yang, W.C . 2006. A Study of Effect of Magnetic Field on Catalytic Activity of Catalase. Chemical Industry Times. 12:23-25.

[10] Çelik, N.Büyükuslu, and Ç. Atak, et al. 2009. Effects of Magnetic Field on Activity of Superoxide Dismutase and Catalase in Glycine max (L.) Merr. Roots. *Polish Journal of Environmental Studies*. 18(2):175-182.

[11] Sui, W.Y., Song, P. Han, T.T., et al. 2011. Contrastive Studies on Experiment of Activated Sludge Method Enhanced by Magnetic Field for Treating Urban Wastewater. *Journal of Anhui Agricultural Sciences*. 39(33):20469-20471，20540.

[12] Zhang, S.F., Wei, W.Z., Zhang, J.Z., et al. 2002. Effect of static magnetic field on growth of Escherichia coli and relative response model of series piezoelectric quartz crystal. Analyst. 127(3):373-377.

[13] Y. L. Jia, and Y. H.Wang and J. S. Sun, et al. 2010. Enhancement of biological treatment of wastewater by magnetic field. *Bioresource Technology*. 101(22):8535-8540.

[14] X. L. Cheng and Y. L. Yi, 2009. Effect of Magnetic Treatment on Amount and Generation Time of Slow Growing Rhizobium (USDA110) and Fast growing Rhizobium (USDA 191). *South west China Journal of Agricultural Sciences.* 5:1400-1403.

[15] Zhang. J., Fan, S., Chen, D.W. 2001. Studies of biological effects of high intensities static magnetic fields on the conformation and activity of vitro catalase in bovine liver. *Chinese Journal of Medical Physics*. 18(1):35-36+53.

[16] He H.J., Zhu, Y.H., Zhong, K. et al.1998. T*he Effect of Magnetic Field on Enzyme Conformation. Journal of Jishou University*. 19(4):25-30.

[17] Ramundo-Orlando, A., Mattia, F., Palombo, A., D'lnzeo, G.2000. Effect of low frequencuy, low amplitude magnetic fields on the permeability of cationic liposomes entrapping carbonic anhydrase. *Bioelectromagnetics*. 21:499-507.

International Proceedings of Chemical, Biological and Environmental Engineering
Volume 94 of IPCBEE (2016)
DOI: 10.7763/IPCBEE. 2016. V94. 3

Technical Features and Thermal Efficiencies of Various Flat Plate Solar Collectors

Turhan Koyuncu [+] and Fuat Lule

Department of Energy Systems Engineering, Faculty of Technology, University of Adiyaman, Adiyaman, Turkey

Abstract. Flat plate solar water collectors are widely used for supplying hot water or hot air for domestic or industrial applications in the world. These collectors provide a pretty big profit when compared with other energy resources. For instance, it was determined by a study that these collectors are approximately 2.0, 3.5, 4.0, 6.0, 7.0 and 12.0 times more profitable than wood, coal, natural gas, oil, LPG, and electricity, respectively for heating water. Therefore, technical features and thermal efficiencies of different type flat plate solar air and water collector (heater) systems such as collector panels (arrays), heat exchangers and hot water storage tanks were presented in this research. Besides, calculation of ideal collector panel tilt angle and different theoretical efficiency analysis methods such as energy balance method and complicated method was discussed in this work. As a result, the high thermal efficiencies were found as 46%, 88% and 95% for an air collector, for a natural circulation corrugated 304 chromium water collector, and for a vertical hot water tank, respectively.

Keywords: Solar Water Collector, Solar Air Collector, Solar Heater, Flat Plate Collector.

1. Introduction

Water is used in households predominantly for drinking, cooking and hygiene purposes such as bathing and the washing of dishes. Each person in a household requires at least 20 L of potable water per day, half of which is for personal hygiene. Water is also needed to be heated to meet hot water necessity for cooking and hygiene. The use of hot water during the day is approximately the same in the morning as it is in the evening, but less during the afternoon in households [1].

Different heat sources are employed for heating water. However, in most developing countries, supplies of non-renewable sources of energy are either unavailable, unreliable or too expensive. In renewable energy sources, solar energy is the most appropriate for heating water. This energy allows independent systems to be constructed and possesses a thermal conversion mode which necessitates a simple technology [2].

Solar energy received on the ground is abundant and inexhaustible. In addition to its inexhaustible nature, solar energy has the advantage of being a source of nonpolluting energy. This energy could be harnessed in several ways. The most promising energy forms are solar collectors with thermal conversion, which can be used to heat water for domestic and industrial applications. These applications are developing most rapidly and are the basis of small but growing industry [3].

Collectors are the heart of the solar processes. In solar collector, energy transfer from a distant source of radiant energy to a fluid or store as latent heat energy by using PCM [4-10]. The flux of incident radiation is, at best, approximately 1100 W/m2 (without optical concentration), and it is variable. The wavelength range is from 0.3 to 3 μm, which is considerably shorter than that of the emitted radiation from most energy absorbing surfaces. Thus, the analysis of solar collectors presents unique problems of low and variable energy fluxes and the relatively large importance of radiation. Flat plate collectors can be designed for

[+] Corresponding author. Tel: +90 416 2233800; Fax: +90 416 2233809.
E-mail address: tkoyuncu@adiyaman.edu.tr

applications requiring energy delivery at moderate temperatures, up to perhaps 100 ℃ above ambient temperature. They use both beam and diffuse solar radiation, do not require tracking of the sun, and require little maintenance. The major applications of these units are in solar water heating, building heating, air conditioning, and industrial process heat [11, 12]. The importance of flat plate collectors in thermal processes is such that their thermal performance is treated in considerable detail. This is done to develop an understanding of how the component functions [13, 14].

Many types of conventional solar collectors with metal absorber plates and glass covers are widely used to transforms solar energy into heat for heating water for domestic applications and industrial processes in Turkey and world [15, 16]. These collectors have high efficiency and they are approximately, 2.0, 3.5, 4.0, 6.0, 7.0 and 12.0 times more profitable when compared with other energy sources such as wood, coal, natural gas, oil, LPG and electricity, respectively for heating water for domestic applications in Turkey [17].

2. Theoretical Analysis

The optimum or ideal collector tilt angle (collector panel slope) for any location can be computed by using Equations 1 and 2. The ideal collector array slope is changing depends on latitude of the location, declination angle and the number of the day [17]. All symbols used in equations are described in the Nomenclature.

$$\beta = (\phi - \delta) \tag{1}$$

$$\delta = 23{,}45 \sin\left(360 \frac{284 + n}{365}\right) \tag{2}$$

Basically, the flat plate solar collectors operate under quasi steady-state conditions (Fig. 1). In these conditions, the thermal performance or efficiency of a solar collector is described by an *main energy balance* that indicates the distribution of incident solar energy into useful energy gain, thermal losses, and optical losses (Fig. 2 and 3) [13, 15, 18, 19].

The useful heat gain by a collector can be expressed as:

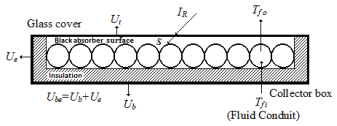

Fig. 1: Description of the flat plate solar water collector (main parts and general heat transfer exchanges).

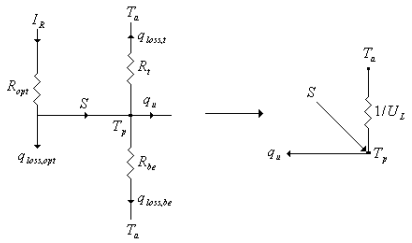

Fig. 2: Equivalent thermal network for flat plate solar water collector.

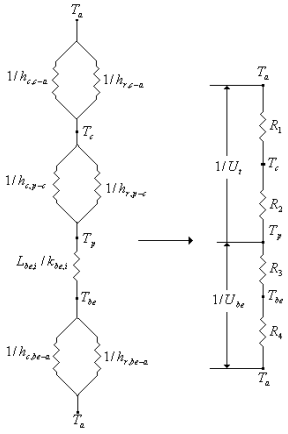

(b)

Fig. 3: Thermal network for the flat plate solar water collector in terms of conduction, convection and radiation (a), and in terms of resistances between plates (b)

$$q_s = I_R A_c = q_{loss} + q_u \tag{3}$$

$$q_u = q_s - q_{loss} = I_R A_c - q_{loss} \tag{4}$$

$$q_{loss} = q_{loss,opt} + q_{loss,t} + q_{loss,be} \tag{5}$$

$$q_u = I_R A_c - q_{loss,opt} - q_{loss,t} - q_{loss,be} \tag{6}$$

$$SA_c = I_R A_c - q_{loss,opt} = I_R A_c \left(\tau_c \alpha_p\right) \tag{7}$$

$$q_u = SA_c - q_{loss,t} - q_{loss,be} \tag{8}$$

$$q_u = I_R A_c \left(\tau_c \alpha_p\right) - q_{loss,t} - q_{loss,be} \tag{9}$$

$$q_u = \dot{m} c_{p,f} \left(T_{f,o} - T_{f,i}\right) \tag{10}$$

A measure of collector performance is the collector efficiency, defined as the ratio of useful heat gain over any time period to the incident solar radiation over the same period we can, thus, define efficiency as,

$$\eta = \frac{q_u}{q_s} \tag{11}$$

$$\eta = \frac{\sum q_u}{\sum q_s} \tag{12}$$

From Equations (3, 10, 11 and 12),

$$\eta = \frac{\dot{m} c_{p,f} \left(T_{f,o} - T_{f,i}\right)}{I_R A_c} \tag{13}$$

In addition, the thermal efficiency of a flat plate solar collector can be determined by using some *complicated equations* as discussed below.

It is convenient to define a quantity that relates the actual useful energy gain of a collector to the useful gain if the whole collector surface were at the fluid inlet temperature. This is quantity is called the collector heat removal factor F_R. The actual useful energy gain and the collector heat removal factor can be expressed as

$$q_u = A_c F_R \left[F_{D,S} S - U_L \left(T_{f,o} - T_{f,i}\right)\right] \tag{14}$$

$$F_R = \frac{\dot{m} c_{p,f} \left(T_{f,o} - T_{f,i}\right)}{A_c \left[S - U_L \left(T_{f,i} - T_a\right)\right]} \tag{15}$$

$$F_R = \frac{\dot{m} c_{p,f}}{A_c U_L} \left[\frac{T_{f,o} - T_{f,i}}{\frac{S}{U_L} - \left(T_{f,i} - T_a\right)}\right] \tag{16}$$

$$F_R = \frac{\dot{m} c_{p,f}}{A_c U_L} \left[\frac{\left(T_{f,o} - T_a - \frac{S}{U_L}\right) - \left(T_{f,i} - T_a - \frac{S}{U_L}\right)}{\frac{S}{U_L} - \left(T_{f,i} - T_a\right)}\right] \tag{17}$$

$$F_R = \frac{\dot{m} c_{p,f}}{A_c U_L} \left[1 - \frac{\frac{S}{U_L} - \left(T_{f,o} - T_a\right)}{\frac{S}{U_L} - \left(T_{f,i} - T_a\right)}\right] \tag{18}$$

U_L is the collector overall heat loss coefficient. The thermal energy lost from the collector to the surroundings by conduction, convection and infrared radiation. U_L is equal to the sum of energy loss through the top (U_t), bottom (U_b) and edge (U_e) of the collectors given below (Fig. 2 and 3) [15] :

$$U_L = U_t + U_b + U_e = U_t + U_{be} \tag{19}$$

The energy loss through the top is the result of convection and radiation between parallel plates. The top loss coefficient from the collector plate to the ambient is

$$\frac{1}{R_1}=\frac{1}{\frac{1}{h_{c,c-a}}}+\frac{1}{\frac{1}{h_{r,c-a}}}=\frac{h_{c,c-a}+h_{r,c-a}}{1} \tag{20}$$

$$R_1=\frac{1}{h_{c,c-a}+h_{r,c-a}} \tag{21}$$

$$\frac{1}{R_2}=\frac{1}{\frac{1}{h_{c,p-c}}}+\frac{1}{\frac{1}{h_{r,p-c}}}=\frac{h_{c,p-c}+h_{r,p-c}}{1} \tag{22}$$

$$R_2=\frac{1}{h_{c,p-c}+h_{r,p-c}} \tag{23}$$

$$\frac{1}{U_t}=R_1+R_2=\frac{1}{h_{c,c-a}+h_{r,c-a}}+\frac{1}{h_{c,p-c}+h_{r,p-c}} \tag{24}$$

$$U_t=\left[\frac{1}{h_{c,c-a}+h_{r,c-a}}+\frac{1}{h_{c,p-c}+h_{r,p-c}}\right]^{-1} \tag{25}$$

Besides, h_w, U_b and U_e must be obtained from the equations as follows [20]:

$$h_{c,c-a}=h_w=2.8+3\upsilon \tag{26}$$

$$U_t=\left[\frac{1}{h_w+h_{r,c-a}}+\frac{1}{h_{c,p-c}+h_{r,p-c}}\right]^{-1} \tag{27}$$

$$R_3=\frac{L_{be,i}}{k_{be,i}}+\frac{A_c}{\left(\frac{k_{be,i}}{L_{be,i}}\right)A_{c,e}} \tag{28}$$

$$\frac{1}{R_4}=\frac{1}{\frac{1}{h_{c,be-a}}}+\frac{1}{\frac{1}{h_{r,be-a}}}=\frac{h_{c,be-a}+h_{r,be-a}}{1} \tag{29}$$

$$R_4=\frac{1}{h_{c,be-a}+h_{r,be-a}} \tag{30}$$

$$\frac{1}{U_{be}}=R_3+R_4 \tag{31}$$

$R_4\cong 0$ is very small and negligible, so

$$\frac{1}{U_{be}}=R_3=\frac{L_{be,i}}{k_{be,i}}+\frac{A_c}{\left(\frac{k_{be,i}}{L_{be,i}}\right)A_{c,e}} \tag{32}$$

$$U_{be}=\frac{k_{be,i}}{L_{be,i}}+\frac{\left(\frac{k_{be,i}}{L_{be,i}}\right)A_{c,e}}{A_c} \tag{33}$$

$$U_t=\left(\frac{1}{h_{c,p-c}+h_{r,p-c}}+\frac{1}{h_w+h_{r,c-a}}\right)^{-1} \tag{34}$$

In order to find $h_{c,p-c}, h_{r,p-c}$ and $h_{r,c-a}$ for these solar water collectors, a series of equations seen below must be used [15].

$$R_a = \frac{g\beta_{p-c}\Delta T_{p-c}{L_{p-c}}^3}{\nu_{a,p-c}\lambda_{a,p-c}} \tag{35}$$

$$\beta = \frac{1}{T_m} \tag{36}$$

$$T_m = \frac{T_c + T_p}{2} \tag{37}$$

$$P_r = \frac{\nu_{a,p-c}}{\lambda_{a,p-c}} \tag{38}$$

$$R_a = \frac{g\Delta T_{p-c}{L_{p-c}}^3 P_r}{T_m {\nu_{a,p-c}}^2} \tag{39}$$

$$R_a = \frac{g\beta_{p-c}\Delta T_{p-c}{L_{p-c}}^3}{{\nu_{a,p-c}}^2} \tag{40}$$

$$N_u = 1 + 1{,}44\left[1 - \frac{1708\left(\sin 1{,}8\beta_{p-c}\right)^{1{,}6}}{R_a \cos\beta_{p-c}}\right]\left[1 - \frac{1708}{R_a \cos\beta_{p-c}}\right] + \left[\left(\frac{R_a \cos\beta_{p-c}}{5830}\right)^{1/3} - 1\right] \tag{41}$$

$$h_{c,p-c} = \frac{N_u k_{a,p-c}}{L_{a,p-c}} \tag{42}$$

$$h_{r,p-c} = \frac{\sigma\left({T_p}^2 + {T_c}^2\right)\left(T_p + T_c\right)}{\frac{1}{\varepsilon_p} + \frac{1}{\varepsilon_c} - 1} \tag{43}$$

$$h_{r,c-a} = \varepsilon_c \sigma\left({T_c}^2 + {T_a}^2\right)\left(T_c + T_a\right) \tag{44}$$

$$T_c = T_p - \frac{U_t\left(T_p - T_a\right)}{h_{c,p-c} + h_{r,p-c}} \tag{45}$$

Another equation to find U_t was developed by Klein. U_t was also calculated by using this equation (46). It was seen that it gives the same results with very small and negligible differences [13].

$$U_t = \left[\frac{n}{\frac{C}{T_p}\left[\frac{\left(T_p - T_a\right)}{\left(n + f\right)}\right]^e} + \frac{1}{h_w}\right]^{-1} + \left[\frac{\sigma\left(T_p + T_a\right)\left({T_p}^2 + {T_a}^2\right)}{\left(\varepsilon_p + 0{,}00591 n h_w\right)^{-1} + \frac{2n + f - 1 + 0{,}133\varepsilon_p}{\varepsilon_c} - n}\right] \tag{46}$$

In Equation (46),

$$f = \left(1 + 0{,}089 h_w - 0{,}1166 h_w \varepsilon_p\right)\left(1 + 0{,}07866 n\right) \tag{47}$$

$$C = 520\left(1 - 0{,}000051{\beta_{a,p-c}}^2\right) \tag{48}$$

$$e = 0{,}430\left(1 - \frac{100}{T_p}\right) \tag{49}$$

As a result of this theoretical analysis, it should be noted that calculated thermal efficiency of any flat plate solar collector by using main energy balance equations (Eq. 3…13) or complicated equations (Eq. 13…49) give the same results with very small differences. In general, the results of main energy balance equations are approximately %2 higher than the results of complicated equations.

3. Results of Various Flat Plate Solar Collectors

Six different solar air heaters have designed, manufactured and tested [21]. The highest thermal efficiency was determines as 46%.

Four identical flat plate solar air collector were experimented at 25 ° (ideal tilt angle from Eq. 1 and 2), 30 °, 35 ° and 40 ° tilt angles. It was seen from the result that the maximum and minimum efficiencies were obtained as % 40 and % 36 for 25 and 40 ° tilt angels, respectively [17].

The effect of some components on thermal efficiencies of flat plate solar water collectors were investigated [22]. It was seen that the efficiencies of aluminum and copper collector panels are changing between 56%...68%. In addition, it was found that the black copper selective absorber surface increase thermal efficiency as 7.13%, the prismatic glass raise the efficiency as 9.37%, the radiation reflector located between absorber and insulater grow the efficiency as 1.12% and the normal tempered glass cover develop the efficiency as 9.63.

A black copper selective surface panel solar water collector system that can be operated as natural circulation closed thermosyphon system with a chromium 304 fluid-to-fluid heat exchanger was designed, manufactured and tested [23, 24]. The efficiency of the collector array and heat exchangers were separately investigated. The results showed that the efficiency of the collector array, horizontal type and vertical type heat exchangers are 63%, 29% and 33%, respectively. The efficiency of combination of both collector array and heat exchangers were also defined as 18% and 21% for horizontal and vertical heat exchangers, respectively.

Three type chromium 304 solar water collectors such as dry type, wet type and storage type was designed, manufactured and tested [25]. The results showed that thermal efficiencies of dry type, storage type and wet type are 22%, 33% and 43%, respectively. The highest efficiency was found for wet type collector when there is fluid (mixture of 60% water and 40% glikol) between pipes.

A domestic type of a 304 stainless steel chromium flat plate solar water collector that can be directly connected to the pressurized city water line system and keep hot water temperature with PCM (phase change material) placed inside the collector during night was designed, constructed and tested [26]. Test results showed that, thermal efficiency of the collector was defined as 12.5% and 62.0% while fluid stored and flows, respectively.

Three different collectors which made of 304 matte chromium that could be directly connected to the city's main waterworks were manufactured for test of experiments [27]. Pipe diameters of collectors were 20mm, 25mm and 32mm. In first step, the collector panels were experimented for their efficiency. In second step, a pressurized and insulated vertical hot water tank was connected with collector panels and tested. The results showed that the efficiencies of collector panels are 67%, 74% and 77% for 20mm, 25mm and 32mm pipe diameters, respectively. Vertical hot water tank's standalone efficiency was found as 70%. The average efficiency of combination of both collector panel with 32 mm pipe diameter and hot water tank was determined as 54%.

A flat plate solar water collector manufactured from matt type stainless steel chromium 304 were designed, constructed and tested [28]. As a result, the thermal efficiency of the collector was defined as 50 % and 64 % when gap between pipes full of air and mixture of water-antifreeze, respectively. The thermal efficiency of natural circulaton and insulated vertical hot water tank was also determined as 95%. The average efficiency of combination of both collector panel (while gap full of water-antifreeze) and hot water tank was determined as 61%. A corrugated solar water collector panel which is natural circulation and made up of 304 matte chromium plate was investigated. The efficiency of the collector panel was determined as 88% [29].

4. Conclusions

1) Flat plate collector panels should be located by considering ideal collector tilt angle.

2) High efficient flat plate solar air collector should be used for air heating.

3) Corrugated and made up of 304 chromium solar water collector panel should be preferred.

4) Natural circulation open thermosiphon collector systems should be used.

5) Natural circulaton and insulated vertical hot water tank should be preferred.

6) It is avoid to use flat plate closed thermosiphon collector systems and heat excahngers.

5. Nomenclature

A_c : Collector area, m^2

$A_{c,e}$: Collector edge surface area, m^2

$c_{p,f}$: Fluid specific heat at constant pressure, J/(kg.K)

$F_{D,S}$: Collector dust and shading factor

F_R : Collector heat removal factor

g : Gravitational acceleration, m/s^2

$h_{c,c-a}$: Convection heat transfer coefficient between cover and ambient air, $W/(m^2.K)$

$h_{c,be-a}$:Convection heat transfer coefficient between bottom-edge and ambient air, $W/(m^2.K)$

$h_{c,p-c}$: Convection heat transfer coefficient between plate and cover, $W/(m^2.K)$

$h_{r,be-a}$: Radiation heat transfer coefficient between bottom-edge and ambient air, $W/(m^2.K)$

$h_{r,c-a}$: Radiation heat transfer coefficient between cover and ambient air, $W/(m^2.K)$

$h_{r,p-c}$: Radiation heat transfer coefficient between plate and cover, $W/(m^2.K)$

h_w : Wind heat transfer coefficient, $W/(m^2.K)$

I_R : Incident solar radiation, W/m^2

$k_{a,p-c}$: Air thermal conductivity between plate and cover, W/(m.K)

$k_{be,i}$: Bottom-edge insulation thermal conductivity, W/(m.K)

$L_{be,i}$: Bottom-edge insulation thickness, m

$L_{a,p-c}$: Air length between plate and cover, m

$\dot{m}$: Fluid mass flow rate, kg/s

n : Number of cover; the day of the year ($1 \le n \le 365$)

N_u : Nusselt Number

P_r : Prandtl number

q_{loss} : Thermal energy losses, W

$q_{loss,be}$: Thermal energy losses through the bottom-edge, W

$q_{loss,opt}$: Optical energy losses, W

$q_{loss,t}$: Thermal energy losses through the top, W

q_s : Incident solar power, W

q_u : Useful thermal power gain, W

R_a : Rayleigh number

R_{be} : Bottom-edge resistance, $(m^2.K)/W$

R_{opt} : Optical resistance, $(m^2.K)/W$

R_t : Top resistance, $(m^2.K)/W$

R_1, R_2, R_3, R_4 : Resistances, $(m^2.K)/W$

S : Absorbed solar radiation, W/m^2

T_a : Ambient air temperature, K

T_{be} : Bottom-edge surface temperature, K

T_c : Cover temperature, K

$T_{f,i}$: Fluid inlet temperature, K

$T_{f,b-1}$: Fluid temperature at point b-1, K

$T_{f,b-2}$: Fluid temperature at point b-2, K

$T_{f,t-1}$: Fluid temperature at point t-1, K

$T_{f,t-2}$: Fluid temperature at point t-2, K

$T_{s-1,s-10}$: Black painted pipe surface temperature at point s-1…s-10, K

$T_{f,o}$: Fluid outlet temperature, K

T_p : Plate surface temperature, K

T_m : Mean temperature, K

U_{be} : Bottom-edge heat loss coefficient, $W/(m^2.K)$

U_L : Collector overall heat loss coefficient, $W/(m^2.K)$

U_t : Top heat loss coefficient, $W/(m^2.K)$

υ : Wind speed, m/s

Greek

$\lambda_{a,p-c}$: Thermal diffusivity of air between plate and cover

α_p : Plate absorptance coefficient

β : Ideal (optimum) collector panel tilt angle (collector panel slope), ° ($0° \le \beta \le 180°$), ($\beta > 90°$ means that the surface has a downward facing component)

$\beta_{a,p-c}$: Volumetric expansion coefficient of air between plate and cover (for an ideal gas $\beta = 1/Tm$),

ϕ : Latitude angle of location, °(the angular location north or south of the equator, north positive; $-90° \le \phi \le 90°$)

δ : Declination angle, °($-23.45° \le \delta \le 23.45°$)

ΔT_{p-c} : Temperature differences between plate and cover, K

ε_c : Cover emittance

ε_p : Plate emittance

η : Collector thermal efficiency

$\nu_{a,p-c}$: Kinematic viscosity of air between plate and cover, m^2/s

σ : Stefan-Boltzmann constant (5.67×10^{-8}), $W/(m^2.K^4)$

τ_c : Cover transmittance

$(\tau_c \alpha_p)$: Transmittance-absorptance product

6. References

[1] M. N. Nieuwoudt and E. H. Mathews. A mobile solar water heater for rural housing in Southern Africa. Building and Environment. 2005, (40): 1217-1234.

[2] T. Koyuncu. Performance of various design of solar air heaters for crop drying applications. Renewable Energy. 2006, (31): 1073-1088.

[3] M. Hazami, S. Kooli, M. Lazaar, A. Farhat and A. Belghith. Performance of a solar storage collector. Desalination.

2005, (183): 167-172.

[4] P.C. Eames and P.W. Griffiths. Thermal behaviour of integrated solar collector/storage unit with 65 0C phase change material. Energy Conversion and Management. 2006, (47): 3611–3618

[5] H. M. S. Hussein, H. H. El-Ghetany and S. A. Nada. Experimental investigation of novel indirect solar cooker with indoor PCM thermal storage and cooking unit. Energy Conversion and Management. 2008, (49): 2237–2246.

[6] M. Mazman, L. F. Cabeza, H. Mehling, M. Nogues, H. Evliya and H. Ö. Paksoy. Utilization of phase change materials in solar domestic hot water systems. Renewable Energy. 2008, 1–5.

[7] W. Saman, F. Bruno and E. Halawa. Thermal performance of PCM thermal storage unit for a roof integrated solar heating system. Solar Energy. 2005, (78): 341–349.

[8] A. Sharma, V. V. Tyagi, C. R. Chen and D. Buddhi. Review on thermal energy storage with phase change materials and applications. Renewable and Sustainable Energy Reviews. 2007, (13): 318–345.

[9] A. Shukla, D. Buddhi and R.L. Sawhney. Solar water heaters with phase change material thermal energy storage medium: A review. Renewable and Sustainable Energy Reviews. 2009, (13): 2119–2125.

[10] E. Talmatsky and A. Kribus. PCM storage for solar DHW: An unfulfilled promise?. Solar Energy. 2008, (82): 861–869.

[11] S.O. Enibe. Thermal analysis of a natural circulation solar air heater with phase change material energy storage. Renewable Energy. 2003, (28): 2269–2299.

[12] A. Kürklü, A. Özmerzi and S. Bilgin. Thermal performance of a water-phase change material solar collector. Renewable Energy. 2002, (26): 391–399.

[13] J. A. Duffie and W. A. Beckman. Solar engineering of thermal process. John Wiley & Sons Ltd., 1991, New York.

[14] M. Smyth, P. C. Eames and B. Norton. Integrated collector storage solar water heaters. Renewable and Sustainable Energy Reviews. 2006, (10): 503–538

[15] T. Koyuncu and M. Ultanir. Economic Analysis of Flat Plate Solar Collectors in Supplying Hot Water in Turkey (in Turkish). 17. National Agricultural Mechanization Congress Proceedings, pp. 179-189, September 17-19, 1997, Tokat, Turkey.

[16] N. M. Nahar. Year round performance and potential of a natural circulation type of solar water heater in India. Energy and Buildings. 2003, (35): 239-247.

[17] T. Koyuncu. Eğim Açılarının Düz Yüzeyli Hava Isıtıcı Güneş Kollektörlerinin Verimleri Üzerine Etkileri (in Turkish), O.M.Ü. Zir. Fak. Dergisi, 17 (3), 2002, 33-42.

[18] Anonymous EN (European Norms) 12972-2. Thermal solar systems and components-Solar collectors-Part 2: Test Methods, April, 2003.

[19] S. B. Riffat, P. S. Doherty and E.I. Abdel Aziz. Performance testing of different types of liquid flat plate collectors. Int. J. Energy Res. 2000, (24): 1203-1215.

[20] M. N. Bagach, R. Tadili, A.S. Dahman and M. Boukallouch. Survey of thermal performances of a solar system used for the heating of agricultural greenhouses in Morocco. Renewable Energy. 2000, (20): 415-433.

[21] T. Koyuncu. Performance of Various Design of Solar Air Heaters for Crop Drying Applications, Renewable Energy, 31, 2006, (7), 1073-1088.

[22] T. Koyuncu, Y. Pınar and F. Lule. The Effect of Some Components on Performance of Flat Plate Solar Water Collectors, Agricultural Mechanization in Asia, Africa and Latin America (AMA),42, (2), 2011, 37-44.

[23] T. Koyuncu, Y. Pınar and F. Lule. Efficiency of a Solar Water Heater System Widely Used for Domestic Applications in Turkey, The Third Int. Exergy, Energy and Environment Symposium (IEEES3 2007), 1-5 July, 2007, Evora, Portugal.

[24] T. Koyuncu, Y. Pınar and F. Lüle. Doğal Dolaşımlı ve Kapalı Tip Güneşli Su Isıtıcı Sistemler İçin Kullanılan Eşanjörlerin Verimlerinin Belirlenmesi (in Turkish), Tarım Makinaları Bilimi Dergisi, 3, (3), 2007, 167-171.

[25] F. Lule and T. Koyuncu. Design, Manufacture and Test of Novel Type Flat Plate Solar Water Collectors, The Fourteenth Int. Energy and Environmental Technology Systems Conference (ICCI 2008), 15-17 May, 2008, Istanbul, Turkey.

[26] T. Koyuncu and F. Lule. Thermal Performance of a Domestic Chromium Solar Water Collector with Phase Change Material, Procedia-Social and Behavioral Sciences, 195, 2015, 2430-2442.

[27] T. Koyuncu, K. E. Engin, A. İ. Kaya, F. Lüle, M. F. Baran, and N. Yükçü ve H. Soğukpınar. Krom Bir Güneşli Su Isıtıcısının Tasarımı, Yapımı ve Denenmesi (in Turkish), Tarım Makinaları Bilimi Dergisi (Journal of Agricultural Machinery Science), 11, (1), 2015, 61-68.

[28] T. Koyuncu, F. Lule, and Y. Pınar ve Y.B. Yurtlu. Basınçlı Açık Sistem Düz Yüzeyli Bir Güneş Kolektörünün Tasarımı, Yapımı ve Denenmesi (in Turkish), Tarımsal Mekanizasyon 25. Ulusal Kongresi, 2009, 129-137, Isparta, Türkiye.

[29] T. Koyuncu, and A.İ. Kaya ve K.E. Engin. Adıyaman Yöresinde Kullanılan Oluklu Kolektörün Veriminin Belirlenmesi (in Turkish), 29. Ulusal Tarımsal Mekanizasyon ve Enerji Kongresi, 501-506, 2-5 Eylül, 2015, Diyarbakır, Türkiye.

International Proceedings of Chemical, Biological and Environmental Engineering
Volume 94 of IPCBEE (2016)
DOI: 10.7763/IPCBEE. 2016. V94. 4

Carbon Effects of Different Land Use Patterns in China During 2004-2013

Xiaokang Li [+], Xiaoming Wang and Guochao Zhao

School of Civil Engineering and Mechanics, Huazhong University of Science and Technology, China

Abstract: Since the 1980s, global warming has become a major problem facing the human all over the world. The main reason of climate becoming warm is due to the excessive emissions of greenhouse gas, especially CO2. Land use is one of the important factors that cause carbon emissions. Different patterns of land use have different carbon emission characteristics, and the results are also different. In this paper, the land was divided into cultivated land, garden land, forest land, grassland, residential and mining land, traffic land, water body, land use change and main ways of carbon emissions and carbon sequestration from different type of land were analyzed. The paper also analyzed the variation tendency of several carbon emission indexes including the amount of carbon emissions and carbon sequestration, the ratio of carbon source and carbon sink, per capita and per hectare carbon emissions from 2004 to 2013. And relevant regulation measurements on land use in China were proposed on the base of low-carbon goals.

Keywords: Different Land Use Patterns, Carbon Effect, Carbon Emission, Carbon Sequestration, China.

1. Introduction

Since the 1980s, the global warming has been the common concern of human beings. The main reason of climate becoming warm is due to the excessive emissions of greenhouse gas, especially CO_2. Land use is one of the important factors that cause carbon emission [1]. Land use changes directly affect the distribution and structure of terrestrial ecosystem, and change the process of carbon storage and carbon flux [2]. According to estimates from the famous carbon cycle research expert Houghton Richard: During 1850-1998, the amount of carbon dioxide emissions caused by the change of land use accounted for 1/3 of the total ones from human activities, and the amount of carbon emissions caused by the change of land use reached 10.6 billion tons, accounted for 30% caused by human activities [3, 4].

Researches about carbon emissions of land use have become hotspots in recent years, which mainly focused on the carbon cycle of land use on the ecosystem [1], regional land carbon emission and carbon flux measurement, low carbon optimization for regional land, while less from the perspective of nationwide, so nationwide land in China was chosen as the research object in this paper, and the time series of land use carbon emission was as the key study point. The paper analyzed the changes of land use and the variation tendency of several carbon emission indexes including the amount of carbon emissions and carbon sequestration, the ratio of carbon source and carbon sink, per capita and per hectare carbon emissions from 2004 to 2013. And relevant regulation measurements on land use in China were proposed on the base of low-carbon goals.

2. Data Sources and Research Methods

2.1. Data sources

[+] Corresponding author. Tel.: + 8615071204030.
E-mail address: lixiaokangkang@163.com.

The acreage of each kind of land comes from “Bulletin of China Land and Resources”. The acreage of urban green space comes from “China City Statistical Yearbook”. The amount of coal, oil, and natural gas caused by industry, traffic, business activities and living, and the acreage of farmland irrigation, total power of agricultural machinery, area of the crops, production of major agricultural products comes from “China Statistical Yearbook”. The usage amount of chemical fertilizer, pesticide and agricultural films comes from “Environmental Statistic”. The data of population comes from “The Statistics Bulletins of the National Economic and Social Development”. The territory of China is 9.6 million km^2.

2.2. Research methods

2.2.1 The main ways of carbon emissions and carbon sequestration for different types of land use

According to the original classification system of land use in China, the land is divided into 8 types: cultivated land, garden land, forest land, grassland, residential and mining land, traffic land, water body and unused land. The main sources of land use carbon emissions include agricultural land (mainly cultivated land), construction land (mainly for residential land and industrial and mining land, transportation land). The main sources of land use carbon sequestration include cultivated land, garden land, forest land, grassland, urban green space and water body. The main ways of carbon emissions and carbon sequestration for various types of land is shown in Table 1.

Table 1: The main ways of carbon emissions and carbon sequestration for different types of land use

Land types		The way of carbon emissions	The way of carbon sequestration
Agricultural land	Cultivated land	The use of agricultural machinery, agricultural irrigation, chemical fertilizer, pesticide and agricultural films	Photosynthesis of crops
	Garden land	—	Photosynthesis of fruit trees
	Forest land	—	Photosynthesis of trees
	Grassland	—	Photosynthesis of grassland
Construction land	Residential and mining land	Energy consumption, human respiration	Photosynthesis of urban green space
	Traffic land	Energy consumption	—
Unused land	Water body	—	Waters carbon sequestration and settlement
	Unused land	—	—

Because it is difficult to obtain the data about the acreage of water body, the carbon sequestration of water body is not calculated.

2.2.2 Measurement of carbon emissions

2.2.2.1 Agricultural land

Most of the carbon emissions from agricultural land are produced by agricultural inputs, and less one is caused by the decomposition of crop residues and the release of soil organic carbon [5]. Carbon emissions of agricultural land mainly come from the use of agricultural machinery, agricultural irrigation, fertilizers, pesticides and agricultural films.

The calculation formula for carbon emissions from agricultural machinery and agricultural irrigation is as follows [6]: $CE_{mach} = S_{mach} \times P + P_{mach} \times Q$ $CE_{irri} = S_{irri} \times R$

CE_{mach} and CE_{irri} represent the amount of carbon emissions from the use of agricultural machinery and irrigation process. S_{mach} represents the area of crops. P_{mach} represents the total power of agricultural machinery, S_{irri} represents irrigated area. P, Q, R represent carbon emission factors, which are separately 16.47 kg(C)/hm^2、0.18 kg(C)/KW、266.48 kg(C)/hm^2 [7].

The calculation formula for carbon emissions from the use of chemical fertilizers, pesticides and agricultural films is as follows [6]: $E_t = \sum T_i \times \delta_i$

E_t represents the amount of carbon emissions from the use of cultivated land. T_i represents the emissions of various carbon emission sources. δ_i represents the emission factors of various carbon emission sources.

The factors of chemical fertilizers, pesticides and agricultural films are shown in Table 2

Table 2: The carbon emission factors of chemical fertilizers, pesticides and agricultural films

Terms	Carbon emission factors	Unit	Data sources
Chemical fertilizers	857.54	g/kg	Oak Ridge National Laboratory
Pesticides	4.9341	kg/kg	Oak Ridge National Laboratory
Agricultural films	5.18	kg/kg	IREEA

2.2.2.2 Construction land

By referring to the carbon emission factors of IPCC, carbon emission calculation formula of construction land is as follows:

$$E_c = \sum_j Q_j C_{fj} + Y\lambda$$

E_c, Q_j, C_{fj}, Y and λ represent construction land carbon emissions, energy consumption of J, energy carbon emission factor of J, amount of population, per capita emission factor.

Carbon emission factors of various types of energy consumption and per capita carbon emission factor are shown in Table 3.

Table 3: Carbon emission factors of various types of energy consumption

Terms	Average value	Unit
Coal	0.7329	t(c)/t
Petroleum	0.5574	t(c)/t
Natural gas	0.4226	t(c)/t
Per capita carbon emission factor	328.5	kg/capita/a

Note: the data come from the average of IEE, climate change project finished by The State Science and Technology Commission in China, DOE/EIA and Xianjin Huang [8], Guoquan xu [9].

2.2.2.3 Measurement of carbon sequestration

2.2.2.3.1. Cultivated land

The amount of carbon sequestration comes from the sum of every crop's carbon sequestration, and each kind of crop's carbon sequestration can be calculated through economic yield, economic factor and the carbon sequestration rate [6]. Its carbon sequestration formula is as follows:

$$Ct = \sum_i C_{di} = \sum_i C_{fi} D_{wi} = \sum_i C_{fi} Y_{wi} / H_i$$

Ct represents the carbon sequestration of cultivated land. C_{di} represents the sequestration amount of carbon in the whole growth period. C_{fi} represents the rate of carbon sequestration. Y_{wi} represents the economic yield. D_{wi} represents biomass production. H_i represents the economic factor.

The economic factor and carbon sequestration rate of main crops in China are shown in Table 4.

Table 4: The economic factor and carbon sequestration rate of main crops in China

Terms	Rice	Wheat	Corn	Soy bean	Tubers	Cotton	Peanut	Rape-seed	Hemp	Sugar cane	Beet	Tobacco
Economic factor	0.45	0.40	0.40	0.35	0.70	0.10	0.43	0.25	0.39	0.50	0.7	0.55
Carbon sequestration rate	0.4144	0.4853	0.4709	0.45	0.4226	0.45	0.45	0.45	0.45	0.45	0.4072	0.45

Note: the data come from Kerang Li [10], Jingyun Fang, Xiulan Wang [11]

2.2.2.3.2. Garden land, forest land, grassland, urban green space

The carbon sequestration calculation formula of garden land， forest land, grassland, urban green space is as follows: $C_i = S_i \times V_i$

C_i represents the amount of carbon sequestration including garden land， forest land, grassland and urban green space, S_i represents the acreage of garden land， forest land, grassland and urban green space, V_i represents rate of carbon sequestration. The carbon sequestration of urban green space is the average of forest land and grassland, taking into account that the urban green space contain both trees, shrubs, and grassland [6]. The carbon sequestration factor of garden land, forest land, grassland and urban green space is shown in Table 5.

Table 5: The carbon sequestration factor of garden land, forest land, grassland and urban green space

Terms	Value	Unit	Data source	Terms	Value	Unit	Data source
Garden land	0.0730	kg(c)/(m^2 a)	Rongqin Zhao [12]	Grassland	0.0021	kg(c)/(m^2 a)	Jingyun Fang [13]
Forest land	0.0577	kg(c)/(m^2 a)	Jingyun Fang [13]	Urban green space	2.8861	kg(c)/(m^2 a)	The average of forest land and grassland

3. Results

3.1. Analysis of land use in China from 2004 to 2013

The acreage of different types of land is shown in Table 6, and changes of land use shown in Fig. 1.

Table 6: The acreage of different types of land during 2004-2013 unit: 10^4 hectares

Year	Cultivated land	Garden land	Forest land	Grassland	Other agricultural land	Residential and mining land	Traffic land	Water body
2004	12244.43	1128.78	23504.70	26270.68	2553.27	2572.84	223.32	358.95
2005	12208.27	1154.90	23574.11	26214.38	2553.09	2601.51	230.85	359.87
2006	12177.59	1181.82	23612.13	26193.20	2554.10	2635.45	239.52	361.52
2007	12173.52	1181.31	23611.74	26186.46	2549.11	2664.72	244.43	362.86
2008	12171.60	1180.00	23606.67	26180.00	2546.67	2693.33	246.67	366.67
2009	13538.46	1125.21	23746.32	24687.76	2434.64	2714.07	255.41	369.10
2010	13526.83	1206.59	24319.19	23710.25	2391.13	2844.65	264.65	372.34
2011	13523.86	1382.21	24691.43	22747.18	2378.18	2974.38	274.36	375.22
2012	13515.85	1417.75	25339.69	21956.53	2362.91	3024.53	283.55	378.07
2013	13516.34	1417.80	25325.39	21951.39	2363.00	3026.04	284.34	379.12

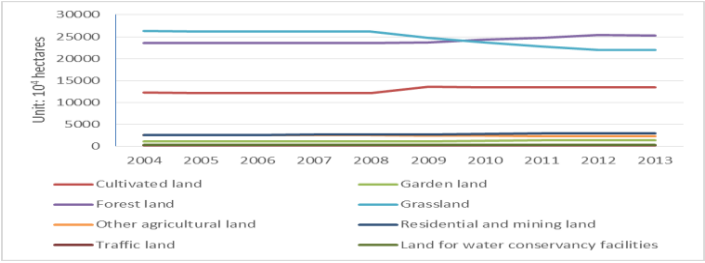

Fig. 1: Changes of land use during 2004-2013

(1) General situation of land use. The area of construction land was obviously less than that of agricultural land, and the main types of agricultural land were grassland, forest land and cultivated land.

(2) The situation of land use change. The overall change of land use is agricultural land. Although the area of construction is increasing because of urbanization, advance of all kinds of infrastructure construction and improvement of the level of industrialization, it increases marginally. The change of construction land is less than agricultural land. The amount of grassland begun to reduce significantly from 2009, while forest

land and cultivated land increased gradually, the reason for this was that Chinese government implemented the policy of "conservation intensive land use and stick to the red line of 1.8 billion mu cultivated land".

3.2. Analysis of land use carbon emissions in China from 2004 to 2013

3.2.1. Analysis of total carbon emissions and carbon sequestration

The carbon emissions, carbon sequestration and net carbon emissions of land use are shown in Table 7

Table 7 The carbon emissions, carbon sequestration and net carbon emissions of land use in China from 2004 to 2013

Year	Carbon emissions /10^4t		Carbon sequestration /10^4t					Net carbon emissions /10^4t
	Cultivated land	Construction land	Cultivated land	Garden land	Forest land	Grassland	Urban green space	
2004	7422.80	110500.37	63470.76	8240.09	13562.21	551.68	3100.26	28998.16
2005	7636.68	117373.25	64752.17	8430.77	13602.26	550.50	3436.57	34237.66
2006	7884.93	123133.43	68139.34	8627.29	13624.20	550.06	3496.52	36580.96
2007	8151.55	129981.25	69890.64	8623.56	13623.97	549.92	4268.96	41175.75
2008	8387.08	133890.23	74381.68	8614.00	13621.05	549.78	4618.83	40491.98
2009	8616.88	140106.82	73510.22	8214.03	13701.63	518.44	4831.38	47948.00
2010	8863.65	145135.58	74654.89	8808.11	14032.17	497.92	4889.66	51116.49
2011	9107.57	150671.30	78157.14	10090.13	14246.96	477.69	5143.48	51663.48
2012	9307.65	150604.99	81326.20	10349.58	14621.00	461.09	5406.12	47748.65
2013	9456.47	152113.24	82918.21	10349.94	14612.75	460.98	5696.90	47530.93

In general, the total amount of carbon emissions and carbon sequestration in China showed an increasing trend and the amount of carbon emissions are always higher than carbon sequestration from 2004 to 2013. Since 2010, the growth rate of carbon emission is lower than that of carbon sequestration (as shown in Fig. 2). The increase of carbon emissions is closely related to the rapid development of urbanization, industrialization and land conversion [14].

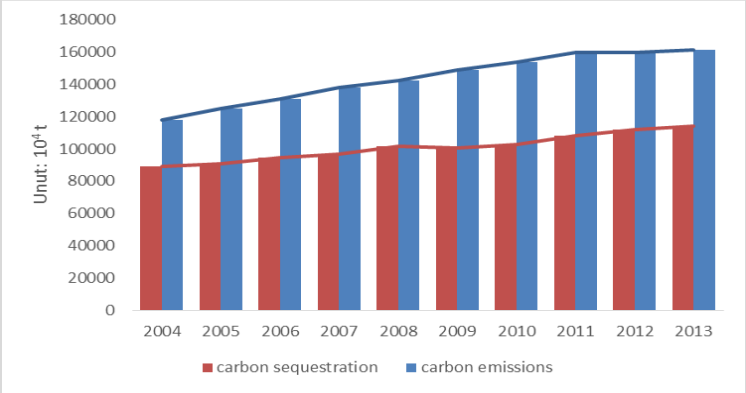

Fig. 2: The change of carbon emissions and carbon sequestration on land use in China from 2004 to 2013

3.2.2. Analysis of carbon emissions and carbon sequestration structure

Table 8: The carbon emissions from agricultural land in China from 2004 to 2013

Year	Agricultural machinery /10^4t	Agricultural irrigation /10^4t	Fertilizers /10^4t	Agricultural films /10^4t	Pesticides /10^4t	Total/10^4t
2004	264.43	1451.74	4152.52	870.23	683.88	7422.80
2005	268.40	1466.42	4268.63	912.88	720.35	7636.68
2006	271.67	1485.64	4413.24	955.96	758.42	7884.93
2007	266.54	1506.10	4574.57	1003.61	800.72	8151.55
2008	272.16	1558.15	4692.07	1039.59	825.11	8387.08
2009	276.99	1579.20	4840.18	1077.28	843.24	8616.88
2010	281.33	1608.15	4981.04	1125.61	867.52	8863.65
2011	284.87	1643.69	5108.71	1188.57	881.72	9107.57
2012	287.61	1665.25	5229.27	1234.40	891.13	9307.65
2013	289.84	1691.44	5294.67	1291.47	889.06	9456.47

Analysis of carbon emissions structure. The carbon emission sources for land mainly include agricultural land and construction land, and the carbon emissions from construction land take a large part. The carbon emissions of agricultural land mainly come from the use of fertilizers, agricultural irrigation, the use of agricultural films, pesticides and agricultural machinery. And the amount of carbon emissions from fertilizers take the large part, accounted for 56%. the second large one is agricultural irrigation, accounted for 19%. The amount of carbon emissions from agricultural land is shown in Table 8.

Construction land is the main source of land carbon emissions, including carbon emissions from industrial land, transportation land, commercial land, residential land and carbon emissions from human respiration. Carbon emissions from industrial land and human respiration accounted for the main part of construction land carbon emissions. The amount of carbon emissions from construction land are shown in Table 9.

Table 9: The amount of carbon emissions from construction land in China

Year	Industry/10^4t	Traffic/10^4t	Commercial/10^4t	Living/10^4t	Human respiration /10^4t	Total/10^4t
2004	51011.09	6206.38	1988.17	8593.67	42701.06	110500.37
2005	56673.30	6707.69	2167.20	8871.71	42953.35	117373.25
2006	61239.44	7284.13	2308.06	9121.13	43180.67	123133.43
2007	67130.18	7734.65	2462.10	9249.94	43404.38	129981.25
2008	70712.93	8181.64	2524.30	8845.91	43625.46	133890.23
2009	76374.36	8238.33	2658.03	8989.90	43846.21	140106.82
2010	79992.74	9025.92	2690.15	9374.92	44051.85	145135.58
2011	83858.92	9779.86	2998.38	9773.69	44260.45	150671.30
2012	82206.62	10700.76	3169.47	10047.92	44480.21	150604.99
2013	82278.05	11357.85	3341.13	10436.55	44699.65	152113.24

Analysis of carbon sequestration structure. The source of carbon sequestration mainly includes cultivated land, forest land, garden land, grassland and urban green space. Carbon sequestration in China increased year by year, and forest land, crop is an important carbon sink.

The carbon sequestration of land use in China from 2004 to 2013 is shown in Table 10, and the change of that is shown in Fig. 3.

Table 10: The carbon sequestration of land use in China from 2004 to 2013

Year	Cultivated land /10^4t	Forest land /10^4t	Garden land /10^4t	Grassland /10^4t	Urban green space /10^4t	Total/10^4t
2004	63470.76	13562.21	8240.09	551.68	3100.26	88925.02
2005	64752.17	13602.26	8430.77	550.50	3436.57	90772.27
2006	68139.34	13624.20	8627.29	550.06	3496.52	94437.40
2007	69890.64	13623.97	8623.56	549.92	4268.96	96957.06
2008	74381.68	13621.05	8614.00	549.78	4618.83	101785.34
2009	73510.22	13701.63	8214.03	518.44	4831.38	100775.71
2010	74654.89	14032.17	8808.11	497.92	4889.66	102882.74
2011	78157.14	14246.96	10090.13	477.69	5143.48	108115.39
2012	81326.20	14621.00	10349.58	461.09	5406.12	112163.99
2013	82918.21	14612.75	10349.94	460.98	5696.90	114038.77

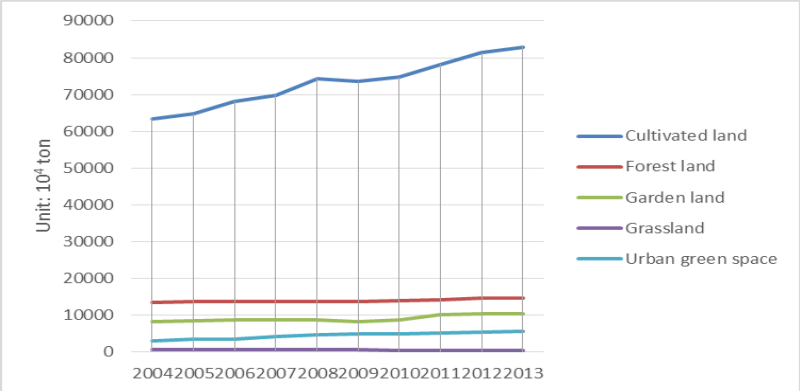

Fig. 3: The change of carbon sequestration of land use in China from 2004 to 2013

3.2.3. Analysis of carbon emission intensity

Ratio between carbon source and carbon sinks. The ratio between carbon source and carbon sinks of land use can intuitively reflect carbon emissions and carbon sequestration of land and has an important value on land use for low-carbon. The ratio between carbon source and carbon sinks is increasing during the year of 2004 to 2010 and it begun to reduce after 2010 (shown in Table 11), it indicates that the relevant measures to protect the ecological environment of land have been effective.

Per capita and per hectare carbon emissions. The carbon emission intensity of per capita and per hectare is increasing gradually during the year of 2004 to 2013, and the reason is mainly because urbanization and industrialization is accelerating, and the carbon emission intensity of construction land has increased.

Table 11: Analysis of carbon emission intensity in China from 2004 to 2013

Year	Ratio between carbon source and carbon sinks	Per capita carbon emissions （t/capita）	Per hectare construction land carbon emissions.（t/hm^2）	Per hectare carbon emissions.（t/hm^2）
2004	1.33	0.91	37.38	1.23
2005	1.38	0.96	39.16	1.30
2006	1.39	1.00	40.48	1.36
2007	1.43	1.05	42.22	1.44
2008	1.40	1.07	43.03	1.48
2009	1.48	1.12	44.55	1.55
2010	1.50	1.15	44.23	1.60
2011	1.48	1.19	44.09	1.66
2012	1.43	1.18	43.38	1.67
2013	1.42	1.19	43.79	1.68

3.3. Effects of land use change on carbon emissions

3.3.1. Analysis on mechanism of the impact of land use changing on carbon emissions

The role of different land use patterns is different in the effects of production, living and ecology, so the process of carbon emissions is different significantly [15], land use change has a significant impact on carbon emissions. The impacts of land use change on carbon emissions include direct and indirect ones. The direct impact is that carbon emissions and carbon sequestration are different in different patterns of land use, and the mutual conversion between different types of land will directly affect the carbon emission of land, also affect soil respiration rate. The indirect impact is that the ways of production, living and energy consumption are different between different land use patterns, so the carbon emissions caused by human are different significantly. Land use change will increase or decrease the demand for some kind of energy consumption and change the combination mode of energy consumption in different type of land, then change the carbon emissions intensity and structure of land use [16].

3.3.2. Analysis of carbon emission effects of land use change

Great changes have taken place in patterns of land use in China because of the accelerating urbanization and industrialization process during the year of 2004 to 2013. Construction land is the main carbon source and owns the largest proportion of carbon emissions, cultivated land is the second largest carbon source. Crops on the cultivated land is the most important carbon sink, followed by forest land, garden land and urban green space. The carbon sequestration capacity of grassland is very small. Cultivated land and forest land increased a large area, so that the amount of carbon sequestration also increased. Because of a substantial increase in energy consumption from construction land , the increase of carbon source far greater than that of carbon sinks, which makes carbon emissions are still higher than the amount of carbon absorbed. From the point of land use type, the increase of 1 hectares of cultivated land, 1.6 tons of carbon emissions increase, while 1 hectares increasing of construction land, carbon emissions increased by 77.9 tons, which indicates that construction land owns the strongest capacity for carbon emissions. The amount of carbon sequestration increased by 15.9 tons for each increase of 1 hectares of cultivated land and forest land, only 20.41% of carbon emissions increasing from construction land. The amount of carbon emissions increasing from construction land is the main reason for the increasing of carbon emissions in China.

4. Conclusion and Suggestion

4.1. Conclusion

Construction land is the main carbon source, cultivated and forest land are the main carbon sink. The trend on change of the carbon emissions in China was increasing from 2004 to 2013. The reason construction became the main carbon source was the increasing of energy consumption, and cultivated land became the second largest carbon source because the use of fertilizers, agricultural irrigation, agricultural films, pesticides and agricultural machinery. Carbon fixation through crops and forest land are the main patterns for carbon sequestration in China, which plays a leading role in reducing carbon in the atmosphere.

Carbon emission reduction efforts still need to be strengthened. Although the ratio between carbon source and carbon sinks begun to reduce after 2010, the lowering range was small，while per capita and per hectare carbon emissions were in the situation of increasing, which indicated that relevant policies formulated by the Chinese government had a certain role in promoting reducing carbon emissions but not obvious, carbon emission reduction efforts still need to be strengthened.

Providing guidance for low carbon optimization of land use structure. According to the research of this paper, different land use patterns have different carbon effects, and the research on carbon emission effects of different land use patterns is of great significance to the optimization of land use structure.

4.2. Suggestion

Explore low carbon utilization mode of land. The amount of land use carbon emissions is significantly greater than that of carbon sequestration, therefore, it is needed to explore low carbon utilization mode of land. It should be efforts to control construction land and cultivated land carbon emissions, improve energy efficiency, reduce the use of fertilizer, expand the area of forest land.

Develop low carbon utilization technology of land. Developing new technologies to reduce energy consumption in the process of cultivated and construction land use, and control carbon emissions.

Carry out the evaluation of low carbon utilization of land. Construction land is the main carbon source of land use carbon emission. If we need to control the construction of carbon emissions, we need to improve the threshold of construction land approval, add more carbon emission index assesses of construction land supply and carry out the evaluation of low carbon use of land.

Implement the regulation policy on low carbon land use. There are two methods to implement the regulation policy on low carbon land use: administrative and economic regulation. To be more specific, the government can levy a certain carbon tax to construction land developer through administrative means, and then these funds can be used to reward the users who have increased carbon sink. The government also can give a certain carbon emission quota for all kinds of construction land. The right of carbon emissions for land use can be traded through market mechanism. The government should also guide the low carbon land use through offering preferential policies, credit policies to developers for low carbon development.

5. Acknowledgements

The research was financed by 12th Five-Year Plan of National Science and Technology Support Program of China (NO.: 2014BAL04B03-3).

6. References

[1] Rongqin Zhao, xianjin Huang, et al. Carbon effect evaluation and low-carbon optimization of regional land use. *Transactions of the Chinese Society of Agricultural Engineering*, 2013, 29(17): 220-228.

[2] Zhiqiang Gao, et al. Effects of land use and climate change on ecosystem productivity and carbon cycle in the transition zone of agriculture and animal husbandry. *SCIENCE CHINA Earth Sciences*, 2004, 34 (10): 946-957.

[3] Houghton R A. The annual net flux of carbon to the atmosphere from changes in land use 1850-1990. *Tellus Series B-Chemical and Physical Meteorology*, 1999, 51(2): 298-313.

[4] Houghton R A, Hackler J L. Sources and sinks of carbon from land-use change in China. *Global Biogeochemical Cycles*, 2003, 17(2): 1034-1047

[5] Kongqing Li. Evaluation and Structural Optimization of Low-carbon Economy-Oriented Regional Land-use. *Huazhong Agricultural University*, 2013.

[6] Rongqin Zhao. *Theoretical and Empirical Research on Regional Carbon Budget Accounting.* Science Press, 2015.

[7] T.O. West, G. Marland. A Synthesis of carbon sequestration, carbon emissions and net carbon flux in agriculture: comparing tillage practices in the United States. *Agriculture Ecosystems & Environment*, 2002, 91: 217-232.

[8] Ying Li, Xianjin Huang, Feng Zhen. Effects of land use patterns on carbon emission in Jiangsu Province. *Transactions of The Chinese Society of Agricultural Engineering*, 2008(24): 102-106.

[9] Guoquan Xu, ZeYuan Liu, ZhaoHua ,Jiang. Decomposition Model and Empirical Study of Carbon Emissions for China, 1995-2004[J]. *China Population Resources and Environment*, 2006, 16(6): 158-161.

[10] Kerang Li. *Land use change and net greenhouse gas emissions and terrestrial ecosystem carbon cycle.* Meteorological Press, 2002.

[11] Xiulan Wang. *Carbon dioxide, climate change and agriculture*. Meteorological Press, 1996.

[12] He Sun, Hongmei Liang, et al. Land use patterns on carbon emission and spatial association in China. *Economic Geography*, 2015, 35(3): 154-162.

[13] Jingyun Fang, Zhaodi Guo, Shilong Piao, et al. Estimation of carbon sink of terrestrial vegetation in China during 1981~2000. *SCIENCE CHINA*, 2007, 37(6): 804-812.

[14] Tingting Zhou. Study on the relationship between land use and carbon emission in China. *Journal of Anhui Agri. Sci.* 2012, 40 (2): 1175-1177.

[15] Rongqin Zhao. *Study on the carbon cycle and land regulation of urban system*. Nanjing University Press, 2012.

[16] Rongqin Zhao, Xianjin Huang, Ying Liu, Minglei Ding. Mechanism and policy framework for land regulation of carbon cycle of regional system. *China Population Resources and Environment*, 2014, 24(5): 51-56.

International Proceedings of Chemical, Biological and Environmental Engineering
Volume 94 of IPCBEE (2016)
DOI: 10.7763/IPCBEE. 2016. V94. 5

Human Health Risk Assessment of Pesticide Residues in Field Grown Yellow Peppers

Raluca Maria Hlihor [1+], Manuela Olga Pogăcean [2], Brîndușa Mihaela Robu Sluser[1] and Maria Gavrilescu [1, 3]

[1] Gheorghe Asachi Technical University of Iasi, Faculty of Chemical Engineering and Environmental Protection, Department of Environmental Engineering and Management, 73 Prof. Dr. Docent D. Mangeron, Iasi, 700050, Romania

[2] Phytosanitary Office Mureş, 80 Dezrobirii Street, T âgu Mureş, Romania

[3] Academy of Romanian Scientists, 54 Splaiul Independentei, RO-050094, Bucharest, Romania

Abstract. A field survey was carried out considering the application of 13 pesticides in normal and double doses on field grown yellow peppers, within the Phytosanitary Office Mureş (Romania). Seven fungicides (based on chlorothalonil, captan, folpet, tebuconazole, triadimenol, myclobutanil and metalaxyl-M), five insecticides (based on deltamethrin, alfa-cypermethrin, lambda-cyhalothrin, chlorpyrifos, biphenthrin) and one acaricide (based on propargite) were applied in three treatments considering the phenological growth stages of yellow peppers. The aim of our study was to assess the health risks associated with pesticides residues by yellow peppers consumption for both adults and children. Based on fruits consumption estimates released in 2015 for 2013, of 188.60 g/capita/day in EU-28, the human health risk assessment revealed that pesticides chlorothalonil and propargite can pose a threat to children health when applied in double doses. Health risks for both adults and children after consumption of yellow peppers treated with pesticides applied in normal dose may be considered negligible.

Keywords: Human Health Risk Assessment, Hazard Index, Maximum Residue Levels, Fruit Consumption, Pesticides

1. Introduction

The application of pesticides in current agricultural practices has lead to serious impacts to human health and the environment. Although, in the effort to prevent and control pests or eliminate yield losses and maintaining high quality products, the use of pesticides is strictly regulated, serious concerns are raised for human exposure to residues from fruits and vegetables [1, 2]. Fruits and vegetables are considered very important components of the human diet. The intake of 5 or more servings per day is considered essential for a good health and it is encouraged for vitamin deficiency prevention and also different diseases such as cancer or obesity [3]. Reports considering monitoring programs of pesticides residues in fruit and vegetable products in Europe, USA and Canada, have shown that most samples (including also fresh and processed foods), have amounts of residues between 6.7 and 58% [4]. Well-known effects of pesticides such as chronic neurotoxicity, endocrine disruption, immune impacts, genotoxicity, mutagenicity and carcinogenesis have been increasing public concern for food safety [4, 5]. Consequently, pesticides contamination of fruits, vegetables and grains has become a health issue across the entire world [6]. To meet the high request for fruits and vegetables, worldwide farmers apply large quantities of pesticides not only to prevent pests and diseases but also to boost their production, with continuous growth of the environmental impact and health risk consequences [7-10].

+ Corresponding author. Tel.: +40 - 232 278683 / int. 2136/2137.
E-mail address: raluca.hlihor@ch.tuiasi.ro; rallu_ca@yahoo.com; mgav@tuiasi.ro

In Europe and across the world, peppers are much appreciated. Pepper crops are attacked by a number of diseases and pests which can lead to great loss of production when pesticides are not used. Chemical protection of peppers is usually carried out by performing 2 or 3 treatments with different types of pesticides. Constant use of pesticides increases the possibility of finding multiple residues of these compounds in peppers, beyond the Maximum Residue Levels (MRLs), creating a significant risk to human health [11].

With respect to the above mentioned information, our primary objective was to assess the human health risk associated with the consumption of yellow peppers at harvest for which three treatments with 13 pesticides were applied in normal and double doses. We have considered both adults and children, as exposed population in the human health risk evaluation.

2. Materials and Methods

2.1. Reagents and analysis

Analytical standards were purchased from Chem Service (West Chester, SUA) and Sigma Aldrich Laborchemikalien GmbH (Seelze, Germany) with certified purity between 95.1% and 99.7%, while Dafcochim SRL (Tg. Mureş, Romania) and Chemark Rom SRL (Tg. Mureş, Romania) were the providers for pesticides applied in the field survey. The pesticide residues were analyzed by a gas chromatograph (Agilent 7890 type with 2 ovens) coupled with a mass spectrometer with flight time, CG*GC-TOF-MS Pegasus 4.21 (LECO, SUA). The working conditions were considered as presented by Pogăcean et al. [12, 13].

2.2. Field survey

In the field survey developed at the Phytosanitary Office Mureş (Romania), the yellow pepper plants were transplanted to the field in late April 2013, in two rows, considering 0.8 m wide and 0.14 m distance between plants on the same row. We considered two types of experiments, and we applied a total of 3 treatments for each survey based on the normal recommended dose (ND) and on the double dose (DD). Treatments were carried out at 2 weeks time interval, from the moment of the first group of yellow peppers appearance and up to 80% of typical yellow peppers (fully ripe). We have ensured a buffer zone between the yellow peppers subjected to the experiments. The sprays with pesticides solution were carried out using a 1.5 L pump, in sunny days, without wind, in the morning, in compliance with Good Agricultural Practices (GAP). We used solutions containing seven fungicides (chlorothalonil, captan, folpet, tebuconazole, triadimenol, myclobutanil, metalaxyl-M), five insecticides (deltamethrin, alfa-cypermethrin, lambda-cyhalothrin, chlorpyrifos, biphenthrin) and one acaricide (propargite). Pesticides treatments were applied according to yellow peppers phenological growth phases considering the BBCH scale (Biologische Bundesanstalt, Bundessortenamt and CHemical industry) [14, 15], as shown in Table 1.

Table 1: Phenological growth stages of yellow peppers.

No	BBCH scale	Fruit description	Time between treatments
1	701-702	Fruits with typical dimension	14 days
2	801-802	10% of fruits show typical size and color of a fully ripe fruit	14 days
3	807-808	80% of fruits show typical size and color of a fully ripe fruit	14 days
4	909	At harvest	25 days (from the last treatment)

2.3. Human health risk assessment

The human health risk was evaluated based on the concentration of pesticides residues in yellow peppers at harvest. The estimated lifetime exposure dose (mg/kg/day), food consumption (kg/person/day) and body weight (kg) were used to determine if there are any health risks to consumers posed by pesticide residues in yellow peppers. Based on latest edition of "Freshfel Consumption Monitor" in the EU-28 released in 2015, per capita fruit consumption in 2013 was estimated at 188.60 g/capita/day [16], while the average body weight of adults in Europe was estimated at 70.8 kg [17] and at 23.1 kg for children (age group, 3 to < 10 years) [18]. Based on food consumption rate for fruits in Europe, the estimated lifetime exposure dose (mg/kg/day) was calculated as indicated by Pogăcean et al. [13] and Bempah et al. [19]. The hazard indices

(HI) for adults and children were assessed based on the ratio between estimated pesticide exposure doses and the corresponding Reference Doses (RfDs) [20] or the analogous Acceptable Daily Intake (ADI) values, when RfDs were not available.

3. Results and Discussion

The field survey indicated that there are significant differences between the MRL and the final concentration of pesticides in yellow pepper samples. Food containing pesticide residues in higher levels than MRLs values can still be considered safe for consumption since the MRLs are always set far below levels considered to be safe for humans. Safety limits are evaluated by analogy with RfDs or ADI values [3].

The results indicated in Table 2 show that the only pesticide residues in yellow peppers at harvest, that are in conformity with European Union rules, by not exceeding the MRLs are: deltamethrin, alfa-cypermethrin and triadimenol. On the other side, pesticides myclobutanil and biphenthrin do not exceed the MRLs only when applied in normal dose. The other pesticides considered in our field survey exceed the MRLs, considering both types of treatments (ND and DD treatments). These findings have raised our concerns when it comes to human exposure to higher levels of pesticides than the acceptable limits set by European Union. By consuming yellow peppers treated with pesticides of which concentrations at harvest exceed the MRLs, the vulnerable population such as children may face exposure risks. These findings lead to our study fundamental objective: assessing the risk posed by consumption of yellow peppers treated with pesticides applied in normal and double doses, by adults and children.

Table 2: Pesticides concentration (mg/kg) in yellow peppers samples after treatments applied in normal dose (ND) and double dose (DD) according to BBCH scale.

Pesticides	BBCH scale								MRL (mg/kg)
	701-702		801-802		807-808		909		
	ND	DD	ND	DD	ND	DD	ND	DD	
Chlorothalonil	1.14	1.75	1.25	3.31	2.75	4.15	1.32	2.28	0.01*
Deltamethrin	0.1	0.18	0.15	0.29	0.11	0.38	0.08	0.12	0.2
Myclobutanil	0.3	0.45	0.22	0.36	0.45	0.8	0.21	0.54	0.5
Alfa-cypermethrin	0.31	0.62	0.22	0.47	0.389	0.55	0.12	0.32	0.5
Biphenthrin	0.301	0.5	0.34	0.76	0.44	0.88	0.34	0.79	0.5
Captan	0.8	2.07	0.96	1.96	1.02	3.73	0.43	1.27	0.1
Folpet	0.7	2.58	1.96	3.57	2.75	4.18	1.83	2.01	0.02*
Tebuconazole	0.69	2.01	0.65	1.02	0.82	2.72	0.62	1.41	0.6
Triadimenol	0.09	0.29	0.21	0.36	0.17	0.47	0.09	0.12	1
Metalaxyl-M	1.18	2.18	0.88	1.86	1.22	2.74	0.65	1.55	0.5
Chlorpyrifos	0.45	0.75	0.5	0.69	0.85	1.62	0.52	1.35	0.5
Lambda-cyhalothrin	0.47	0.61	0.09	0.29	0.17	0.48	0.09	0.14	0.01
Propargite	1.38	3.16	2.02	4.96	2.63	3.11	1.62	2.82	0.01*

MRL - Maximum Residue Level set by European Union legislation [21]

* *= Limit of determination*

In our study, the U.S Environmental Protection Agency's guidelines for human health risk assessment have been taken into consideration. Therefore, we considered that the maximum absorption rate and the bioavailability rate are 100% [22]. The lifetime exposure dose was calculated for pesticides residues in yellow peppers at harvest considering the two types of experiments developed (for pesticides applied in both ND and DD). A comparison of lifetime exposure dose for the exposed population, both adults and children, with the RfDs is available in Table 3. When comparing the lifetime exposure dose with the available RfDs, it can be observed that chlorothalonil and propargite are the only pesticides that exceed the RfD values, if applied in double doses and when children are considered as exposed population. For the rest of 11 pesticides, the lifetime exposure dose value is under the value of RfD, although simultaneous exposure to multiple pesticides can lead to toxicological effects for both adults and children health.

The next step in our evaluation was to assess the health risk by considering the HI for adults and children. A concern can also be raised by considering the values of HI, as seen from Figs. 1 and 2. If HI is higher than 1, the pesticide residues in yellow peppers can be considered a risk to consumers, while for a HI lower than 1,

the pesticide residues are considered to be in an acceptable limit with no risk to human health [12, 13, 23]. When treatments with pesticides were applied in normal doses (Fig. 1) the HI do not exceed the value 1, so it can be considered that there are no risks involved for adults and children. The values of HI higher than 1 in the case of pesticides chlorothalonil and propargite, when applied in double doses (Fig. 2) indicate a risk to children health associated with the consumption of yellow peppers. Since children consume more calories of food per unit of body weight compared adults, their exposure to pesticide residues in foods is higher.

Table 3: Lifetime exposure dose calculated for pesticides residues in yellow peppers at harvest.

Pesticide	Reference dose (mg/kg-day)	Lifetime exposure dose (mg/kg/day)			
		ND		DD	
		Adults	Children	Adults	Children
Chlorothalonil	0.015	0.0035	0.0107	0.0060	0.0186
Deltamethrin	0.01*	0.0002	0.0006	0.0003	0.0009
Myclobutanil	0.31*	0.0005	0.0017	0.0014	0.0044
Alfa-cypermethrin	0.1	0.0003	0.0009	0.0008	0.0026
Biphenthrin	0.015	0.0009	0.0027	0.0021	0.0064
Captan	0.13	0.0011	0.0035	0.0033	0.0103
Folpet	0.1	0.0048	0.0149	0.0053	0.0164
Tebuconazole	0.03*	0.0016	0.0050	0.0037	0.0115
Triadimenol	0.05*	0.0002	0.0007	0.0003	0.0009
Metalaxyl-M	0.06	0.0017	0.0053	0.0041	0.0126
Chlorpyrifos	0.1*	0.0013	0.0042	0.0035	0.0110
Lambda-cyhalothrin	0.005	0.0002	0.0007	0.0003	0.0011
Propargite	0.02	0.0043	0.0132	0.0075	0.0230

*ADI

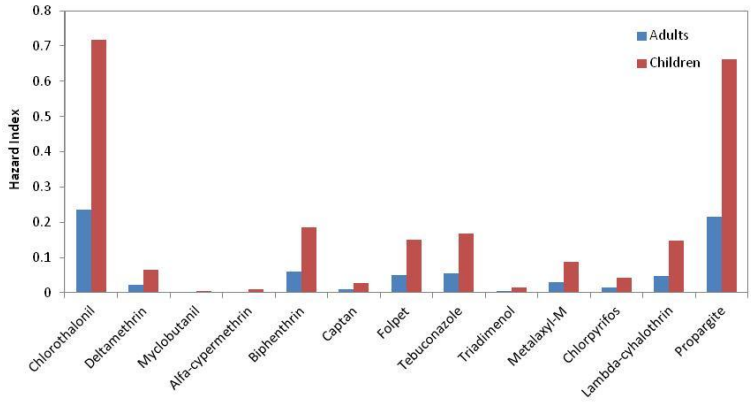

Fig. 1: Hazard Index calculated for pesticides residues in yellow peppers at harvest considering the ND treatments.

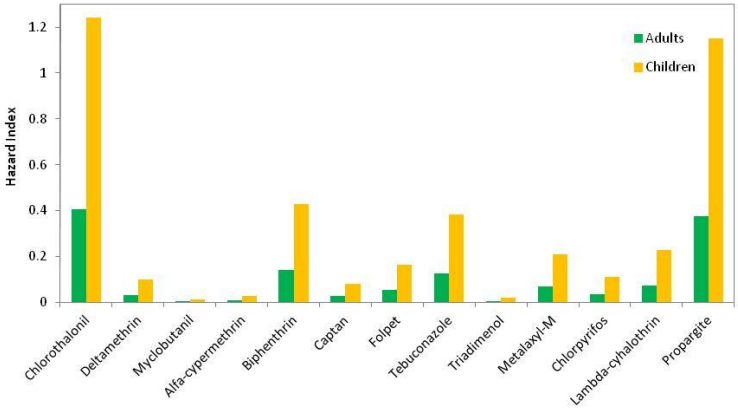

Fig. 2: Hazard Index calculated for pesticides residues in yellow peppers at harvest considering the DD treatments.

4. Conclusions

A number of 13 pesticides were applied in normal dose (recommended) and double dose treatments on field grown yellow peppers. Three treatments with pesticides were considered according to BBCH phonological growth stages of yellow peppers. Our findings have shown that although most of the pesticides residues in yellow peppers exceed the MRLs at harvest, only chlorothalonil and propargite are a threat to children health, if applied in double doses. The lifetime exposure dose which exceeds the RfDs, and the Hazard Index >1 for chlorothalonil and propargite applied in double dose also sustain these findings. Potential consumer risks should be taken into account, since continuous consumption of fruits and vegetables containing pesticides residues could result in higher toxicity, leading to deadly chronic effects.

5. Acknowledgements

This paper was elaborated with the support of a grant of the Romanian National Authority for Scientific Research, CNCS – UEFISCDI, project number PN-II-ID-PCE-2011-3-0559", Contract 265/2011 and with the support of Phytosanitary Office Mureş, Romania.

6. References

[1] C.A. Damalas and I.G. Eleftherohorinos. Pesticide Exposure, Safety Issues, and Risk Assessment Indicators. *Int. J. Environ. Res. Public Health* 2011, 8 (5): 1402-1419.

[2] M.O. Pogăcean and M. Gavrilescu. Plant protection products and their sustainable and environmentally friendly use. *Environ. Eng. Manag. J.* 2014, 8 (3): 607-627.

[3] B.M. Keikotlhaile and P. Spanoghe. Pesticide residues in fruits and vegetables. In: M. Stoytcheva (Ed.) Pesticides - formulations, effects, fate. InTech 2011, pp. 243-252.

[4] M.A. Dalvie and L. London. Risk assessment of pesticide residues in South African raw wheat. *Crop Protection* 2009, 28 (10): 864–869.

[5] S. Wanwimolruk, O. Kanchanamayoon, S. Boonpangrak, and V. Prachayasittikul. Food safety in Thailand 1: it is safe to eat watermelon and durian in Thailand. *Environ. Health. Prev. Med.* 2015, 20 (3): 204–215.

[6] Y. Latif, S.T.H. Sherazi, and M.I. Bhanger. Monitoring of pesticide residues in commonly used fruits in Hyderabad Region, Pakistan. *American Journal of Analytical Chemistry* 2011, 2: 46-52.

[7] C.K. Bempah and A.K. Donkor. Pesticide residues in fruits at the market level in Accra Metropolis, Ghana, a preliminary study. *Environ. Monit. Assess.* 2011, 175 (1-4): 551–561.

[8] K.R. Everett, I.P.S. Pushparajah, J.T. Taylor, O.E. Timudo-Torrevilla, T.M. Spiers, A.A. Chee, P.W. Shaw, and D.R. Wallis. Evaluation of fungicides for control of bitter and sprinkler rots on apple fruit. *New Zealand Plant Protection* 2015, 68: 264-274.

[9] B. Robu, O. Jitar, C. Teodosiu, S.-A. Strungaru, M. Nicoara, and G. Plavan. Environmental impact and risk assessment of the main pollution sources from the Romanian Black Sea coast. *Environ. Eng. Manag. J.* 2015, 14 (2): 331-340.

[10] H. Wei, Z. Le, L. Shuxian, W. Dan, L. Xiaojun, J. Lan, and M. Xiping. Health risk assessment of heavy metals and polycyclicaromatic hydrocarbons in soil at coke oven gas plants. *Environ. Eng. Manag. J.* 2015, 14 (2):487-496.

[11] M. O. Pogăcean. *Studies on accumulation of some pesticides in vegetable products*. PhD thesis, Gheorghe Asachi Technical University of Iasi, Romania, 2013.

[12] M. O. Pogăcean, R. M. Hlihor, C. Preda, and M. Gavrilescu. Humans in the environment: Comparative analysis and assessment of pesticide residues from field-grown tomatoes. *Eur. J. Sci. Theol.* 2013 9 (6): 79-95.

[13] M. O. Pogăcean, R. M. Hlihor, and M. Gavrilescu. Monitoring pesticides degradation in apple fruits and potential effects of residues on human health. *J. Environ. Eng. Landsc.* 2014 22 (3):171-182.

[14] D. Gericke, J. Nekovar, and C. Hörold. Estimation of plant protection product application dates for environmental fate modeling based on phenological stages of crops. *J. Environ. Sci. Health B.* 2010 45 (7): 639-647.

[15] U. Meier, H. Bleiholder, E. Weber, C. Feller, M. Hess, H. Wicke, T. van den Boom, P.D. Lancashire, L. Buhr, H. Hack, R. Klose, and R. Stauss. *BBCH Monograph - Growth stages of mono-and dicotyledonous plants, 2nd Edition*. Uwe Federal Biological Research Centre for Agriculture and Forestry, 2001.

[16] FRESHFEL. *Freshfel Consumption Monitor* [online] 2015. Available from Internet: http://www.freshfel.org/docs/2015/Press_Releases/20150610_-_Consumption_Monitor.pdf.

[17] S. C. Walpole, D. Prieto-Merino, P. Edwards, J. Cleland, G. Stevens, and I. Roberts. The weight of nations: an estimation of adult human biomass. *BMC Public Health* 2012 12: 439.

[18] EFSA. Guidance on selected default values to be used by the EFSA Scientific Committee, Scientific Panels and Units in the absence of actual measured data. *EFSA Journal* 2012 10 (3): 32 pp.

[19] C. K. Bempah, A. Buah-Kwofie, D. Denutsui, J. Asomaning, and A. O. Tutu. Monitoring of pesticide residues in fruits and vegetables and related health risk assessment in Kumasi Metropolis, Ghana. *Res. J. Environ. Earth Sci.* 2011 3 (6): 761-771.

[20] USEPA. *Integrated Risk Information System (IRIS)* [online] 2015. Available from Internet: http://cfpub.epa.gov/ncea/iris/index.cfm?fuseaction=iris.showSubstanceList.

[21] HSE. *Maximum Residue Level (MRL) Database* [online] 2015. Available from Internet: https://secure.pesticides.gov.uk/MRLs.

[22] USEPA. *Exposure Factors Handbook. 2011 Edition*. National Center for Environmental Assessment Office of Research and Development U.S. Environmental Protection Agency, Washington DC, 2011.

[23] R. M. Hlihor, L .C. Apostol, C. Smaranda, L. V. Pavel, F. A. Căliman, B. M. Robu, and M. Gavrilescu. Bioavailability processes for contaminants in soils and their use in risk assessment. *Environ. Eng. Manag. J.* 2009, 8 (5): 1199-1206.

International Proceedings of Chemical, Biological and Environmental Engineering
Volume 94 of IPCBEE (2016)
DOI: 10.7763/IPCBEE. 2016. V94. 6

Extraction of Nitrophenols Using Pseudo-emulsion Based Hollow Fiber Strip Dispersion

Gedela Ashok Kumar Naidu, Smita Gupta and Mousumi Chakraborty[+]

Department of chemical Engineering, S. V. National Institute of Technology, Surat 395007, Gujarat, India

Abstract. The extraction of nitrophenols from aqueous solutions through a pseudo-emulsion hollow fiber strip dispersion (PEHFSD) system were conducted in a microporous hydrophobic polypropylene hollow fiber membrane contactor. The study had focused on the effects of various parameters, viz., feed and pseudo emulsion phase flow rates, types of carrier and concentration etc. Effect of multiple cycles using the same pseudo-emulsion on nitrophenols extraction was also analyzed. Almost 99% extraction of all three nitrophenols (individually) was achieved at optimum conditions.

Keywords: Nitrophenol Extraction, Pehfsd System, Feed and Pseudo Emulsion Phase Flow Rates, Carrier Concentration.

1. Introduction

Para-nitrophenol (PNP) is an important intermediate in dye and pesticide synthesis. In this role PNP contaminates large amounts of water; water that eventually must be treated or disposed off [1]. It is a typical biorefractory organic compound and considered to be one of the 114 priority toxic pollutants by US Environmental Protection Agency. Nitrophenol is highly toxic and resistant to biological treatment, so it is very important to treat nitrophenol before discharging with waste stream. In degradation methods, nitrophenols are converted into substances that are nontoxic and satisfactory for release to the environment. The main disadvantage of these degradation methods is the high cost because of the large consumption of chemicals (as in chemical degradation) or major investment in land requirement (as in biological treatment).

The liquid membrane process was used for the removal of phenol from wastewater and also for the treatment of formulated and real wastewater containing *o*-nitrophenol (ONP), m-nitrophenol (MNP) and *p*-nitrophenol (PNP) [2,3]. Supported liquid membranes (SLMs) are also very effective for the removal and recovery of nitrophenol from waste waters as they are also associated with simultaneous extraction and stripping [1-4]. In last 5 years, hollow fiber supported liquid membranes (HFSLMs) were used effectively for the separation of various metal ions, phenols, nitrophenols and its derivatives [5-8]. Despite these advantages, three major limitations in applying HFSLM are fouling of suspended or dissolved substances on the surface of the hollow fibers, instability and long-term performance of SLM and HFSLM are the important issue for industrial applications [9]. In view of this, recently, a more stable technique, that is Pseudo-emulsion hollow fiber strip dispersion (PEHFSD) technique, has been developed which utilized the merits of LM techniques and suitable for industrial use.

Till date, no investigations is reported for the removal of nitrophenols through the PEHFSD, so an effort has been made to investigate the behavior of the PEHFSD system for the extraction of p-nitrophenol from aqueous solution using NaOH as stripping solution and Trioctylmethyl ammonium chloride, Tri butyl phosphate and Tri Octyl amine as carriers. The influence of the various process variables, such as feed and pseudo emulsion phase flow rates, types of carrier and concentrations on the transportation of nitrophenol

[+] Corresponding author. Tel.: +00919904003862.
E-mail address: mousumi_chakra@yahoo.com.

molecule in the PEHFSD system have been studied. Extraction of o-nitrophenol and m-nitrophenol are also carried out using same optimum conditions.

2. Experimental

2.1. Materials and method

The chemicals used in the study for the transport of Nitrophenols through PEHFSD were p-Nitrophenol, m-Nitrophenol and o-Nitrophenol (Loba Chemie, Mumbai, India). For the preparation of pseudo-emulsion, n-hexane (Finar chemicals, Ahmedabad, India) of specific gravity 0.6548 g mL^{-1} and viscosity of 0.294 cP, containing carrier like Tri butyl phosphate (TBP) (Otto Kemi, Mumbai, India), Trioctylmethyl ammonium chloride (TOMAC) (Merck, Mumbai, India) and Tri Octyl amine (TOA) (Merck, Mumbai, India) in membrane phase and NaOH (Finar, Ahmedabad, India) in stripping phase were used. 1-Decanol (Otto Kemi, Mumbai, India) to dissolve TOMAC in the n-hexane and sulfuric acid (Merck, India) are used to maintain the pH of the feed phase.

2.2. HFSLM experiments

In order to prepare HFSLM, the preferred organic solvent has been circulated in the tube side of the module for at least 45 min. During this period of time the outlet pressure of the tube side is maintained at 5-10 psi so that the solvent has been passed through the micro pores of the fibers and come out through the shell side of the module. This phenomenon is performed to ensure that the solvent is embedded in the micro pores of the fibers. The excess organic solvent has been removed by circulating distilled water at zero pressure on both sides (i.e. Tube side and shell side) of the membrane. The feed solution and the stripping solution are then pumped counter currently into the tube side and shell side of the HFSLM, respectively, in recycle mode at zero pressure.

2.3. PEHFSD experiments

The PEHFSD process comprises a single membrane contactor for extraction and stripping. One stirred tank is used for preparing and as a reservoir of the pseudo-emulsion containing carrier + n-hexane and NaOH and another stirred tank as a feed phase reservoir. The experimental conditions are shown in Table 1. The hollow fiber device used for the investigation was obtained from membrane: Celgard ® X50-215 [9]

Table 1: Experimental conditions for PEHFSD system.

Pseudo-emulsion phase	Membrane phase + Stripping phase
Membrane phase	n-Hexane
Carrier	Tri butyl phosphate (TBP) (varied from 0.5 to 1.5% w/v)
Stripping phase	NaOH (varied from 0.01 to 1.0 M)
Flow rate of pseudo emulsion through PEHFSD	200 mL/min
Stirring speed in pseudo emulsion tank	700 rpm
Volume of pseudo-emulsion	600 mL
Feed phase Aqueous solution	p-nitrophenol (varied from 25 to 75 mg L^{-1})
Flow rate of feed through PEHFSD	300 mL/min
Stirring speed in feed tank	Maintained at 300-350 rpm
Feed: strip ratio	5:1 (22)
pH (Feed phase)	2.5

The experimental set-up also contained two gear pumps of variable flows for both phases and flowmeters. The organic solution wets the porous wall of the fiber because of its hydrophobic nature. The interface is maintained at the mouth of the pores by applying a higher pressure to the feed side (tube side) than to the pseudo-emulsion side (shell side). The differential pressure should always be kept below the breakthrough pressure. In the present case, the pressure of the feed side is 2.5 psi higher than in the pseudo-emulsion phase. The operation is carried out by passing an acidic aqueous feed containing PNP through the tube side and pseudo-emulsion through the shell side in countercurrent recirculation mode. The feed reservoir tank and the

pseudo-emulsion reservoir tank are stirred to homogenize the solution and to maintain the homogeneity of the pseudo-emulsion respectively. The recovery of PNP from pseudo-emulsion can be accomplished by breaking down the pseudo-emulsion and separating organic and stripping solutions. The recycle mode of a single-module HFSLM operation is shown in Fig. 1.

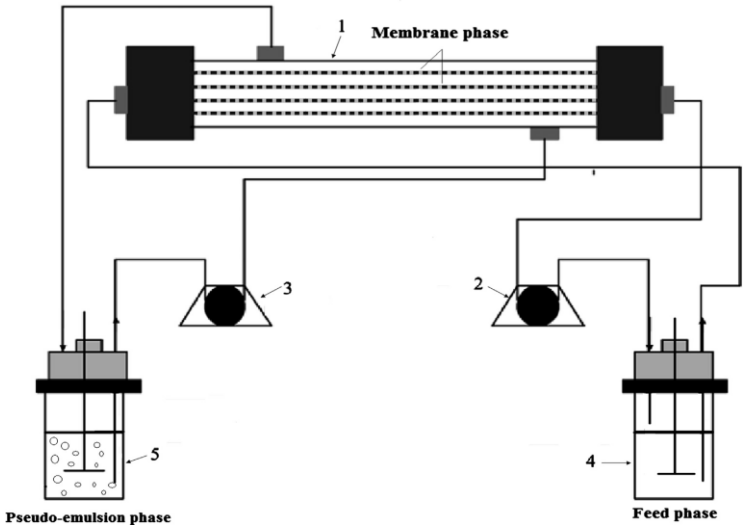

Fig. 1: Schematic view of pseudo-emulsion hollow fiber strip dispersion system operated in recycling mode for p-nitrophenol extraction from aqueous solution: (1) hollow fiber contactor; (2) feed pump; (3) pseudo-emulsion pump; (4) feed reservoir with stirrer; and (5) pseudo-emulsion reservoir with mixing arrangement; volume of feed: 1500 mL, organic phase: 300 mL and stripping phase: 300 mL.

A small volume of the aqueous streams was taken at different time intervals and analyzed for PNP concentration by UV-vis spectrophotometry (HACH make, Germany) at 317 nm wavelength. The percentage extraction of p-nitrophenol through PEHFSD can be evaluated by:

$$\%Extraction\,(Y) = \frac{[PNP]_{f,t=0} - [PNP]_f}{[PNP]_{f,t=0}} \times 100 \tag{1}$$

Reproducibility of the results was checked and found to be satisfactory using three sets of data.

The equations describing the material balance for PEHFSD system would result in the following equation, which shows first-order kinetics:

$$V_f \left(\ln \frac{[PNP]_{f,t=0}}{[PNP]_f} \right) = St \tag{2}$$

where S is the coefficient dependent on the linear velocity of the fluids, the geometry of the fibers and module the overall permeability of the system and V_f Volume of the feed (cm^3). This overall permeability can be obtained for the system running in the recycling mode, from the experimental values of the slope S, as :

$$P_{PNP} = \frac{-Q_f}{2\pi r_i LN} \left[\ln \left(1 - \frac{S}{Q_f} \right) \right] \tag{3}$$

where L, Length of fibre (cm), N number of fiber in module, P permeability coefficient (cm s^{-1}), Q_f total flow rate of feed solution flowing through tube side ($cm^3 s^{-1}$), r_i internal radius of hollow fiber membrane(cm).

3. Results

3.1. Effects of feed and pseudo emulsion phase flow rates of PNP transport

In order to attain effective permeation of PNP in a PEHFSD system, it is necessary to examine the effect of the feed flow and strippant flow on permeability coefficients. For that a series of experiments were

conducted, keeping PNP concentration at 25 ppm in feed phase, the NaOH concentration of 1 M in stripping phase and n-hexane with 0.5% (w/v) TBP as membrane phase to acquire satisfactory hydrodynamic conditions.

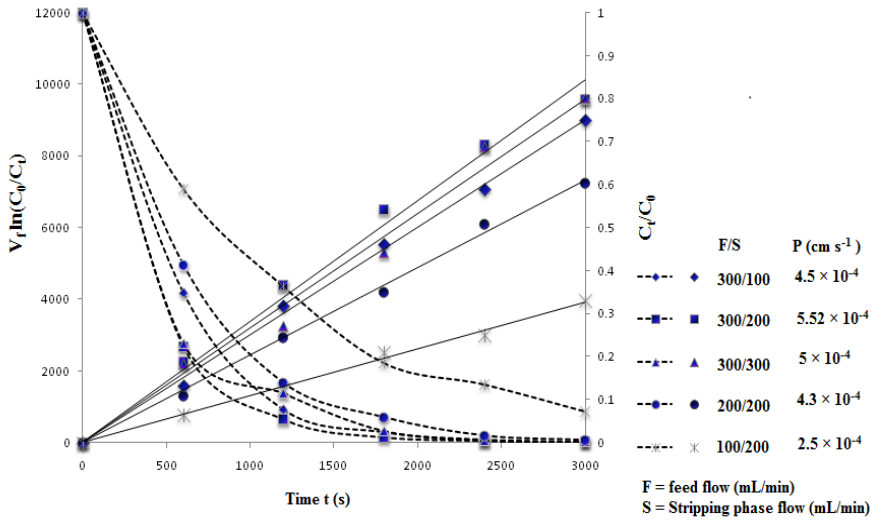

Fig. 2: Effect of feed and pseudo emulsion phase flow rates on the extraction of p-nitrophenol through PEHFSD.

The permeability coefficient was studied as a function of the flow in the feed and strippant solutions. The obtained results are shown in Fig. 2 in terms of permeability coefficient and extraction efficiency, respectively. The increase of the permeability coefficient with the increase of feed flow was due to decrease in the thickness of the aqueous feed boundary layer and aqueous strippant boundary layer, whereas the decrease of P_{PNP} value might be because of lower residence time at higher flow rates, which provided insufficient time for solute to react with the strippant. Agarwal et al. [10] noticed similar result in the recovery of Cu(II) from sulphate solutions using PEHFSD. From Fig. 2, it is observed that permeability coefficient is more dependent on the feed flow as compared to the strippant flow. Thus, 300 cm^3 min^{-1} of feed flow and 200 cm^3 min^{-1} of strippant flow were taken as optimum hydrodynamic conditions for further experiments.

3.2. PEHFSD system versus HFSLM system

To determine the advantages and uses of the pseudo emulsion hollow fiber strip dispersion (PEHFSD) system over the hollow fiber supported liquid membrane (HFSLM) system, the experiments were conducted by keeping PNP concentration at 25 ppm in feed phase, the NaOH concentration of 1 M in stripping phase and n-hexane with 0.5% (w/v) TBP as membrane phase in both of the systems. It was observed that PEHFSD system extracted more p-nitrophenol over the HFSLM system during the 40 min of time span due to stability of the pseudo emulsion membrane. Thus, on the basis of operational stability, PEHFSD is more preferable as compared to HFSLM. Sheng et al. [11] also observed the same result in the recovery of fumaric acid by hollow-fiber supported liquid membrane with strip dispersion using trialkylamine carrier.

3.3. Effect of types of carriers and carrier concentrationon the extraction of PNP

In this series of experiments, three different carriers like TOMAC, TOA and TBP were used in order to choose the right one for the transport of the PNP. The experiments were carried out in PEHFSD by keeping PNP concentration at 25 ppm in feed phase, the NaOH concentration of 1 M in stripping phase and n-hexane with 0.5% (w/v) of the respective carrier in membrane phase. In case of TOMAC, 2.0 % (v/v) of n-decanol was also added in the membrane phase to avoid the formation of third phase. From Fig. 3, it was observed that TBP as a carrier extracted maximum amount of PNP (99% within 40 min) and showed highest permeability (P_{PNP} $\times 10^4$ cm s^{-1} = 5.52) as compared to TOMAC and TOA (0.639 and 0.223).

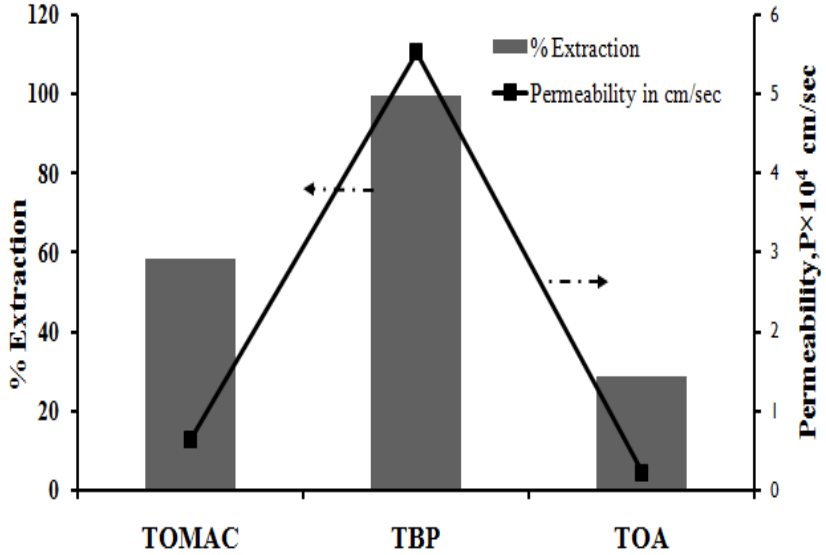

Fig. 3: Effect of carriers on the extraction of p-nitrophenol through PEHFSD.

3.4. Effect of multiple cycles

Multiple operations of the PNP extraction using the same strip solution were conducted under optimum process conditions to increase the concentration of PNP in the strip solution and to examine the availability of the extraction module for cyclic use, which minimizes time and efforts of module cleaning, drying and reassembling. In this experiment, the feed solution was replaced at each cycle of five hours of extraction operation. It was observed that up to four cycles, there was no considerable drop in the PNP transport rate through PEHFSD.

3.5. Facilitated transport of o-nitrophenol and m-nitrophenol through PEHFSD system

So far, the study of extraction of p-nitrophenol through PEHFSD was investigated using tri butyl phosphate as a carrier, n-hexane as an organic solvent and NaOH as a stripping reagent.

Table 2: Facilitated transport of nitrophenols through PEHFSD.

Type of nitrophenol	Organic solvent used	Carrier used	Ratio of feed to strippant flow	Feed concentration in mg/L	Carrier concent-ration % (w/v)	Stripping phase concentration (M)	% Removal of Nitro-phenols
p-nitrophenol	n-hexane	TBP	300/200	25	1.5	1	99.12
o-nitrophenol	n-hexane	TBP	300/200	25	1.5	1	99.41
m-nitrophenol	n-hexane	TBP	300/200	25	1.5	1	99.23

The parameters optimized were feed and pseudo emulsion flow rates, types of carrier and carrier concentration. The facilitated transport of the of the o- and m-nitrophenols through PEHFSD system have been also studied using optimum conditions of all parameters obtained from the above study. The results obtained are tabulated as shown in Table 2.

4. Conclusion

The present study demonstrates the feasibility of the PEHFSD technology for the extraction and recovery of p-nitrophenol from the aqueous solutions employing various carriers such as Tri butyl phosphate (TBP), TOMAC and Tri Octyl amine. Among these, Tri butyl phosphate was found to be the best carrier in the extraction of the p-nitrophenol from the aqueous solutions. Effects of other parameters, viz., feed and pseudo emulsion phase flow rates, carrier concentration etc were also studied. Almost 99% extraction of all three nitrophenols (individually) was achieved at optimum conditions.

6. References

[1] Tompkins CJ, Michaels AS, Peretti SW. Removal of p-nitrophenol from aqueous solutions by membrane supported solvent extraction. J. Membr. Sci. 1992, 75, 277-292.

[2] Luana J, Plaisier A. Study on the treatment of wastewater containing nitrophenol compounds by liquid membrane process. J Membr Sci. 2004; 229: 235-239.

[3] Anitha P, Kavitha N, Palanivelu K. Removal and recovery of p-nitrophenol from aqueous solution using natural solid triglycerides. Desalination. 2011; 272: 196-200.

[4] Venkateswaran P, Palanivelu K. Recovery of phenol from aqueous solution by supported liquid membrane using vegetable oils as liquid membrane. J Hazard Mater. 2006; 131: 146-152.

[5] Peretti SW, Tompkins CJ, Goodall JL, Michaels AS. Extraction of 4-nitrophenol from 1-octanol into aqueous solution in a hollow fiber liquid contactor. J Membr Sci. 2001; 195: 193-202.

[6] Praveen P, Loh KC, Trioctylphosphine oxide-impregnated hollow fiber membranes for the removal of phenol from wastewater. J Membr Sci. 2013; 437: 1-6.

[7] Gonzalez MJ, Luque S, Álvarez JR, Coca J. Recovery of phenol from aqueous solutions using hollow fiber contactors. J Membr Sci. 2003; 213: 181-193.

[8] Gupta S, Chakraborty M, Murthy ZVP. Performance study of hollow fiber supported liquid membrane system for the separation of bisphenol A from aqueous solutions. J Ind Eng Chem. 2014; 20: 2138-2145.

[9] Gupta S, Chakraborty M, Murthy ZVP. Optimization of process parameters for mercury extraction through pseudo-emulsion hollow fiber strip dispersion system. Sep Purif Technol. 2013; 114: 43-52.

[10] Agarwal S, Teresa M, Rosinda M, Ismael C, Joana M, Correia N, Carvalho JMR. Application of pseudo-emulsion based hollow fiber strip dispersion (PEHFSD) for the recovery of copper from sulphate solutions. Sep Purif Technol. 2013; 102: 103-110.

[11] Sheng J, Chena HL, Zhanga L. Recovery of fumaric acid by hollow-fiber supported liquid membrane with strip dispersion using trialkylamine carrier. Sep Purif Technol. 2009; 66: 25-34.

International Proceedings of Chemical, Biological and Environmental Engineering
Volume 94 of IPCBEE (2016)
DOI: 10.7763/IPCBEE. 2016. V94. 7

Scr of No with Nh_3 over Fe_2o_3 Particles at Low Temperature

Xiaobo Wang[1, 2+], Keting Gui[3] and Lin Dong[1, 2]

[1] Key Laboratory of Mesoscopic Chemistry of MOE, School of Chemistry and Chemical Engineering, Nanjing University, Nanjing 210093, Jiangsu, China

[2] Jiangsu Key Laboratory of Vehicle Emissions Control, Center of Modern Analysis, Nanjing University, Nanjing 210093, Jiangsu, China

[3] Key Laboratory of Energy Thermal Conversion and Control of Ministry of Education, School of Energy and Environment, Southeast University, Nanjing 210096, Jiangsu, China

Abstract. Fe_2O_3 particles were used for selective catalytic reduction (SCR) of NO with NH_3 at low-temperature in a fixed bed reactor. Mössbauer spectroscopy and H2-TPR were employed to characterize the Fe_2O_3 particles. It was found that Fe_2O_3 particles showed high activity in a wide temperature range of 150-270℃ and more than 95% of NO conversion could be obtained at 180℃. Moreover, the reaction order was found to be nearly 1, 0 and 0.42 with respect to NO, NH_3 and O_2, respectively. Apparent activation energy was calculated to be 28.8kJ/mol and lower than that for most of the catalysts reported by previous studies.

Keywords: Low-Temperature Scr, Fe_2o_3, Mössbauer Spectroscopy, Kinetics, Apparent Activation Energy

1. Introduction

The selective catalytic reduction (SCR) of NOx by ammonia is one of effective post-treatments for the abatement of nitrogen oxide emissions from stationary sources [1-5]. The general reaction is as follows:

$4NO+4NH_3+O_2 \rightarrow 4NO+6H_2O$

Many catalysts have been reported to be active for the above NO-NH_3-O_2 reaction. The commercial catalysts for this SCR process are based on V_2O_5/TiO_2 mixed with WO_3 or MoO_3. Although the commercial catalysts are highly active and resistant to SO_2, there are also some disadvantages [1-5]. This catalyst shows high activity within a narrow temperature range of 300-400℃ and thus the SCR process is necessary to locate upstream of the desulphurization and particle removal in order to avoid the flue gas reheating. In addition, the formation of the N_2O is another drawback for the vanadium-based catalysts [2]. For the reasons above, there is strong interest to develop highly active SCR catalysts at low temperature. In this way, such a catalyst would show high catalytic activity at low temperature and thus the SCR system can be located downstream of the desulfurizer and the particulate-removal device without gas preheating.

Based on our previous study [6], we found that Fe_2O_3 particles were highly active for low temperature SCR of NO with NH_3 and the external magnetic field could improve low-temperature SCR activity of the Fe_2O_3 particles. Due to the fact that the reaction orders with respect to NO and NH_3 varied with the catalyst and the reaction conditions, it is important to understand the reaction kinetics of the NO-SCR over the catalyst. Consequently, more work should be done for the low-temperature SCR of NO with ammonia with Fe_2O_3 particles.

In this report, the catalytic property of the Fe_2O_3 particles was experimentally studied in a fixed bed. Experiments were also carried out to understand the reaction kinetics of NO-SCR over the Fe_2O_3 particles

+ Corresponding author. Tel.: +86-25-83592290; fax: +86-25-83317761.
E-mail address: winstonwell@126.com.

and calculate the apparent activation energy, which could be used to compare the performance of Fe_2O_3 particles with that of other catalysts at low-temperature.

2. Experimental

2.1. Catalyst preparation

The particulate Fe_2O_3 particles was prepared by the Research Institute of Nanjing Chemistry Industry Group. The typically preparation of Fe_2O_3 particles was as follows: a solution of ammonia (1:1,*V*/*V*) was continuously added into the aqueous solutions of ferric sulfate and ferrous sulfate until the pH of the solution reached 8. After that, the resulting precipitate was washed several times with deionized water and separated by filtration under suction, followed by extrusion molding and evaporation to dryness at 120 ℃. At last, the particles were calcined at 300 ℃ in air for 3hr and collected in the diameters of 35-65 mesh by crushing and sieving. The bulk density of the Fe_2O_3 particles was 1.06 g/cm^3 and the BET surface area, pore volume, and pore size of the Fe_2O_3 particles were 90.79m^2/g, 0.2582cm^3/g and 11.38nm, respectively.

2.2. Catalyst characterization

Mössbauer spectroscopy was used to study the phases of iron presented in the Fe_2O_3 particles and the spectra were measured with a radioactive source of 57Co (Pd) moving in a constant acceleration mode at room temperature. The α-Fe foil was exploited as a reference and the experimentally observed Mössbauer spectra were curve-fitted by a least squares method, assuming Lorentzian line shapes. The corresponding Mössbauer parameters, i.e. isomer shift (IS), quadrupole splitting (QS), and magnetic hyperfine field (B_{hf}) were used for description of the individual iron species.

Temperature-programmed reduction (TPR) was carried out in a quartz U-tube reactor connected to a thermal conduction detector (TCD), under the following conditions: a hydrogen-argon mixture (7%H_2) at a flow rate of 60ml/min; a 50 mg sample; a heating rate of 10 ℃/min from room temperature to 600 ℃. The sample was pretreated in N_2 stream at 100 ℃ for 1h before reduction and then cooled to the room temperature.

2.3. Activity measurements

The SCR activity measurement was carried out in a fixed-bed quartz reactor. The reaction conditions were as follows: 500ppm NO, 500ppm NH_3, 3% O_2, balance N_2, 1500 ml/min or 1000 ml/min total flow rate. The feed gases were premixed in a glass chamber, but the NH_3 was fed directly into the reactor by passing the mixing chamber to avoid possible reaction before the reactor. All the data were obtained when the SCR reaction reached steady state, and the product components in the outlet gases were measured online by an online flue gas analyzer.

Steady-state kinetics studies were carried out in a fixed-bed quartz flow reactor (differential reactor). An amount of 0.65g of catalyst was placed in the reactor in this work. The flue gas was simulated by blending different gaseous reactants. The typical reactant gas composition was as follows: 500-2000ppm NO, 500-2000ppm NH_3, 0.5-5% O_2 and balance N_2. The total flow rate was 1500 ml/min (ambient conditions). The instrument is the same as for the catalytic activity measurement mentioned above.

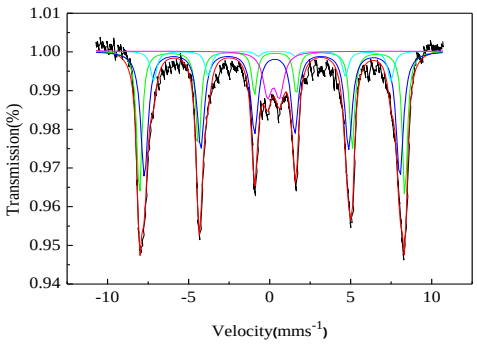

Fig. 1: Mössbauer spectra of the Fe_2O_3 particles

3. Results and Discussion

3.1. Catalyst characterization

The ^{57}Fe Mössbauer spectra of the Fe_2O_3 particles are shown in Fig. 1 and the Mössbauer parameters are summarized in Table 1. It can be seen from Fig. 1 that the ^{57}Fe Mössbauer spectra of the Fe_2O_3 particles were fitted with three sextets and one doublet. The values of IS calculated for the samples were characteristic of Fe^{3+} ions and near-zero values of QS for the sextets indicated the defect spinel structure for the samples [7, 8]. The IS of sub-spectrum 1 and sub-spectrum 2 were 0.271mms^{-1} and 0.249 mms^{-1} with B_{hf} of 51T and 49T, respectively, which could be assigned to γ-Fe_2O_3 [8-10]. The components described by IS=0.318 mm/s and B_{hf}= 45.56T were characteristic for α-Fe_2O_3 [11]. Based on the discussion above, the Fe_2O_3 particles mainly consisted of γ-Fe_2O_3 and α-Fe_2O_3. The γ form of Fe_2O_3 had the spinel structure and the cation vacancies were confined to the octahedral sites in the γ-Fe_2O_3 crystal, which could be written: $[Fe^{3+}]_T[Fe^{3+}_{5/3}\square_{1/3}]_O O_4$. The presence of vacancies could improve electron transfer on the Fe_2O_3 surface in the reaction and increase the catalytic performance of the catalysts.

Table 1: ^{57}Fe Mössbauer parameters at RT calculated for Fe_2O_3 particles

Sample	Sub-spectrum	Fitted spectrum	IS (mm/s)	QS (mm/s)	Γ (mm/s)	B_{hf} (T)	Relative Intensity (%)	Composition
Before reaction	S1	Sextet	0.271 ±0.008	-0.098 ±0.005	0.375	51.017 ±0.039	33.223	γ-Fe_2O_3[8,9]
	S2	Sextet	0.249 ±0.013	-0.079 ±0.006	0.538	49.063 ±0.069	50.090	γ-Fe_2O_3[10]
	S3	Sextet	0.318 ±0.037	-0.143 ±0.023	0.452	45.560 ±0.184	8.391	α-Fe_2O_3[11]
	S4	Doublet	0.253 ±0.028	-0.735 ±0.055	0.658		8.297	Fe(III)[8]

Key: IS = isomer shift given relative to α-Fe at RT; QS=quadrupole splitting; Bhf=hyperfine magnetic field; Γ=line width.

The redox property of the catalyst had an important influence on the SCR reaction. In particular, the redox property of the catalyst at low temperature with low activation energy had been shown to be the main factors for the SCR reaction [12]. In order to investigate the redox property of the Fe_2O_3 particles, H_2-TPR experiments were carried out and the results are shown in Fig. 2. It can be clearly seen from Fig. 2 that there were three reduction peaks at 231.9 ℃, 261.4 ℃ and 309.5 ℃ before 400 ℃, respectively, and an incomplete reduction peak after 400 ℃, showing a stepwise reduction of Fe_2O_3.It is generally accepted that the reduction of iron oxide involves a two-step process, with Fe_2O_3 first reduced to Fe_3O_4 (FeO·Fe_2O_3) at low temperature (<400 ℃) and then to metallic Fe at high temperature (>350 ℃) [13-16]. Therefore, the reduction peaks observed before 400 ℃ might be attributed to the reduction of Fe_2O_3, while the incomplete reduction peak after 400 ℃ might be ascribed to the reduction of Fe_3O_4 (FeO·Fe_2O_3).In addition, the reduction temperature of catalyst was proved to be closely correlated with the reaction temperature for SCR of NO. It can be seen from Fig. 2 that Fe_2O_3 particles were found to be reduced by H_2 at lower temperatures at around 150-300 ℃. Therefore, the lower reducible temperature of Fe_2O_3 particles may contribute to the higher activity of Fe_2O_3 particles at lower temperature.

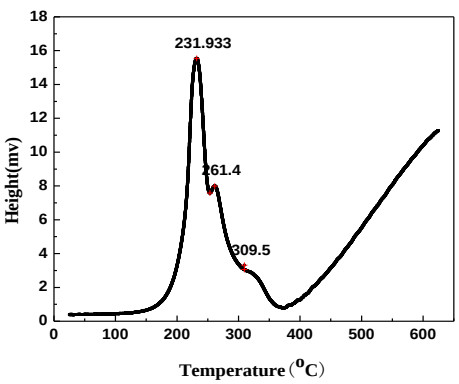

Fig. 2: TPR profiles of the Fe_2O_3 particles

3.2. Catalytic activity of Fe_2O_3 particles

Catalytic activity of Fe_2O_3 particles as a function of temperatures is shown in Fig. 3. Compared the results of the NO conversion by SCR on Fe_2O_3 particles in the absence/ presence of O_2, it can be seen from Fig. 3 that the catalytic performance over Fe_2O_3 particles monotonically increased with temperature until 210 ℃, but the discrepancy of reactivity for catalysts under different O_2 concentration is obvious. More than 90%, 95.5% and 98.5 NO conversion could be achieved at 150 ℃, 180 ℃ and 210 ℃ over the Fe_2O_3 particles with 3% oxygen, respectively. Compared with that without oxygen, only 86.4%, 91.2% and 92% NO conversion could be obtained at 150 ℃, 180 ℃ and 210 ℃, respectively. Then NO conversion decreased with increasing temperatures. With the feeding of 3% oxygen, the NO conversion was increased from 91.2% to 95.5% and 92% to 98.5% at 180 ℃ and 210 ℃, respectively. The results in Fig. 3 showed that the Fe_2O_3 particles was highly active for the low-temperature SCR of NO with NH_3 in the presence of excess oxygen and the addition of oxygen caused enhancement of the catalytic activity.

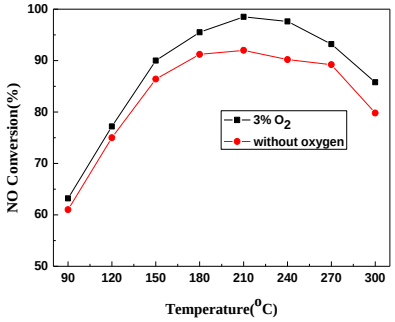

Fig. 3: NO conversion on the Fe_2O_3 particles in the absence/ presence of O_2. Reaction conditions: [NO]=[NH_3]=500ppm, [O_2]=3%, balance N_2, total flow rate 1500 ml/min, catalyst 12mL

3.3. Kinetics of the reaction and apparent activation energy

To determine the reaction orders with respect to NO, NH_3 and O_2, the differential reaction experiments were performed at 120, 150, 180 and 210 ℃, respectively. For calculating the reaction order with respect to NO, the concentration of NH_3 and O_2 was kept constant at 2000ppm and 3%, respectively, while the concentration of NO was varied between 500 and 2000ppm. Similar experiments were performed to determine the reaction orders with respect to NH_3 and O_2. The experimental results for the rate of NO conversion with the concentration of nitric oxide, ammonia and oxygen are presented in Fig. 4-6, respectively. As seen from Fig. 4-6, the rate of NO conversion increased with the increase of NO concentration, but it was nearly no change with the increase of NH_3 concentration (shown in Fig. 5). Fig. 6 showed the effect of oxygen on the reduction of NO by NH_3 at different temperatures. The Fe_2O_3 particles presented a low rate of NO conversion at different temperatures under a small concentration of O_2.However, when a higher concentration of O_2 was feeded into the simulated flue gas, the NO conversion increased sharply.

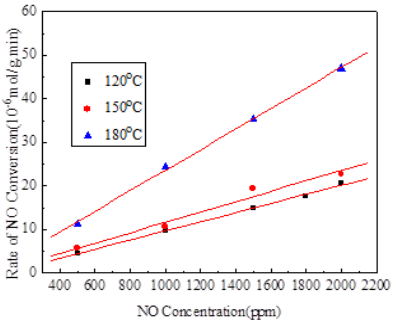

Fig. 4: Dependence of NO conversion rate on NO concentration over Fe_2O_3 particles at different temperatures. Reaction conditions: [NO]=500-2000ppm, [NH_3]=2000ppm, [O_2]=3%, balance N_2, total flow rate 1500 ml/min, catalyst 0.65g.

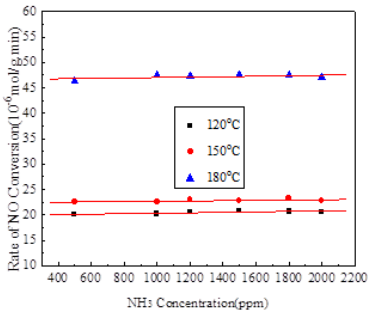

Fig. 5: Dependence of NO conversion rate on NH_3 concentration over Fe_2O_3 particles at different temperatures. Reaction conditions: [NO]=2000ppm, [NH_3]=500-2000ppm, [O_2]=3%, balance N_2, total flow rate 1500ml/min, catalyst 0.65g.

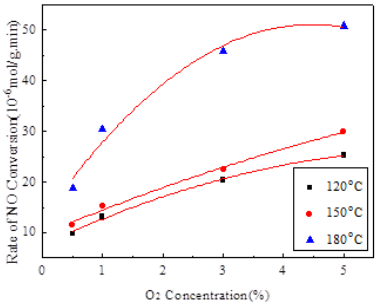

Fig. 6: Effect of O_2 concentration on NO conversion rate over Fe_2O_3 particles at different temperatures. Reaction conditions: [NO]=[NH_3]=2000ppm, [O_2]=0.5-5%, balance N_2, total flow rate 1500ml/min, catalyst 0.65g.

The reaction rate of NO conversion as a function of reactant concentrations can be expressed simply as follows [1]:

$$R_{NO}=-k[NO]^{\alpha}[NH_3]^{ß}[O_2]^{\gamma} \quad (1)$$

Where, R_{NO} is the SCR reaction rate, k is the apparent rate constant, α and, ß, and γ are the reaction orders for NO, NH_3 and O_2, respectively.

The SCR reaction order with respect to NO, NH_3, O_2 was calculated to be nearly 1, 0, and 0.42, respectively. Then the SCR reaction rate of NO conversion was expressed simply as:

$$R_{NO}=-k[NO][O_2]^{0.42} \quad (2)$$

In this system, only when the oxygen partial pressure was below approximately 0.5at%, this rate equation can be established [2]. Based on the experimental conditions used (the partial pressure of O_2 was all 0.03atm), the Eq. (3) could be used as the rate equation.

$$R_{NO}=-k[NO] \quad (3)$$

The amount of oxygen was in excess during SCR reaction, the relationship between apparent rate constant (k) and NO conversion (x) could be given as follows:

$$k=-F_0\frac{\ln(1-x)}{[NO_0]w} \quad (4)$$

where F_0 was the molar NO feed rate (mol/min), $[NO]_0$ was the molar NO concentration at the inlet (mol/L) and W was the amount of catalyst(g).

The relationship between ln(1-x) and $[NO]_0\ W/F_0$ was shown in Fig. 7. And the value of the apparent rate constant (k) at different temperatures had been calculated and a summary comparison made for the Fe_2O_3 particles with other reported excellent catalysts is listed in Table 2.

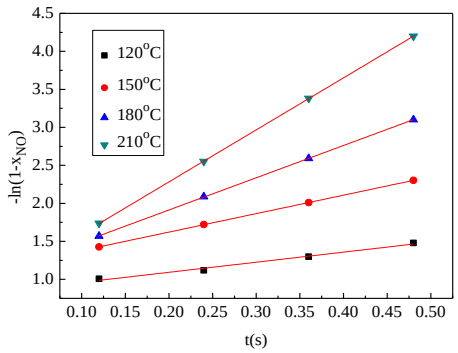

Fig.7: First-order plots with respect to NO with different gas flow rate at different temperatures.

Table 2: Performance of the Fe_2O_3 particles for low-temperature SCR of NO with NH_3

Sample	Reaction conditions	t(℃)	x_{NO}（%）	k($cm^3g^{-1}s^{-1}$)
Fe_2O_3[this work]	[NO]=[NH_3]=500ppm,O_2=3%, balance N_2, total flow rate 1500 ml/min, catalyst 12mL	120	77.2	1.33
		150	90	2.43
		180	95.5	4.25
		210	98.5	6.85
$MnOx/Al_2O_3$ [17]	[NO]= 500ppm, [NH_3]=550ppm, O_2=2%, SV(cm^3 g^{-1} h^{-1})=24000	150	63	9.40
10%Mn-14%Ce /USY [2]	[NO]= [NH_3]=1000ppm, O_2=2%, SV(cm^3 g^{-1} h^{-1})=30000	80	50	6.84
		100	59	9.31

It is well known that apparent activation energy of a reaction is a significant parameter to evaluate the performance of catalyst. The apparent activation energy could be obtained by using Arrhenius equation:

$$k = k_0 e^{\frac{-Ea}{RT}} \tag{5}$$

where E_a is the apparent activation energy.

When ln$k$ was plotted vs 1/T, the activation energy and the pre-exponential factor for SCR reaction could be obtained by the slope and intercept (as shown in Fig. 8). The activation energy for Fe_2O_3 in SCR process was calculated to be 28.8kJ/mol. This is consistent with our previous study and is lower than values obtained by other researchers, such as MnOx/TiO_2 [1](38kJ/mol), H-ZSM-5 [18](55kJ/mol), V_2O_5/TiO_2 [19] (85kJ/mol) and Fe-ZSM-5 [20](68kJ/mol). It indicated that less energy was needed for activation than other catalysts in the reaction. Therefore the Fe_2O_3 particles would be substantially more active than all other catalysts at low temperature.

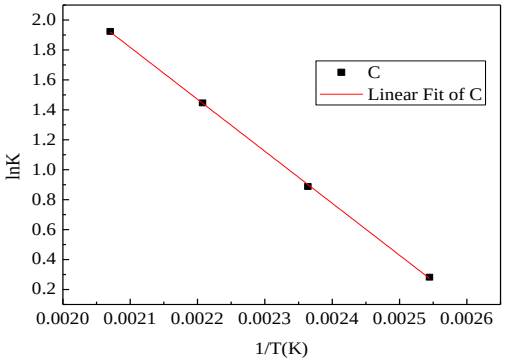

Fig. 8: Arrhennius plots of the NO-NH_3-O_2 reaction on Fe_2O_3 particles

4. Conclusion

Based on the above results, it can be concluded that the Fe_2O_3 particles were highly active for the selective catalytic reduction of NO with NH_3 in the presence of excess oxygen at low temperatures. More

than 90% NO conversion was obtained over a broad temperature range of 150-270℃ under the conditions used. The reaction order of NO, NH_3, O_2 was determined to be nearly 1, 0, and 0.42, respectively. And the apparent active energy of the reaction was calculated to be 28.8kJ/mol, which was consistent with our previous study and was lower than the values obtained by other researchers.

5. Acknowledgments

This work was supported by the National High Technology Research and Development Program of China (863 Program) (No. 2015AA03A401), the National Natural Science Foundation of China (No. 51276039), the Fundamental Research Funds for the Central Universities (No. 020514380020, No. 020514380030) and Postdoctoral Science Foundation of Jiangsu Province, China (No. 1501033A).

6. References

[1] Z. Wu, B. Jiang, Y. Liu, W. Zhao, B. Guan. Experimental study on a low-temperature SCR catalyst based on MnO_X/TiO_2 prepared by sol-gel method. *J. Hazard. Mater.*2007, 145:488-494.

[2] G. Qi, R. T. Yang, R. Chang. Low-temperature SCR of NO with NH_3 over USY-supported manganese oxide-based catalysts. *Catal. Lett.* 2003, 87:67-71.

[3] X. Tang, J. Hao, H. Yi, H. Li. Low-temperature SCR of NO with NH3 over AC/C supported manganese-based monolithic catalysts. *Catal. Today*. 2007, 126(3-4):406-411.

[4] G. Qi, R. T. Yang. Low-temperature selective catalytic reduction of NO with NH_3 over iron and manganese oxides supported on titania.*Appl Catal B-Environ.*2003, 44:217-215.

[5] M. Kang, E. D. Park, J. M. Kim, J. E. Yie. Cu-Mn mixed oxides for low temperature NO reduction with NH_3.Catal. *Today*.2006, 111:236-241.

[6] G. Yao, F. Wang, X. Wang, K. Gui. Magnetic Field Effects on Selective Catalytic Reduction of NO by NH_3 over Fe_2O_3 Catalyst in a Magnetically Fluidized Bed.*Energy*.2010, 35:2295-2300.

[7] C. Sudakar, T. R. N. Kutty. Structural and magnetic characteristics of cobalt ferrite-coated nano-fibrous γ-Fe_2O_3. *J.Magn. Magn. Mater.*.2004, 279:363-374.

[8] E. Tabor, K. Závěta, N. K. Sathu, Z. Tvarůžková, Z. Sobal ík. Characterization of iron cationic sites in ferrierite using Mössbauer spectroscopy.*Catal Today*.2011, 169:16-23.

[9] M. Jeleńska, A. Hasso-Agopsowicz, B. Kopcewicz. Thermally induced transformation of magnetic minerals in soil based on rock magnetic study and Mössbauer analysis. *Phys Earth Planet In.*2010, 179:164-177.

[10] D. Ortega, J. S. Garitaonandia, C. Barrera-Solano, M. Ram írez-del-Solar, E Blanco, M Domínguez. γ-Fe_2O_3/SiO_2 nanocomposites for magneto-optical applications: Nanostructural and magnetic properties.*J. Non-Cryst. Solids.*2006, 352:2801-2810.

[11] C. V. Cromphaut, V. G. Resende, E. D. Grave, A. V. Alboom, R. E. Vandenberghe, G. Klingelh öfer. Characterisation of the magnetic iron phases in Clovis Class rocks in Gusev crater from the MER Spirit Mössbauer spectrometer.*Geochim. Cosmochim. Ac.*2007, 71:4814-4822

[12] D. W. Kwon, K. H. Park, S. C. Hong. The influence on SCR activity of the atomic structure of V2O5/TiO2 catalysts prepared by a mechanochemical method. *Appl. Catal. A-Gen.*2013, 451:227-235.

[13] K. Li, H. Wang, Y. Wei, M. Liu. Preparation and characterization of Ce1-xFexO2 complex oxides and its catalytic activity for methane selective oxidation. *J. Rare. Earth.*2008, 26:245-249.

[14] M. Liang, W. Kang, K. Xie. Comparison of reduction behavior of Fe_2O_3, ZnO and $ZnFe_2O_4$ by TPR technique. *J.Nat. Gas. Chem.*2009, 18:110-113.

[15] G. Munteanu, L. Ilieva, D. Andreeva.Kinetic parameters obtained from TPR data for α-Fe_2O_3 and Au/α-Fe_2O_3 systems .*Thermochimica. Acta.*1997, 291:171-177.

[16] P. S. Lambrou, A. M. Efstathiou. The effects of Fe on the oxygen storage and release properties of model Pd-Rh/CeO2-Al2O3 three-way catalyst .*J. Catal.* 2006, 240(2):182-193.

[17] L. Singoredjo, R. Korver, F. Kapteijn, J. Moulijn. Alumina supported manganese oxides for the low-temperature selective catalytic reduction of nitric oxide with ammonia. *Appl. Catal. B-Environ.*1992, 1:297-316.

[18] S. A. Stevenson, J. C. Vartuli, C. F. Brooks. Kinetics of the Selective Catalytic Reduction of NO over HZSM-5. *J. Catal.* 2000, 190:228-239.

[19] M. D. Amiridis, J. P. Solar. Selective catalytic reduction of nitric oxide by ammonia over V_2O_5/TiO_2, $V_2O_5/TiO_2/SiO_2$, and V_2O_5-WO_3/TiO_2 Catalysts: Effect of vanadia content on the activation energy. *Ind. Eng. Chem. Res.* 1996, 35(3): 978-981.

[20] M. Iwasaki, K. Yamazaki, H. Shinjoh. Transient reaction analysis and steady-state kinetic study of selective catalytic reduction of NO and NO + NO2 by NH3 over Fe/ZSM-5.*Appl. Catal. A-Gen.*2009, 366:84-92.

International Proceedings of Chemical, Biological and Environmental Engineering
Volume 94 of IPCBEE (2016)
DOI: 10.7763/IPCBEE. 2016. V94. 8

Precipitation and Soil Quality in a Small Watershed

Erdem Ahmet Albek [1], Mine Albek [1], Burcu Şimşek Uygun[1+], Meltem Uyar[2], Müge Taş[1], and Latife Tatlıpınar[1]

[1] Anadolu University, Environmental Engineering Department, Eskişehir, Turkey
[2] Pisagor Environmental Consultancy and Engineering, İzmir, Turkey

Abstract. Anthropogenic sources began to adversely impact the environment especially after the industrial revolution. With the increasing use of water by domestic, industrial and agricultural activities, the importance of keeping water resources in unpolluted shape has grown. To abate pollution of water resources knowledge about the pollutants arriving from the atmosphere and other sources is of prime importance. In this study, pollutants which are deposed by precipitation and from the soil are determined for the Borabey Pond, Eskişehir, in Inner Anatolia of Turkey. The pond's surface covers 0.16 km2 has volume 1.4 Mm3. Precipitation contains many pollutants, also from agricultural activities which find their way to the atmosphere principal among them are nitrogen and phosphorus species. The maximum total nitrogen concentration in precipitation was found to be 9.7 mg/L and total phosphorus concentration 1.97 mg/L. Besides, the soil has a total nitrogen concentration 50 mg/kg and total phosphorus concentration of 3.5 mg/kg. Strategies must be developed to protect the water source and improve water quality.

Keywords: Water Pollution, Precipitation Quality, Nutrients in Soil

1. Introduction

Water resources are used for drinking water, irrigation, industrial use, energy production and it is being excessively polluted due to rapid growth of population and human activities. Because of these activities, eutrophication of many lakes is a global problem which reduces water quality [1]. Once a lake is eutrophic, it will lose its functions and this will reflect negatively in the economy and society [2]. Besides, precipitation can be one of the major source of pollutants for a lake because it contains atmospheric pollutants [3]. Moreover, agricultural activities are a major source of eutrophication, because excessive amounts of nutrients such as nitrogen and phosphorus enter water bodies with the precipitation and cause algal blooms, eroded soil is another source of pollutants [4]. Algal blooms can lead to decreases in clarity and dissolved oxygen levels so this has negative effects on organisms living in the lake.

In addition, decomposition of organic matter can cause deterioration of the ecosystem [5]. Besides, physicochemical properties of water such as turbidity, odor, taste are negatively affected with eutrophication. As a result, eutrophic water sources can contain dead zone [6].

Eutrophication of a lake is combined with two major nutrients; nitrogen and phosphorus. Phosphorus is usually known as the growth-limiting nutrient for the growth of algae [4]. If the N:P weight ratio is larger than 7,2N:1P, the limiting element is phosphorus; smaller than 7,2N:1P, nitrogen becomes the limiting element [7]. It has been determined that nitrogen is responsible for controlling phytoplankton production in olgotrophic marine regions, while phosphorus controls continental water bodies [6].

Monitoring the environmental factors is essential to manage and maintain water quality of lakes and also nutrient sources coming to the lake must be investigated [8]. In this study, the nitrogen and phosphorus

+ Corresponding Author : Tel:+(902223350580)
E-mail address: bsimsek1@anadolu.edu.tr

concentration are determined which are brought by precipitation to the Borabey Pond and N-P concentrations of the watershed's soil are established. Soil is unable to keep nitrate, so excess nitrate above the needs of plants, move to around water. Because of being responsible for creating conditions of producing algal blooms, the critical concentrations of nitrogen and phosphorus (including total phosphorus, orthophosphates, total nitrogen, ammonium, nitrite and nitrate) are important.

2. Study Area

The study area is the Borabey Pond which is located in Eskişehir, Turkey. Eskişehir is a large city in northwestern part of Inner Anatolia. There have been many of agricultural products in the region are principally wheat, barley, rye, corn, sugar beet. Industrial activities include brick and tile, food and textiles production. There are also mining activities, especially for chromium and coal in Eskişehir.

The pond lies in a hilly region at an elevation of 900 meters above mean sea level and covers 0.16 km^2 and its main usage is for irrigation of farmlands to the downstream. The watershed area is 8.6 km^2. Eskişehir has continental climate due to geographical area, altitude and land forms. The summers are hot and arid, the winters are cold and wet.

The water body serves as a habitat to waterbirds and fish, but the pond obtains runoff from farmlands which brings nitrogen and phosphorus. Agricultural areas are nonpoint pollution sources so run off from these areas cause pollution unless precautions are taken.

3. Material and Methods

In this study, a meteorological station established in the watershed close to the pond was used and to collect the pollutants coming with precipitation to the watershed (Fig. 1-b). The samples were brought to the laboratory and analyses were made with Hach DR2400 spectrophotometer. For measuring ammonia nitrogen the Nessler Process, for nitrate-N the Cadmium Reduction method; for nitrite-N the Diazotization method; for total N the Persulphate Digestion method were used and for phosphorus species; for total phosphorus the Persulphate Digestion method and for orthophosphate the Ascorbic Acid method were used. Soil samples were taken from two sides (Fig. 1-a). Then, they were brought to the laboratory and analyzed with Hach DR2400 spectrophotometer. The soil's pollutants are determined with spectrophotometer after extraction.

Fig. 1.a: Borabey Pond with soil sampling sites

Fig. 1.b: Precipitation collection device

4. Results and Discussion

Precipitation analysis were carried out on a monthly basis at a station situated at the shore of the pond. Precipitation is collected and analyzed later in the laboratory. The values at a particular date reflect the concentrations in the collected water in the period beginning with the last date. They also represent total atmospheric deposition. This is not the case for the analysis in December 2014 which begins after a long period. While this does not affect phosphorus concentrations to a significant degree, nitrogen concentration must be viewed with care. Especially after waiting ammonia can escape from the samples and decrease total nitrogen levels.

As seen in Fig. 2 total nitrogen in precipitation has a maximum value of 9.7 mg/L in March 2013. At the same time, ammonia nitrogen takes a maximum value of 3.21 mg/L. Increasing total nitrogen concentrations were observed in the spring 2013. The average of nitrate concentration is 0.47 mg/L. Besides, nitrite concentrations generally have low values of which the maximum is 0.006 mg/L.

Total phosphorus concentration is another important parameter which creates eutrophication. Kaya (2013) determined the eutrophication status of the pond as mesotrophic and the limiting nutrient as phosphorus [9]. Total phosphorus maximum concentration which comes from precipitation is 1.97 mg/L and also orthophosphate concentration has a maximum value 1.92 mg/L in precipitation in March 2013 (Fig. 3). The reason of increased nitrogen and phosphorus concentration (Fig. 2 and 3) is thought to be dust particles from the Sahara Desert reaching Turkey in the period of sampling [9].

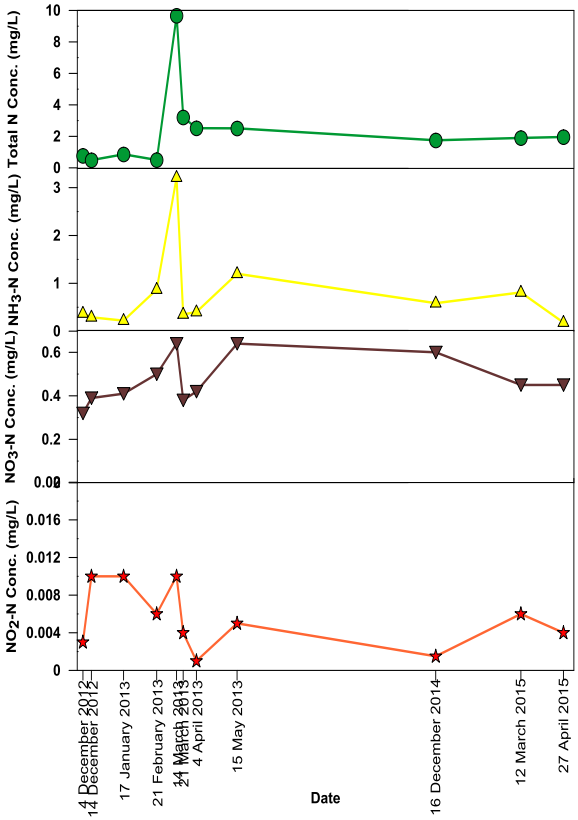

Fig. 2: Nitrogen concentrations in precipitation

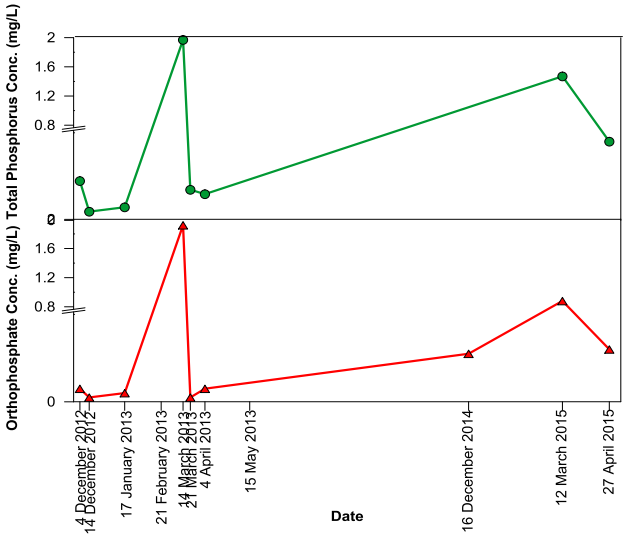

Fig. 3: Phosphorus concentrations in precipitation

The soil is another important source of pollutants carried to the lake. In 2015, two analysis were made about nitrogen and phosphorus concentration in the soil and the results are shown in the Table 2. Total nitrogen concentrations in diffrent soils change between 20-200 mg/kg [10]. Besides, the phosphorus concentrations in a variety of soils lie in a range of 1-50 mg/kg in the soil [11]. Measured concentrations in the Borabey Pond have been found to lie within these ranges.

Table 1: Pollutant concentrations on soil

	Total N (mg/kg)	NH_3-N (mg/kg)	NO_3-N (mg/kg)	NO_2-N (mg/kg)	Total P (mg/kg)	Orthophosphate (mg/kg)
12 March 2015	23	4,5	0,035	1,5	3,5	1
27 April 2015	50	1	0,035	1	3,5	0,5

5. Conclusion

In this study, pollutants contained in precipitation reaching the Borabey Pond were measured and the nitrogen and phosphorus content of the watershed soil was determined. As in the case of the high loads in precipitation in March 2013, atmospheric sources can be an important pathway of pollutants to the pond and its watershed can carry loads of nitrogen and phosphorus from the soils which receive their loads from agricultural activities.

In this study, total nitrogen in precipitation has a maximum value of 9.7 mg/L. Besides, ammonia nitrogen takes a value of 3.21 mg/L. The average nitrate concentration is 0.47 mg/L. Moreover, nitrite concentrations generally have low values of which the maximum is 0.006 mg/L.

Total phosphorus maximum concentration of precipitation is 1.97 mg/L and also orthophosphate concentration has a maximum value 1.92 mg/L. Soil analysis values are within ranges found in literature.

6. Acknowledgements

This study is supported by Research Fund of Anadolu University under Project No. 1206F097.

7. References

[1] Sanchez-Carrillo, S., L. C. Alatorre, et al. (2007). Eutrophication and sedimentation patterns in complete exploitation of water resources scenarios: An example from Northwestern semi-arid Mexico.*Environmental Monitoring and Assessment* **132**(1-3): 377-393.

[2] Yang, X. E., X. Wu, et al. (2008). Mechanisms and assessment of water eutrophication. *Journal of Zhejiang University-Science B* **9**(3): 197-209.

[3] Zhang, Y.L., Shi, K. et al. (2016). Monitoring the river plume induced by heavy rainfall events in large, shallow, Lake Taihu using MODIS 250 m imagery. *Remote Sensing of Environment* 173: 109-121.

[4] Galvez-Cloutier, R., S. K. M. Saminathan, et al. (2012). An Evaluation of Several In-Lake Restoration Techniques to Improve the Water Quality Problem (Eutrophication) of Saint-Augustin Lake, Quebec, Canada. E*nvironmental Management* **49**(5): 1037-1053.

[5] Ali, E. M. (2011). Impact of drain water on water quality and eutrophication status of Lake Burullus, Egypt, a southern Mediterranean lagoon. *African Journal of Aquatic Science* **36**(3): 267-277.

[6] Frumin, G. T. and I. M. Gildeeva (2014). Eutrophication of water bodies - A global environmental problem. *Russian Journal of General Chemistry* **84**(13): 2483-2488.

[7] Chapra, S. C. (1997). *Surface Water Quality Modeling*. United States of America, McGraw-Hill Companies.

[8] Liu, W. C., W. B. Chen, et al. (2009). Impact of phosphorus load reduction on water quality in a stratified reservoir-eutrophication modeling study. *Environmental Monitoring and Assessment* **159**(1-4): 393-406.

[9] Kaya, M., 2013 Interaction of Water Quality with Basin Components in Small Water Bodies, M.Sc. Thesis, Anadolu University, Environmental Engineering Department.

[10] Li, Q., Wang, C., et al. (2016). Spatiotemporal variations and factors affecting soil nitrogen in the purple hilly area

of Southwest China during the 1980s and the 2010. *Science of the Total Environment* 547:173-181.

[11] Yang, X. E., X. Wu, et al. (2008). Mechanisms and assessment of water eutrophication. *Journal of Zhejiang University-Science B* **9**(3): 197-209.

International Proceedings of Chemical, Biological and Environmental Engineering
Volume 94 of IPCBEE (2016)
DOI: 10.7763/IPCBEE. 2016. V94. 9

Effect of Impoundment on Physico-chemical Properties of Water in the Flowing through stream, the Case of the Turawa Reservoir

Marek Ruman[1], Żaneta Polkowska[2] and Bogdan Zygmunt[2 +]

[1]University of Silesia, Faculty of Earth Sciences, Centre for Polar Studies KNOW (Leading National Research Centre), ul. Będzińska 60, 41-200 Sosnowiec, Poland

[2] Department of Analytical Chemistry, Chemical Faculty, Gdansk University of Technology, 80-952 Gdańsk, 11/12 Narutowicza Str.

Abstract. The Turawa reservoir is one of the most important storage reservoirs in Poland. Quite many physico-chemical parameters of water in the reservoir itself and also in the Mała Panew, the river flowing through the reservoir were measured at various periods of the year. Measuring and sampling points were situated at the river inflow, over the reservoir, and at the river outflow. The parameters included temperature, electrical conductivity, total hardness, salinity, oxygenation conditions, pH, concentration of organic matter, nutrient anions and cations and some other cationic metals and also heavy metals in different chemical forms, periods of ice laying on the river, algal blooms, etc. The differences in the parameters, their origin and consequences were thoroughly discussed.

Keywords: The Turawa Reservoir, The Mała Panew River, Physico-Chemical Parameters, Sampling and Measuring Points, Water Quality

1. Introduction

The resources of surface water in Poland are relatively low and not uniformly distributed over the country. Water availability is strongly dependent on season. Moreover, due to the strong anthropopressure still observed water quality happens to be poor for some purposes. Though the efforts have been undertaken to store water in large reservoirs, the storage capacity of the present Polish reservoirs is rather not sufficient. Impoundment or the storage water within flowing streams is generally beneficial for handling large amounts of pollution downstream. However, it can be damaging to the water quality. Generally, water storage behind large dams is applied whereby the water is used for power generation, municipal water supply, and flood control. Large storage reservoirs with controlled discharge provide larger amounts of water for periods of drought or low flow in the streams. However, the water quality downstream can be affected by storage during part of the year.

One of the larger storage reservoirs in Poland is the Turawa reservoir, which has been operated since 1948. It is localized between 50°42'27'' and 50°44'32'' north latitude and 18°04'51'' and 18°10'59'' east longitude in Mała Panew Velley, which is the part of Równina Opolska (Opole Plain). The reservoir is situated on the Mała Panew river 16 km away from where it flows into the Odra river. There are two smaller rivers inflowing to the reservoir; they are the Libawa and the Rosa.

The Turawa reservoir plays an important role for the above mentioned part of Poland but due to strong agricultural and industrial anthropopressure its ecological state is rather poor and the strong efforts have been taken to improve it. The remedial program needs the assessment of the actual quality of water in the reservoir.

+ Corresponding author. Tel.: + 48 58 347 23 94
E-mail address: bogdan.zygmunt@pg.gda.pl

It is also important to know the influence of the reservoir on the characteristics of the Mała Panew river water. From ecological point of view, each river is an open system being in dynamic equilibrium. Disturbance of the river flow by building up the dam changes the hydrological conditions and hence physical, chemical and biological processes determining the water quality in the reservoir and in the river downstream the dam [1-5].

The aim of the first part of the research on the surface water quality in the area of the Turawa reservoir was to study the effect of the reservoir on the selected parameters of water in the Mała Panew river which is the main river supplying the reservoir with water and then flowing into the Odra river.

2. Measured Parameters and Localization of Sampling Points

The measurements were made for the selected points situated at the Mała Panew river inflow (Fig. 1, 13), over the reservoir, and at the river outflow (Fig. 1, 14; just after the dam). The points for on–site measurement and for collecting samples for laboratory analysis are presented in Fig. 1.

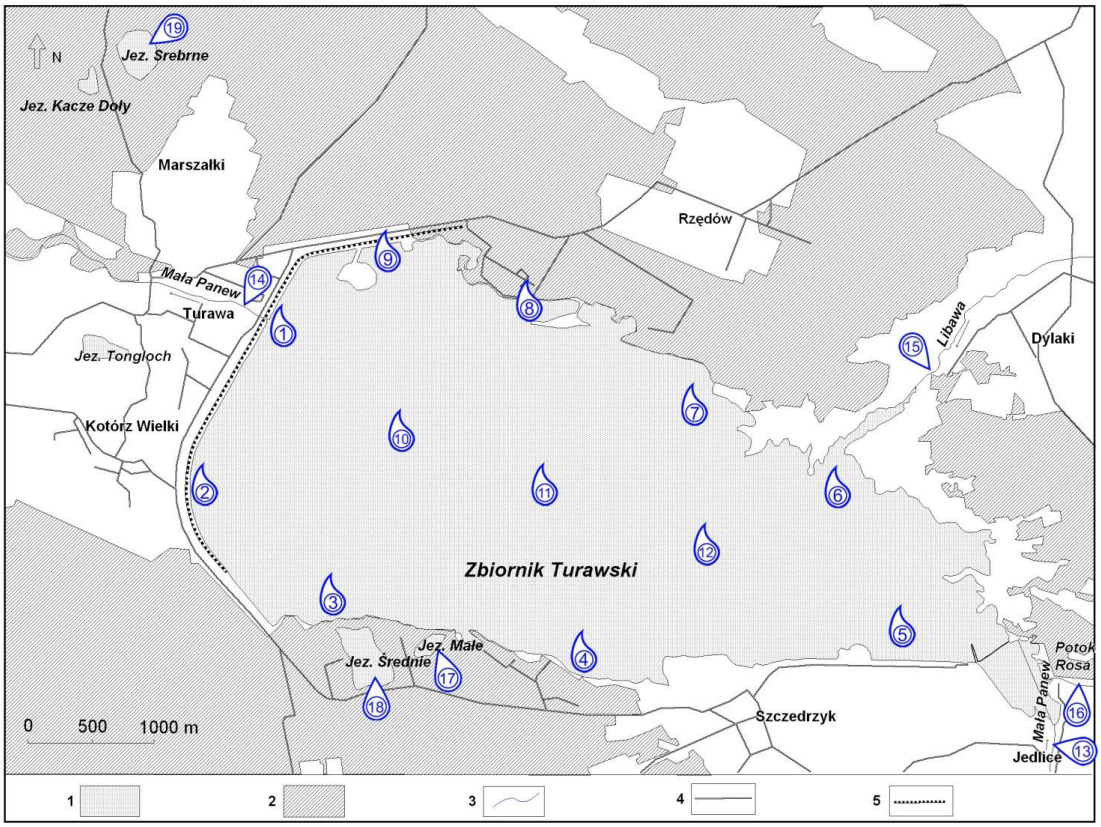

Fig. 1: Location of the points for collecting samples for physico-chemical measurements: 13 – the Mała Panew river inlet, 14 – the river outlet. Geographical features: 1 – natural (Jez. - lake) and artificial (Zbiornik Turawski – the Turawa reservoir) water reservoirs; 2 – forests; 3 – rivers; 4 – roads; 5 – dam

There are quite a number of parameters characterizing the water which can be influenced to a smaller or higher degree by building the dam to accumulate water. In the case of the Turawa reservoir the most important parameters are thought to be: temperature, electrical conductivity, total hardness, salinity, oxygenation conditions, pH, content of organic matter, nutrient anions and cations and some other metal cations and also heavy metals in different chemical forms, period of ice laying, and intensity of algal blooms etc. Some of the parameters were measured on-site; however most of them were determined in the laboratory analysing the samples properly collected, transported and stored. The methods and instrumentation for on-site measurements as well as for collecting samples and their laboratory analysis will be described elsewhere.

3. Water Temperature of The Mała Panew River

The Turawa reservoir has had the significant effect on the temperature of the Mała Panew water outflowing the reservoir. The differences in temperature of river water inflowing and water outflowing the reservoir are significant and depend on the season (Fig. 2).

In the period of spring and summer the water at the inflow had higher temperature than that at the outflow. The difference was in the range of 2.5 – 6.5 ^{0}C. In autumn-winter seasons the reservoir effect on water temperature was opposite; the outflowing water temperature was higher by 1.4 – 2.5 ^{0}C. This is because of the thermal stratification in that period and the fact that, due to the reservoir construction and the use of bottom sluices, the outflowing water comes from hypolimnion. The average surface water temperature in the reservoir was higher than the water delivered by the Mała Panew. The minimal difference was 0.37 ^{o}C, the maximum 3 ^{o}C, and the average 0.86 ^{o}C (Fig. 2). Moreover, the average and maximum temperatures of water outflowing the reservoir were lower than those at the inflow of the Mała Panew by 0.33 ^{o}C, and 2.7 ^{o}C, respectively; only minimum temperature was slightly higher (0.1 ^{o}C).

Summing up, in the spring-summer period the Turawa reservoir effect is lowering the temperature of the Mała Panew water (outflow with respect to inflow) while in the fall-winter period the opposite effect is observed. This is disadvantageous, though typical for storage reservoirs as shown by some researchers.

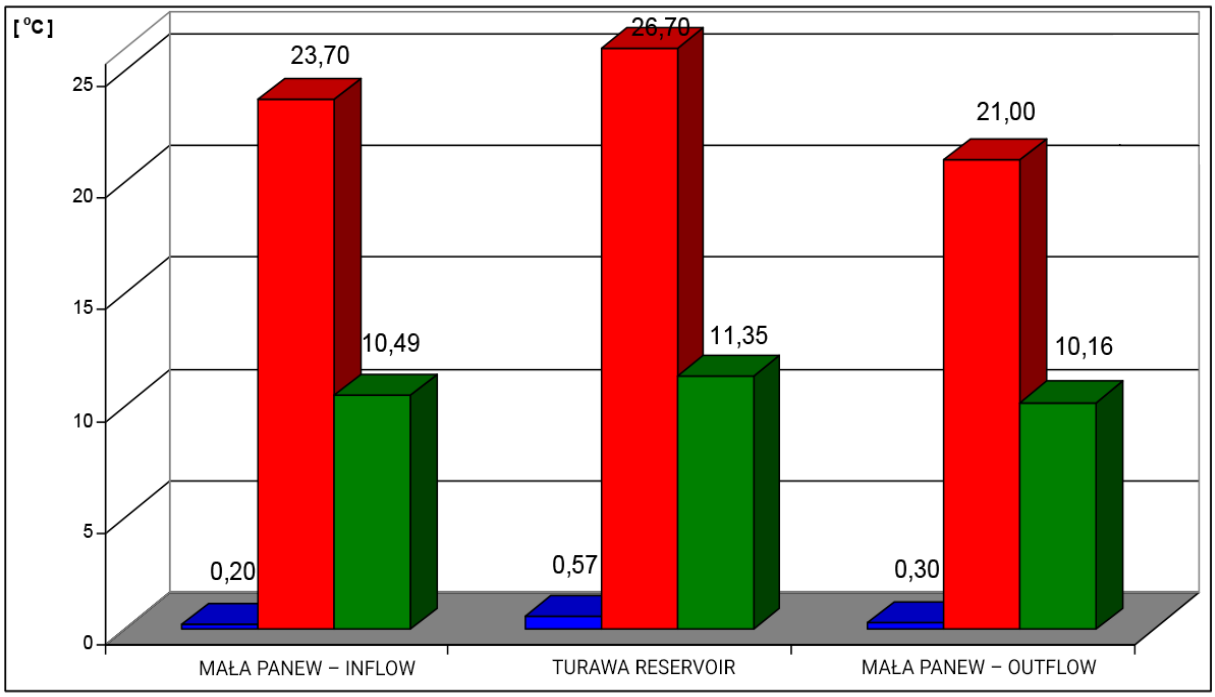

Fig. 2: Temperatures (minimum, maximum and average) of water at the following stations: the Mała Panew – inflow to the Turawa reservoir; the Turawa reservoir, and the Mała Panew – outflow from the reservoir, in the hydrological years 2004-2006

The period of ice laying was also influenced by the reservoir; it was longer for the Mała Panew downstream the reservoir than upstream the reservoir. This is typical for dam reservoirs.

4. Oxygen Saturation

The Turawa reservoir influenced saturation of water with oxygen in the Mała Panew river. In the whole period of studies the average oxygen content in the water of the river downstream the reservoir was a bit higher than that upstream. However, due to intensive eutrophication of the reservoir during summer quite high oxygen deficiency (40-60 %) was observed for the river downstream; it was so because the river was supplied with hypolimnion water which was oxygen deficient at that time of the year. All this can be detrimental for the river fauna.

Intensive eutrophication of the Turawa reservoir and resulting water blooming and then decay of algae and blue-green algae causes deterioration of taste and odour of water outflowing the reservoir. Water colour changed significantly, as well. During intensive blooming, water was intensively green (Photo 1).

Photograph 1: The intensively green colour of water in the Mała Panew downstream the reservoir.

The increase in suspended matter content and water turbidity resulted in the drop in water transparency. In fact, the use of the water for municipal water supply system and for power plant required additional purification. Moreover, the presence of blue-green algae prohibited the use of the water for domestic animal watering.

The mass dying of algae after blooming increased the content of organic matter expressed, e.g., as BOD_5 and COD_{Mn}. In the hydrologic years 2004 and 2006 the water in the Mała Panew downstream the reservoir was characterized by 8% and 16% increase (with respect to upstream) in BOD_5 and COD_{Mn}, respectively.

COD_{Mn} level in the Mała Panew water upstream the reservoir ranged from 4.3 to 14.7mg O_2 dm^{-3} (average 7.6mg O_2 dm^{-3}) while BOD_5 level ranged from 0.0 to 16mg O_2 dm^{-3} (average 2.6mg O_2 dm^{-3}).

5. Other Selected Importnt Physico-Chemical Parameters

The Turawa reservoir affects the water content of many inorganic cations and anions at the outflow of the Mała Panew. The most common anions are bicarbonates, nitrates, phosphates, sulphates, chlorides, while cations are Ca^{2+}, Mg^{2+}, K^{+}, and Na^{+}. The improvement in water quality, at least for some purposes, results from self-purification and dilution of the Mała Panew water with less polluted water of the two inflowing smaller rivers. Due to strong season dependent eutrophication and intensive CO_2 consumption during algae blooming the water outflowing the reservoir is characterized by relatively large increase in pH with respect to the inflowing water of the Mała Panew river. Moreover, pH changes within the wide range. The total hardness or the content of calcium and magnesium ions, generally expressed as mg $CaCO_3$ dm^{-3}, depends on the season. It was the lowest in winter and spring. The observed lowered water hardness in the Mała Panew downstream the reservoir is mainly due to biogenic precipitation of calcium in the form of $CaCO_3$. Similarly, the content of chlorides and the total salinity is lower by ca. 10% at the outflow of the Mała Panew. The problem will be described in more details and thoroughly discussed elsewhere.

6. Conclusion

Building-up of the dam on the Mała Panew river and formation of the storage reservoir, called the Turawa reservoir, has affected, to a significant degree, the water characteristics of the river downstream the reservoir [6].

Some changes such as drop in conductivity, hardness, salinity, content of nitrates and phosphates can be regarded as advantageous for most purposes. However, many of the changes are surely unwanted. They include deterioration of water colour, odour and taste; increase in oxygen deficiency in some periods; an increase in organic pollution and in pH; and in the content of quite a few heavy metals.

Many changes result from the strong eutrophication of the reservoir. Numerous recreational centres and villages situated around the reservoir did not have sewage system and are the important source of some pollutants. Moreover, the way of water is managed causes fluctuations of water level resulting in reservoir bottom uncover. This reduces the self-purification capability of the water body and deteriorates water quality.

A lot of efforts have been successfully undertaken to reduce unwanted effects and improvement in water quality is being observed. Further studies on monitoring of the quality of the water in the reservoir itself and in the Mała Panew river flowing through are in progress.

7. References

[1] Z. Masood, H. Ur Rehman, A.B Baloch, N. Ul Akbar, M. Zakir, I. Gul, N. Gul, N. Jamil, N. Din, B. Ambreen, I. Shahid, T. Ahmad, T. Shah, M. Masab, A. Ha, Analysis of Physicochemical Parameters of Water and Sediments Collected from Rawal Dam Islamabad. American-Eurasian Journal of Toxicological Sciences. 7, 123-128, 2015

[2] R. Kornijów, Controversies around dam reservoirs: benefits, costs and future, Ecohydrology & Hydrobiology, 9, 141-148 2009,

[3] O.J Achadu, F.E Ako, C.L Dalla, Quality Assessment of Stored Harvested Rainwater in Wukari, North-Eastern Nigeria: Impact of Storage Media. IOSR Journal Of Environmental Science, Toxicology And Food Technology (IOSR). 7, 25-32, 2013

[4] P. Mihailova, I. Traykov, A. Tosheva, M. Nachev, Changes in biological and physicochemical parameters of river, Water in a small hydropower reservoir Cascade. Bulgarian Journal of Agricultural Science.19, 286–289, 2013

[5] B.U Ibrahim, J. Auta, J.K Balogun, An assessment of the physico-chemical parameters of Kontagora reservoir, Niger state, Nigeria. Bayero Journal of Pure and Applied Sciences. 2, 64 – 69, 2009

[6] S. Tsakovski, B. Kudlak, V. Simeonov, L. Wolska, J. Namiesnik, Ecotoxicity and chemical sediment data classification by the use of self-organising maps. Analytica Chimica Acta. 631, 142-152, 2009

International Proceedings of Chemical, Biological and Environmental Engineering
Volume 94 of IPCBEE (2016)
DOI: 10.7763/IPCBEE. 2016. V94. 10

Research on Landfill and Composting Guidelines in Kigali City, Rwanda Based on China's Experience

Josephine Isugi, Dongjie Niu [+]

The State Key Laboratory of Pollution Control and Resource Reuse, School of Environmental Science and Engineering, Tongji University, Shanghai 200092, China

Abstract. Due to the population growth and the improvement of life standards, there is a growing concern associated with waste generation in Kigali city. All collected waste goes to the only one landfill in Kigali and the waste composition is dominated by organic waste up to 68%. Some efforts were made to handle solid waste in Kigali City, but there are still some weaknesses related to waste disposal facilities. Most of data used in this paper are collected directly or indirectly from literature, government websites, and institution reports which are related to solid waste management and official media. This paper used a comparative analysis for Kigali city and China in order to propose guidelines that could be referred to improve the design of landfill and composting plants in Kigali city. This paper is proposing Kigali City to refer to Chinese standards on landfill and composting plants. China has important standards on liner system, leachate collection, cover standards, environmental monitoring standards that can be referred to in construction and monitoring the functionality of a landfill in Kigali city. The materials such as geotextile, Perforated HDPE pipe and others used in China should be tested if they are compatible with soil, weather, and other environment issues in Kigali City before using them. Composting is very necessary in Kigali City because 68% of solid waste generated is organic waste. MSW aerobic static composting standards in China such as moisture content, leachate collection, temperature could be followed in order to introduce the standards of composting in Kigali city, compost can be used in agriculture as 90% of Rwandans are formers.

Keywords: China'S Experience, Compost, Guidelines, Kigali, Landfill.

1. Introduction

Rwanda is a small country located at the east central Africa. Rwanda has a capital city called Kigali, covering an area of 730 km^2 in the central part of Rwanda, serves about 1,223,000 people and Kigali's population density is 1600 per km^2 Currently GDP per capita is 724$, a 3 fold increase from 2000 and the GDP target is $1,240 by 2017 [1-3].

Nduba dumpsite remains the current only facility in Kigali that deals with collected solid waste which receives about 400 tons per day of unsorted waste or 140,000 tons per year [4]. Solid wastes in Kigali City are mainly made by food remnants up to 68 %, the average waste generation is between 1800 and 2000 t per day [5, 6]. Organic solid waste should be composted for use in agriculture or kitchen gardening, which is mainly kitchen waste, plants, leaves [7, 8]. If a portion of the waste stream consists of organics or can be easily separated into organics and non-organics, composting may become a viable waste management strategy [9].

Kigali is facing significant challenges in relation to solid waste disposal. Waste generation is increasing, while a sizeable portion of it is disposed on improperly located and operated dumpsites and resulting in adverse impacts on environment and health [10]. Reports from various institutions claim that garbage management in Kigali has had diverse effects on both the natural environment and human society [4]. Deep seated fires, methane explosions, landslides and leachates threatening rivers and groundwater are some of the

[+] Corresponding author. Tel.: 86-13917100764.
E-mail address: isujo20@gmail.com.

common problems of such basic dumpsite [11]. Launched in 2012, the Nduba dumpsite was established to avoid these potential disasters, poor sanitation practices and among other issues but it has problems of not being a sanitary landfill, with no proper engineered lining system to prevent leachate from contaminating the ground and no gas collection facilities.

Although many studies have been done regarding solid waste management systems in Kigali City (J BAZIMENYERA, Qiang Fu, Karangwa Antoine [5], Innocent Kahigana [12], REMA 2013 [13], and RURA 2009 [14]) there is no reported study which was focused on landfill and composting guidelines.

This paper referred to Chinese guidelines such as pollution Control on the Landfill Site of Municipal Solid Waste (GB16889) which was first released in 1997 and then amended in 2008; technical specification for operation, maintenance and safety of municipal solid waste composting plant (CJJ/T86-2000) for MSW composting [15]. These guidelines were issued by the Ministry of construction, the State Environmental Protection Administration, and the Ministry of Science and Technology.

Landfill and composting are promising for a developing country as Rwanda which is solid waste are increasing quickly and organic waste are dominating in solid waste composition. China has experience in landfill and composting, therefore, this paper is proposing Kigali City to refer to Chinese guidelines on landfill and composting. China has important standards on liner system, leachate collection, cover standards, environmental monitoring standards that can be referred in construction and monitoring the functionality of a landfill in Kigali city.

2. Current Situation of MSWM in Kigali City of Rwanda

2.1. Location

Rwanda has a capital called Kigali city, covering an area of 730 km^2 in the central part of Rwanda, serves about 1,223,000 people, Kigali's population density is 1600. Kigali City is built on interlocking hills, has an annual average temperature of about 20˚C [4].

Kigali city has only one landfill located at North East of Kigali at Gasabo District, Nduba hill at Muremure cell at 10 Km from Kigali Center [13]. The dumpsite in Kigali receives about 400 tons per day of solid, not sorted waste or 140,000 tons per year. Even though, all waste collected in Kigali City are brought to Nduba landfill according to Kigali state of environment 2013 [16], a big part of Kigali city doesn't have collection system.

Kigali, which is very hilly, has changing wind directions throughout the day [17]. As the general annual trend of wind direction is from North and North-East to the South, the southern part of Kigali would expect to have highest concentration air pollution than other area in the entire city [18].

Rwandan soils are naturally fragile. They are generated by physicochemical alteration of basic schistose, quartzite, gneissic, granite and volcanic rocks that make up the superficial geology of the country [19]. Granitic and meta-sedimentary rocks underlie the City of Kigali; these include schists, sandstones and siltstones. Lateritic soils, rich in iron and aluminium, dominate the city's hillside surfaces while alluvial soils (fertile soil deposited in river valleys) and organic soils are found in the lowlands and wetlands. Inappropriate development on Kigali's hilly slopes has caused extensive soil erosion in some areas [1]. The City of Kigali has a hilly topography with soil permeability and stability of 0.01- 0.7 cm/min [20].

2.2. Data collection and methodology

Data of any kind involving solid waste is generally not widely valued, available or shared in Rwanda. In order to obtain the potential materials regarding solid waste, most data used in this paper are collected directly or indirectly from literature, government websites, reports and institutions which are related to solid waste management and official media. Kigali was expanded in 2007, so data for population, GDP per capita and solid waste generation starts from 2007.

This paper uses a comparative analysis for Kigali city and China in order to propose guidelines that could be referred to improve the design of plants and environmental monitoring. In order to profit from China's experience in MSWM and learn some lessons for Rwanda. This research uses a descriptive study to show the situation of MSWM in both countries Rwanda and China and then it will discuss some guidelines

on composting and landfill made by Rwandan government and Chinese government to conclude some recommendations for Rwanda.

3. Results and Discussion

3.1. Problem analysis

Rwanda is facing significant challenges in relation to solid waste management. Waste generation is increasing, while a sizeable portion of it is disposed on improperly located and operated dumpsites, resulting in adverse impacts on environment and health. Reports from various institutions claim that garbage management in Rwanda has had diverse effects on both the natural environment and human society [4]. While meeting demands for waste disposal, larger landfills can reduce the costs of land acquirement and environmental assessments, and can be equipped with better pollution control facilities [21].

Kigali city could learn from China technical standards pertaining to MSWM. Such as Pollution Control Standard for MSW Landfills (GB16889-1997) which was amended by the Ministry of Environmental Protection in July 2008. The new standard (GB 16889-2008) placed stricter regulations on the construction of landfill sites and established more rigorous pollution controls.

3.2. Waste increase

Kigali City's solid wastes are highly increasing in the quantity and quality as the number of population and economic activities are increasing while the land for disposal is becoming scarce. Composting and good landfill methodologies are the most viable alternatives for managing solid waste in Kigali City; however, no single method will control the waste problem as effectively as a comprehensive program that relies on a number of solutions for different situations and the direct involvement of citizens is essential.

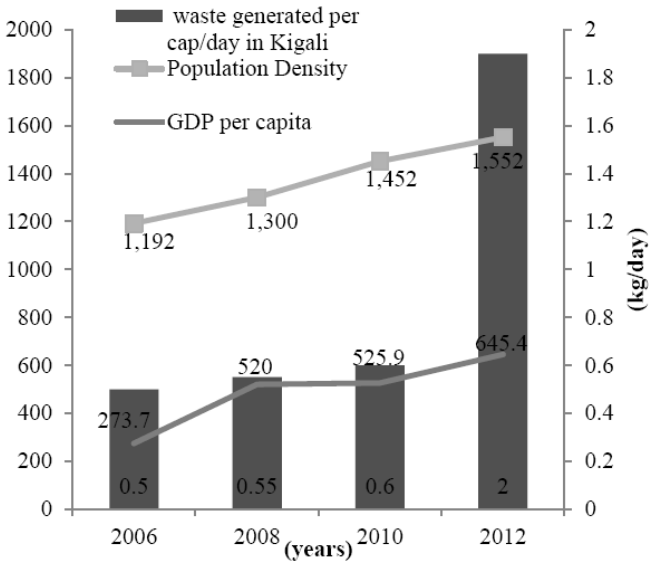

Fig. 1: Waste generation per capita, population density and GDP per capita per year in Kigali City.

Kigali city has currently reached a density of 1600 population per km square from 1,192 in 2007 and Kigali is ranked as the first city in Africa which has the highest density. Rwanda is a developing country in 2007, GDP per capita was $273.7 and in the same year waste generation per day per capita was 0.5 Kg however in 2012 GDP reached $645.4 per capita and waste generated was times four more than in 2007 and reached 2kg per capita per day as shown Fig. 1. All these data prove the necessity of improving solid waste disposal because of increasing of solid waste linked with high population and economic development.

The average waste generation is between 1800 and 2000 t per day in Kigali but 400t are collected to Nduba landfill. Kigali City's population is expected to double by 2020 to 2 million inhabitants; currently the City of Kigali has 1,223,000 million inhabitants with annual growth of 4.0 percent. This growth goes with increasing demand for basic services and puts an unrelenting pressure on the environment in general.

3.3. Mixed waste

Solid wastes composition in Kigali City as shown in Fig. 2 are mainly made by food remnants up to 68 % and in China also organic waste takes 56% of waste generated as shown in Fig. 1. If organic waste is diverted for composting, it can be beneficial to agricultures as 90% of Rwanda are formers [22], [6].

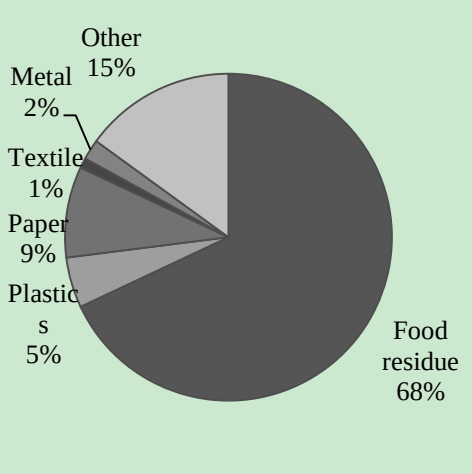

Fig. 1: Waste composition in Kigali City.

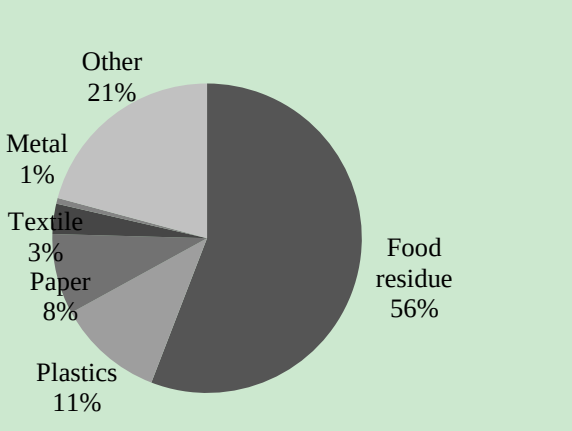

Fig. 2: Waste composition in China.

3.4. Comparision of technical requirements on Landfill between China and Kigali City.

Kigali city could learn from China how liner system and a barrier liner are accomplished, double liner and barrier layers are very necessary for a sanitary landfill. Chinese materials might not perform well in Rwanda because the soil, climate are not the same for both countries that is why some test are required such as soil test, geomembrane, geotextile and other materials.

Leachate facilities are very necessary for a sanitary landfill, if leachate is not collected, it can penetrate and pollute ground water. So, a strategic plan should be applied in Kigali City in order to collect well leachate, sand drainage layer is not enough that is why constructors of landfills in Kigali should refer to Chinese methods of using nonwoven geotextile, perforated HDPE pipe and other materials and test them before if they will perform well in Rwanda.

Pollution control is essential for a sanitary landfill; China has a Code for pollution control: GB16889-2008 that Rwanda can be referred to set pollution control in the landfill. China's code for pollution control is very detailed and easy to understand for a developing country as Rwanda.

A sanitary landfill should have a monitoring system of groundwater, landfill biogas, and leachate as it is mentioned in Chinese Code of monitoring: MOC/NCEC2001, CJJ/T 3037-1995 and GB/T18772-2008. Kigali city should refer to these codes in order to set adequate requirements of environmental monitoring.

A sanitary landfill has also a daily cover, intermediate cover and a top cover system but in Kigali's landfill, they try to put a daily cover only but also intermediate covers are also needed with adequate materials which are adaptable on Kigali city's environment. In Kigali sand, clay, gravel can be found easily but geomembrane and nonwoven geotex should be tested in order to know if they will not cause other problems.

3.5. Composting standards in China that could be referred to in Rwanda

According to Rwanda Environmental Management Agency, 50 % of wastes which goes to Nduba landfill are of good quality for composting, such as waste from purely residential neighborhoods, and wastes from special generators such as markets, restaurants, and slaughterhouses [23].

Temperature is a critical factor in determining the rate of decomposition that takes place in a composting pile. Composting temperatures largely depend on how the heat generated by the microorganisms is offset by the heat lost through controlled aeration, surface cooling, and moisture losses [24]. Kigali's average high temperature through the year is 26.89˚C and average low temperature through the year is 15.73˚C.

Composting should be considered as part of an integrated solid waste management strategy with appropriate processing technologies selected based on market opportunities, economic feasibility, and social acceptance.

Composting plant construction evaluation should address the following elements according to urban wastes for agricultural control standards in China GB8172 with life waste composting plant evaluation criteria CJJ / T 172-2011 and also MSW Composting plant technical evaluation CJ / T 3059 requirements [25].

A composting plant overall design in China has (unloading feed system; garbage sorting system; waste fermentation system; reprocessing facilities; ventilation dust and odor control system and leachate treatment facilities).

China's applicable standards compost 8 CJJ / T52 93 gives the static aerobic composting of municipal solid waste disposal requirements. MSW Aerobic Static Composting shall have relevant standards which are total nitrogen organic matter less than 8%, total phosphorus less than 0.2% and the total potassium less than 0.8%, ph value does not exceed the maximum.

The compost biological parameters control standards are compost products pathogen content should be less or even zero, moisture content should meet the following requirements should be 25% to 35% carbon-nitrogen ratio. To achieve this purpose, the stack body temperature should be maintained at 55°C, and hold duration of not less than 5 days.

The static aerobic composting of municipal solid waste could be used in Kigali city since 68% of Municipal solid waste is organic waste. The process could be successful because the compost can adapt to Kigali's temperature. The compost can be used in agriculture sector as a fertiliser since 90% of Rwandans are farmers.

4. Suggestion Guidelines on Landfill and Composting in Kigali City

In Kigali city, there is a gap in designing landfill and composting plants, also, pollution control should control the whole system of these plants. China has a lot of experience that Rwanda could learn.

On Landfill, there should be:

(1) Liner system: In Nduba landfill, there is no liner system; therefore, this paper is suggesting double liner and barrier liner systems because their materials are available in Rwanda.

(2) Leachate system: Sand drainage layer is not enough for Nduba landfill, so, test of some materials such as perforated HDPE pipe, woven geotextile and nonwoven geotextile should be performed in order to know if they can be adaptable in Rwanda to facilitate leachate extraction.

(3) Cover system design: Daily cover is not sufficient for Nduba landfill, there should be provision of an intermediate cover and top cover systems.

(4) Pollution Control: Pollution control such as Methane, leachate and groundwater monitors should be established in order to protect groundwater and surrounding environment of landfill.

On Composting plant, Kigali city could learn:

Design of composting plant should have (unloading feed system; garbage sorting system; waste fermentation system; reprocessing facilities; ventilation dust and odor control system; leachate treatment facilities and daily waste volume should be known).

5. Summary

Landfill and composting are promising for a developing country as Rwanda which is solid waste are increasing quickly and organic waste are dominating in solid waste composition. China has experience in landfill and composting, therefore, this paper is proposing Kigali City to refer to Chinese standards on landfill and composting. China has important standards on liner system, leachate collection, cover standards, environmental monitoring standards that can be referred to in construction and monitoring the functionality of a landfill in Kigali city. The materials such as geotextile, Perforated HDPE pipe and others used in China should be tested if they are compatible with soil, weather, and other environment issues in Kigali City before using them.

Composting is very necessary in Kigali City because 68% of solid waste generated is organic waste. MSW aerobic static composting standards in China such as moisture content, leachate collection, temperature could be followed to introduce the standards of composting in Kigali city, compost can be used in agriculture as 90% of Rwandans are formers.

6. Acknowledgements

The contributions of individual through scholarship, advice, moral and participation herein mentioned contributed immensely to the completion of this paper.

7. References

[1] WorldBank, *Rwanda Electricity Sector Strengthening Project (P150634).* 2015.

[2] BK, *Bank of Kigali Investor Presentation Q1 2015.* 2015.

[3] BAD, <*Investing_in_Rwanda.pdf*>. 2014.

[4] Innocent, K., *Selection and implementation of an optimal system to handle garbage in Kigali, Rwanda.* 2011.

[5] J BAZIMENYERA, Qiang Fu, and K. Antoine, *Solid waste management in Kigali City, Rwanda.* East African Journal of Science and Technology, 2012. 2: p. 46-58.

[6] CoK, *Terms of reference for waste to energy project in the City of Kigali.* 2013.

[7] Knausenberger, W.I., et al., *Environmental Guidelines for Small-Scale Activities in Africa.* USAID Bureau for Africa, Office of Sustainable Development, SD Technical Paper, 1996. 18.

[8] Bernstein, J., *Social assessment and public participation in municipal solid waste management.* Worldbank, Urban Environment Thematic Group, Washington, 2004.

[9] UNEP-IETC, H., *International source book on environmentally sound technologies for municipal solid waste management, United Nations Environment Programme (UNEP).* International Environmental Technology Centre (IETC), 1996.

[10] RBS, *The special edition of the Rwanda Burreau of StandardsNewsletter*. March 2014.

[11] Rema, *National Implementation Plan for the Basel Convention on the Control of Transboundary Movements of Hazardous Wastes and Their Disposal 2014 – 2021.* August 2014.

[12] Kahigana, I., *Selection and Implementation of an Optimal System to Handle Garbage in Kigali, Rwanda*. 2011.

[13] REMA, *Kigali State of Environment and Outlook Report 2013.* 2013.

[14] RURA, *Guidelines on Minimum Requirements for Collection, Transportation, Recycling/Treatment and Disposal of Solid Wastes and on Management of Dumping Sites*. 2009.

[15] Yang, Z., H. Zhang, and D. Van Den Bulcke, *China Consulting Projects (CCP) Green means clean: Investing in China's Municipal Solid Waste Industry.* 2011.

[16] REMA, *Kigali State of Environment and Outlook Report 2013.* 2013.

[17] Rich, P.P., *Kigali Master Class.* 8/2014.

[18] NUR-CB, *A Study on Air Pollution in Rwanda with Reference to Kigali City and Vehicular Emissions*. May 2011.

[19] TWAGIRAMUNGU, D.F., *ENVIRONMENTAL PROFILE OF RWANDA.* July 2006.

[20] Kayitesi, M., *IMPROVING SANITATION SYSTEMS:"TECHNICAL AND SOCIO-ECONOMIC PERSPECTIVES".* 2008.

[21] Chen, X., Y. Geng, and T. Fujita, *An overview of municipal solid waste management in China.* Waste management, 2010. 30(4): p. 716-724.

[22] Zhou, H., et al., *An overview of characteristics of municipal solid waste fuel in China: Physical, chemical composition and heating value.* Renewable and Sustainable Energy Reviews, 2014. 36: p. 107-122.

[23] REMA, *Practical Tools on Solid Waste Management of Imidugudu, Small Towns and Cities : Landfill and Composting Facilities*. 2010.

[24] Richard, T.L., *Municipal solid waste composting: physical and biological processing.* Biomass and Bioenergy, 1992. 3(3): p. 163-180.

[25] Jie, J., *SUN Shi-qun~ 1, Michael Nelles~ 3, CAI Jing-min~ 2, YU Zhi-min~ 2, WU Ke~ 2 (1. School of Resources and Environmental Engineering, Hefei University of Technology, Hefei 230009, China; 2. Department of Biological and Environmental Engineering, Hefei University, Hefei 230022, China; 3. Fachhochschule Hildesheim/Holtzminden/Goettingen, Goettingen 37078, Germany); Comparison of Compost Standards for Bio-wastes Between Germany and China [J]*. Journal of Hefei University (Natural Sciences), 2006. 1.

International Proceedings of Chemical, Biological and Environmental Engineering
Volume 94 of IPCBEE (2016)
DOI: 10.7763/IPCBEE. 2016. V94. 11

Traffic Emitted PM10 Modelling Based on NaSch Model with Periodic Boundary

Wei Pan [1], Yu Xue [2] and Wei-Zhen Lu [1+]
[1] Department of Architecture and Civil Engineering, City University of Hong Kong, Hong Kong, HKSAR
[2] Institute of Physics Science and Engineering, Guangxi University, Nanning, China

Abstract. Congestion has always been considered as a big trouble due to large amount of time wasting. Moreover, as high frequency outbreak of haze weather and particulate matter (PM) related diseases, traffic congestion has once again appear in the forefront for its inescapable obligation. However, the effects of congestion on emitted particulate matter are only seldom incorporated in the predictions and measurements, which also hard to accomplish. Hence, by using classical NaSch model and emission function based on empirical measurements, this study aims to investigate the effect of congestion on the emitted PM emission from vehicles on-road. The simulation results show that when vehicle emitted particulate matter levels start to increase as traffic system get into jamming states, and no matter congestion occurs or not, acceleration is the major pollutant maker for total PM emission load. Related analysis of PM emission, fuel consumption and energy dissipation are also conducted.

Keywords: Particulate Matter, Nasch Model, Traffic Congestion, Energy Dissipation, Energy Consuming

1. Introduction

Increasing health awareness and longstanding concerns to the environment have largely prompted the subject of particulate matter (PM) research in the past two decades with bunch of works regarding the mechanisms of production, transformation and removal of particulate matter [1-3]. Meanwhile, road traffic is the dominant anthropogenic source of air pollution in urban areas around the world [4-6] and its contribution to particulate matter concentration is multidimensional. Hence, many researches that aiming at providing sound understanding on physiochemical properties, temporal-spatial distribution, and dispersion characteristics, of traffic related particulate matter emission, either experimentally or numerically have been conducted world widely [7]. Among all traffic related emission processes, traffic congestion has repeatedly been indicated as a major factor in road traffic emissions and urban air quality degradation [8-10], which imply the need to explore the dynamic behavior between traffic emission and traffic-flow [11].

Congestion is the most important contributor and impact factor for total traffic emission. The variables that determine vehicular exhaust emissions are mainly fleet composition, speed, speed limit, acceleration and deceleration rates, queuing time in idle mode during the red phase, queue length, traffic flow rate and ambient wind conditions [10]. The estimation of PM emissions from road traffic requires in-depth understanding of traffic characteristics, which cannot be told by using traditional statistical method that lacking capability to capture the dynamic process of traffic flow [11]. And it is difficult to depict the relationship between traffic congestion and PM emissions by carrying out mobile measurements in a solo car. As a consequence, the effects of congestion are only partially incorporated in the predictions and measurements.

In this paper, we want to investigate how does traffic congestion have impact on PM emission by combining the NaSch model and speed-acceleration emission relation. Note that this study is only a preliminary results that aims at finding a general trend between congestion and emission. According to the

+ Corresponding author. Tel.: + +852-34424316.
E-mail address: bcwzlu@cityu.edu.hk.

results, it seems that the emission load of particulate matter and traffic flow cannot reach best situation at the same time. Hence, the preliminary result here may benefit the future research on optimal planning.

2. Methodology

The whole model consists of two parts: traffic modelling and emission component. The application of NaSch model can provide the speed and acceleration of every agent (vehicle car) in the system at every time step during the whole (traffic activity) simulation life span. Meanwhile, fuel consumption (fc), energy dissipation (ed) and PM10 emission at each current time will be calculated by using above instantaneous information. Finally, analysis about the collective behavior of every individual car and corresponding PM emission would be provided

3. Traffic flow Component Submitting

The aim of introducing traffic component is to gain the needed information that enable whole model with the ability to depict the macroscopic flux, consumption and emission of the traffic flow by simulating every individual vehicle movement microscopically. Among multiple traffic models [12], cellular automaton (CA) ones, microscopically, are most popular for their simple algorithm, high generalization and rich phenomena.

NaSch model[13], a CA model proposed by Nagel and Schreckenberg in 1992, was able to reproduce the spontaneous emergence of traffic jams. It explicitly includes a stochastic noise term in one of its rules, commonly knowns as the first stochastic traffic cellular automaton model, which makes it different from the many previously deterministic CA models.

Generally, NaSch model is defined on a one-dimensional array L in dimensionless manner with each site may either be empty, or be occupied by one vehicle. Because in every time step, the vehicle can only change its position from grid to grid, hence, the velocity is an integer number in the range between zero and maximum velocity ($v_{\max}$) that expressed as the number of cells per time step. For an arbitrary configuration, NaSch model following four consecutive step, which are performed in parallel for all vehicles [14]:

1) Acceleration
$$v(i,t+1/3) \to \min(v(i,t)+1, v_{\max}), \tag{1}$$
2) Deceleration
$$v(i,t+2/3) \to \min(v(i,t+1/3)+1, gap_n), \tag{2}$$
3) Randomization with probability p
$$v(i,t+1) \to \min(v(i,t+2/3)-1, 0), \tag{3}$$
4) Car motion:
$$x(i,t+1) \to x(i,t+1)+v(i,t+1). \tag{4}$$

where $v(i,t)$ and $x(i,t)$ are the speed and position of the vehicle i on the road at time step t. Before the determination of its motion for the next time step $t+1$, the vehicle i should go through three steps (i.e. acceleration, deceleration and randomization), which indicated three commonly situations during driving process. Comparing to realistic traffic, it is easy to scale the model to make comparison with realistic traffic by converting the length of one site and a simulation time step into 7.5 meters of place and one second of time in real road scenario when $v_{\max}=5$, respectively, which is a velocity of about $135 km/h$ on a freeway.

4. Dimensionless Energy Consumption and Dissipation Component

According to the theorem of statistical mechanics, the kinetic energy of a moving car with mass m and velocity v is depicted in the formation as $mv^2(i,t)/2$, which could also be recognized as the fuel consumption of the moving car as the result of combustion, i.e., energy needed for acceleration, deceleration and following (cruising) the front car. Moreover, the reduced kinetic energy can be defined as dissipated energy [15]. Generally, energy dissipation was considered only in the scenario of deceleration occurred for kinetic energy decreasing. However, a board number of in-situ experiments indicate that, the biggest emission load emergence when vehicles accelerate [16], as energy dissipated due to road roughness affects rolling resistance and the resulting fuel consumption and pollutant emission [17]. Hence, energy dissipation would be considered in both acceleration and deceleration situation in our investigation.

For simplicity, it is supposed that the mass distribution of a car is uniform, which means if m_0 the mass of unit car length is, then the mass of the car with length l would be written as $m = m_0 \times l$. Hence, the dimensionless fuel consumption (fc) and energy dissipation (ed) for an arbitrary vehicle i at time step t are defined as:

$$fc(i,t) = \frac{l}{2} v^2(i,t) \tag{5}$$

$$ed(i,t) = \begin{cases} \frac{l}{2}[v^2(i,t-1) - v^2(i,t)], & for \quad v(i,t) < v(i,t-1) \\ 0 & for \quad v(i,t) = v(i,t-1) \\ \frac{l}{2}[v^2(i,t) - v^2(i,t-1)] & for \quad v(i,t) > v(i,t-1) \end{cases} \tag{6}$$

And the average fuel consumption of each car in every time step (F_C) is obtain as:

$$F_C = \frac{1}{T}\frac{1}{N}\sum_{t=1}^{T}\sum_{i=1}^{N} fc(i,t) \tag{7}$$

where N and T are the total number of vehicles in the system and corresponding total statistical time, respectively. Moreover, the fuel consumption fc can be catalogued into three types according to the speed of vehicles as acceleration (fc_a), deceleration (fc_d) and following (fc_f), which is shown as:

$$F_C = fc_a + fc_d + fc_f \tag{8}$$

Similarly, the energy dissipation ed is the sum of acceleration (ed_a) and deceleration (ed_d).

5. Dimensional Emission Component

The estimation modelling of pollutants cannot get rid of the help from emission factors which obtained from in-situ vehicle tracing measurements. Generally, the required 'factor' information can be categorized into two types: distance-based (g/km) and time-based (g/s). And in light of the NaSch model is distance-dimensionless with its simulation time step is equivalent to the real time, time-based (g/s) emission factor would be the priority choice. Hence, a general emission function proposed by using non-linear multiple regression techniques based on empirical measurements is given as [18]:

$$em(i,t) = \max[E_0, f_1 + f_2 v(i,t) + f_3 v^2(i,t) + f_4 a(i,t) + f_5 a^2(i,t) + f_6 v(i,t) a(i,t)] \tag{9}$$

where E_0 is a lower limit emission specified for both pollutant type and vehicle cetology, and f_1 to f_6 are emission constants determined by the regression analysis. As the study here concerns about only about the emitted particulate matter (PM_{10}) from petrol motor vehicles on the freeway which caused by acceleration (em_a), deceleration (em_d) and following (em_f), Table 1 only shows related values that would be used in after simulation.

Table 1: Parameters for Eq. (9)

E_0	f_1	f_2	f_3	f_4	f_5	f_6
0.0	0.0	1.57×10^{-5}	-9.21×10^{-7}	0.0	3.75×10^{-5}	1.89×10^{-5}

6. Results and Discussion

The simulation of the traffic behavior and related fuel consumption (fc), energy dissipation (ed) and PM_{10} emission is performed under periodic boundary condition, which means the number of vehicles in the system is conservation. In general, the averages are obtained by averaging over 30 independent initial realizations up to 3×10^5 iteration steps for each run and discarding the first 2×10^5 iteration steps as transient time. The length of the lane is set to be $L = 1\times10^5 \times l$ with related fixed parameters as $v_{\max} = 5, p = 0.2, l = 1$.

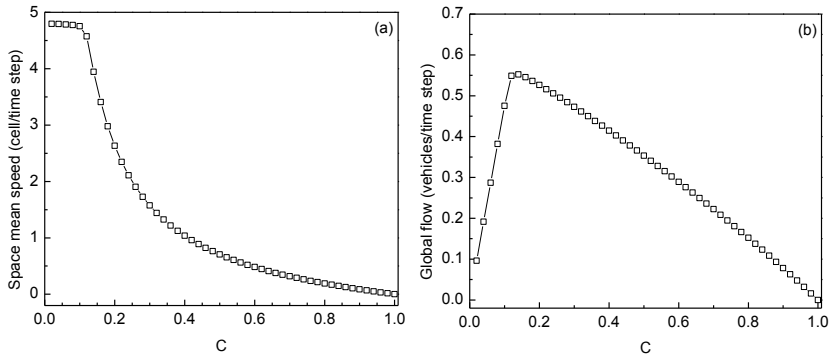

Fig. 1: Fundamental diagrams of the NaSch model (a) space mean speed; (b) global flow.

According to classical traffic theory, the estimation of vehicles moving capability on the road is based on the mean speed or flux, which we called fundamental diagrams as shown in Fig. 1. Here, the occupancy c indicates the proportion of lattices that have been occupied, which amount to the lane usage rate. As more and more cars occupy the road, space mean speed change (Fig. 1(a)) from a platform ($\bar{v} \approx 4.7$) into a slow crash at $c \approx 0.12$, which corresponding to a first phase transition process from free flow into jamming phase that increase first then collapse in global flow, and finally global congestion (Fig. 1(b)).

Fig. 2 presents the average of fuel consumption (fc) and energy dissipation (ed) of the NaSch model. It can be easily found the phase transition points (or critical point), both fc and ed, occur around the same occupancy rate shown in Fig. 1, which indicates that the trends of fc and ed are decided by the law of fundamental diagrams. Specifically, before the critical point, most of the fuel consumption was caused by the following behavior of the cars, then comes after acceleration and deceleration (Fig. 2(a)). After that the total of fuel consumption decrease for all three factors share goes down, which is the result of decreasing mean speed. Then, at some point (here about $c \approx 0.30$), acceleration took the place of following as the dominant contributor to the fuel consumption, which was caused by all vehicles in the system got stuck in the 'go and stop' mode. And the energy dissipation (Fig. 2(b)) told that the acceleration and deceleration had almost the same contribution to the total energy dissipation in the case study.

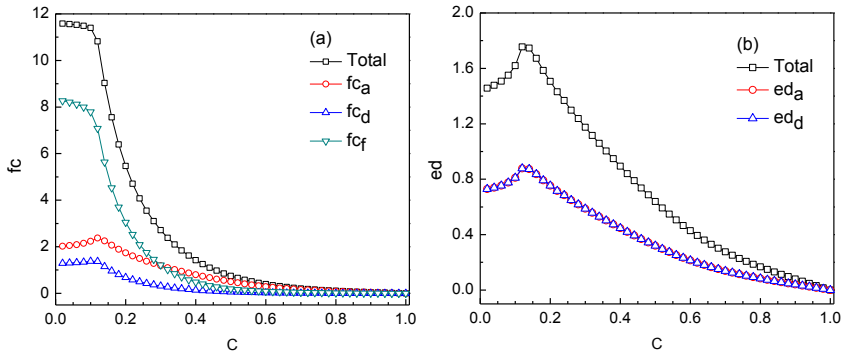

Fig. 2: Average of (a) fuel consumption and (b) energy dissipation of the NaSch model.

According to the emission function given by Eq.(9), we can calculate the average emission of PM_{10} per vehicle in every time step by using the instantaneous velocities and accelerations obtained from the NaSch model as provided in Fig. 3(a). Firstly, the acceleration vehicles had always lead the dominant role to the total PM_{10} emission in the whole span of the simulation, which agrees to most of the previous in-situ experiments. While car following behavior, vehicle speed at this moment was the same as last time step, produced least particulate matter. Another important point is that, before the critical value $c \approx 0.12$, almost all of the emission was caused by the behaviour of acceleration. And after that, where system goes into jamming phase, the emission suddenly climbed up, and the peaks of PM_{10} emission appeared at about $c \approx 0.30$, when acceleration began to act as the biggest fuel consumer as shown in Fig. 2(b).

In order to get better understanding of the emission activities, it is necessary to analyze the ratio of vehicles states. Fig. 3(b) presents the average ratio of vehicle states (acceleration, deceleration, following the frontal car, and jamming that speed equals zero) according to the increasing occupancy. In all situations of different vehicle lengths, before reaching the critical transition point, the majority of cars maintain in the

following states within almost full speed (v_{max}), while can hardly spot the car in jamming states. Moreover, vehicles in the states of acceleration and deceleration receive the same share. When reaching the critical point, jamming cars begin slowly emerging and the proportion of cars in the states of following drops sharply. Meanwhile, the acceleration cars present a small growing peak and the deceleration cars slightly raise, where cross points are observed around $c \approx 0.30$ correspondingly among the ratio of deceleration, following and jamming with the emergence of the total PM emission peak values (Fig. 3(a)); while at the last stage, except the ratio of jamming states, all other three phases' proportions shrink to zero.

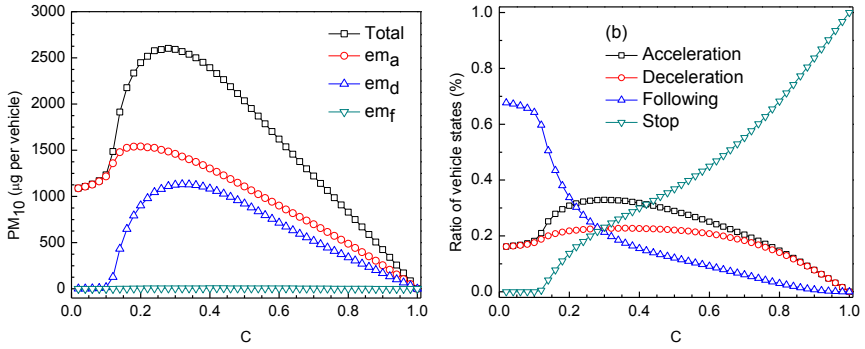

Fig. 3: (a) PM10 emission and (b) corresponding ratio of vehicle states of the NaSch model.

Lastly, rescaled parameters were used to quantify the trend of the PM emission per fuel consuming and dissipation as the traffic flow change from free flow to congestion with results shown in the Fig. 4. As a whole, the total PM_{10} per unit fuel consuming has little change until the system turn into the jamming phase that began to grow as the more cars appeared on the road. However, it is interesting to find that although acceleration produced most emission (Fig. 3(a)), it was the emission load for every unit fuel consuming for deceleration and following that grow exponentially after phase transition into traffic congestion, which means that the aggravating traffic jamming may have great influence on the emission load that made by energy combustion in unit for the broadening behavior of low speed following-deceleration-following. Although not in exponentially manner, the PM_{10} emission per unit energy dissipation reveals some similarities as PM_{10} emission per unit fuel consumption.

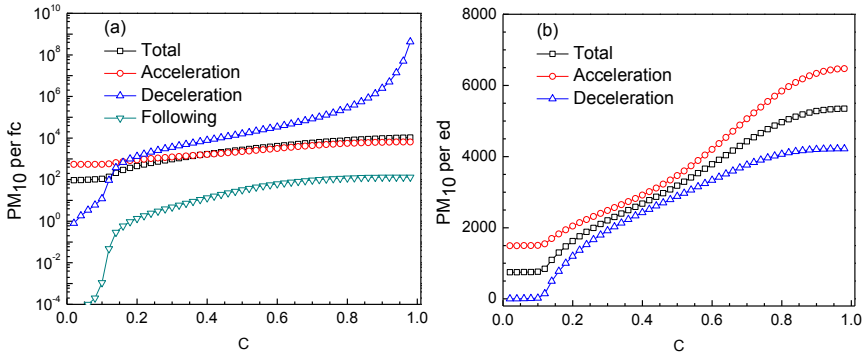

Fig. 4: PM10 emission per (a) fuel consumption and (b) emission dissipation of the NaSch model.

7. Conclusion

This study investigated the impact of congestion on traffic emitted PM_{10} based on NaSch model and empirical emission function. From the simulation results, the model here could well agree to daily measurement experience that vehicles produced more PM_{10} when congestion happened and acceleration was the major contributor to traffic emitted PM_{10}. Although results here were only obtained from a specific case study with limited traffic factors been considered, the model has shown its potential on studying the relation between congestion and emitted PM_{10} that called for further investigation and discussion.

8. Acknowledgements

The work was partially supported by Strategic Research Grant, City University of Hong Kong Grant (SRG-7004360), and National Natural Science Foundation of China (No. 11262003 & 11302125).

9. References

[1] Harrison RM, Yin J. Particulate matter in the atmosphere: which particle properties are important for its effects on health? Science of the total environment, 2000, 249(1), 85-101.

[2] M.J. Kleeman, J.J. Schauer, and G.R. Cass. Size and composition distribution of fine particulate matter emitted from motor vehicles. Environmental science & technology, 2000, 34(7), 1132-1142.

[3] P. Pant, and R.M. Harrison. Estimation of the contribution of road traffic emissions to particulate matter concentrations from field measurements: a review. Atmospheric Environment, 2013, 77, 78-97.

[4] P. Wåhlin, R. Berkowicz, and F. Palmgren. Characterization of traffic-generated particulate matter in Copenhagen. Atmospheric Environment, 2006, 40(12), 2151-2159.

[5] Querol X, Alastuey A, Moreno T, Viana MM, Castillo S, Pey J, De La Campa AS. Spatial and temporal variations in airborne particulate matter (PM 10 and PM 2.5) across Spain 1999–2005. Atmospheric Environment, 2008, 42(17), 3964-3979.

[6] M. Sillanpää, A. Frey, R. Hillamo, A.S. Pennanen, and R.O. Salonen. Organic, elemental and inorganic carbon in particulate matter of six urban environments in Europe. Atmospheric Chemistry and Physics, 2005, 5(11), 2869-2879.

[7] N.S. Holmes, and L. Morawska. A review of dispersion modelling and its application to the dispersion of particles: an overview of different dispersion models available. Atmospheric Environment, 2006, 40(30), 5902-5928.

[8] K.O.K. Oduyemi, and B. Davidson. The impacts of road traffic management on urban air quality. Science of the total environment, 1998, 218(1), 59-66.

[9] D. Carr, von O. Ehrenstein, S. Weiland, C. Wagner, O. Wellie, T. Nicolai, and von E. Mutius. Modeling annual benzene, toluene, NO2, and soot concentrations on the basis of road traffic characteristics. Environmental research, 2002, 90(2), 111-118.

[10] R. Smit. An examination of congestion in road traffic emission models and their application to urban road networks, 2006 (Doctoral dissertation, Griffith University).

[11] A. Goel, and P. Kumar. A review of fundamental drivers governing the emissions, dispersion and exposure to vehicle-emitted nanoparticles at signalised traffic intersections. Atmospheric Environment, 2014, 97, 316-331.

[12] D. Chowdhury, L. Santen, and A. Schadschneider. Statistical physics of vehicular traffic and some related systems. Physics Reports, 2000, 329(4), 199-329.

[13] K. Nagel, and M. Schreckenberg. A cellular automaton model for freeway traffic. Journal de physique I, 1992, 2(12): 2221-2229.

[14] S. Maerivoet, and B.D. Moor. Cellular automata models of road traffic. Phys. Rep., 2005, 419, 1-64.

[15] Y. Xue, S.J. Kang, W.Z. Lu, and H.D. He. Energy dissipation of traffic flow at an on-ramp. Physica A: Statistical Mechanics and its Applications, 2014, 398: 172-178.

[16] P. Kumar, A. Robins, S. Vardoulakis, and R. Britter. A review of the characteristics of nanoparticles in the urban atmosphere and the prospects for developing regulatory controls. Atmospheric Environment, 2010, 44(39), 5035-5052.

[17] A. Louhghalam, M. Tootkaboni, and F.J. Ulm. Roughness-Induced Vehicle Energy Dissipation: Statistical Analysis and Scaling. J. Eng. Mech., 2015, 04015046.

[18] L.I. Panis, S. Broekx, and R. Liu. Modelling instantaneous traffic emission and the influence of traffic speed limits. Science of the total environment, 2006, 371(1): 270-285.

International Proceedings of Chemical, Biological and Environmental Engineering
Volume 94 of IPCBEE (2016)
DOI: 10.7763/IPCBEE. 2016. V94. 12

The Impact of Road Blockage on Local Particulate Matter Multifractal Nature during the Hong Kong Protest

Wei-Zhen Lu [1 +], Wei Pan [1] and Yu Xue[2]

[1] Department of Architecture and Civil Engineering, City University of Hong Kong, Hong Kong, HKSAR
[2] Institute of Physics Science and Engineering, Guangxi University, Nanning, China

Abstract. Traffic emitted particulate matter in urban area has arisen concern both from public and authorities. In addition to technology improvement, traffic control is also considered as a promising way to enhance local air quality, but relevance effectiveness is always hard to describe and quantify. As an unexpected road blockage arose during Hong Kong protest and lasted more than 70 days, the aim of this study is to assess the influence of traffic flow transfer on the multifractality of local particulate matters (PMs). Based on the data sets before, during and after the protest, results show that road blockage does not interfere the daily cycle of PM in urban area, but can change the multifractality trend by intensifying their long-term persistence.

Keywords: Particulate matter, Road Blockage, Autocorrelation, Multifractality.

1. Introduction

Previous studies and observations have shown that motor vehicle emissions constitute the major anthropogenic source of particulate matter (PM) in the urban environment, which threat public health though daily inevitable exposure. Although traffic control is assumed to be the most effective ways to better the situation as they cut off the emission directly, but improvements from socio-political mechanisms like reroute traffic is always hard to detect and quantify [1]. The emergence of blockages during Hong Kong protest from late September to mid-December in 2014 offered an unexpected chance to evaluate the influence of emission control oriented traffic reroute plan on local air pollutant.

Moreover, measured database, similar to complicated system, contains large information like seasonal and meteorological change, complicated oscillations and interference, and etc., which need further analysis in detail, either qualitatively or quantificationally. Multifractality is regarded as the inherent property of complex systems, which may result from long-range correlation or strong fluctuation with persistence enhancement [2]. And this persistence of atmospheric time series is not only dangerous to public health, but also makes management and control of air pollution very difficult. Meanwhile, Multifractality has been found and analysed for air pollutant sequences broadly [3-6].

By using combined statistical methods, i.e. autocorrelation and multifractal detrended fluctuation analysis (MF-DFA), this paper analyses particulate matter data from a roadside station (Causeway Bay) and a background station (Tap Mun) to evaluate the influence of shift traffic flow on local PM sequences. The outputs are expected to benefit the future reroute planning.

2. Data and Methodology

2.1. Materials

+ Corresponding author. Tel.: + +852-34424316.
E-mail address: bcwzlu@cityu.edu.hk.

The key protest emerged with traffic closed for more than 70 days in Admiralty, Causeway Bay and Mong Kok ever since 27th September 2014, where are very close to three Hong Kong Environment Protection Department (HKEPD) roadside monitoring stations at Central, Causeway Bay and Mong Kok. Hence, the study picked the Causeway Bay on Hong Kong Island as the study object, and Tap Mun (or Grass-Island) as the background site in the north-eastern part of Hong Kong which is far away from the protest region. And the timeline of study period is set to be 79 days since the traffic blockage in Causeway Bay was cleared eventually on 15th December: before the protest (from 11th July to 27th September), during the protest (from 28th September to 15th December), and after the protest (from 16th December to 4th March 2015).

The hourly time series are available at HKEPD official website [7] and the original data sets are described in Fig. 1 accordingly with 1896 data points for both respirable suspended particulates (RSP) and fine suspended particulates (FSP). It is found that before the protest happened, the average hourly concentration of RSP and FSP in Causeway Bay were largely above the levels in Tap Mun. However, during the protest period, it seemed that roadside PMs concentrations have dropped into the same level. And when road blockage was cleared, the PMs gradually returned to historical levels. Hence, comments like road blockage has made the air was much fresh than before aroused.

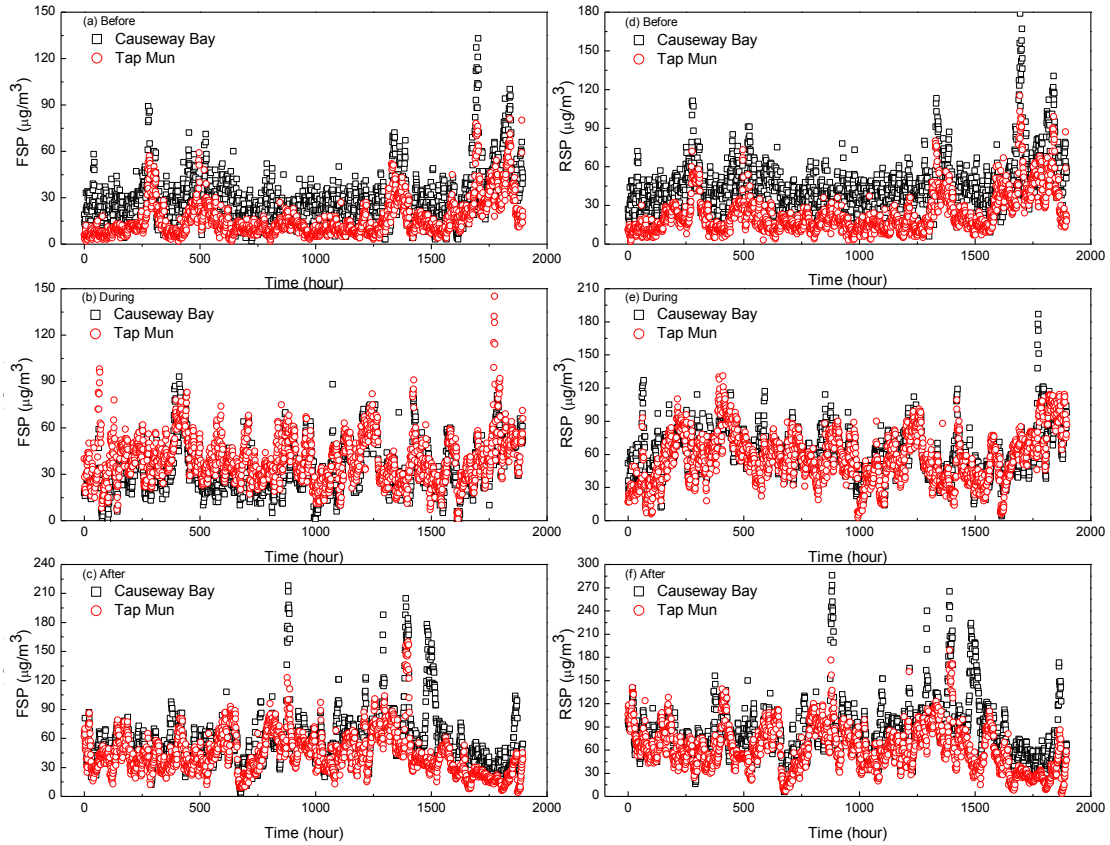

Fig. 1: Sequence of concentration of RSP and FSP in Causeway bay and Tap Mun

2.2. Autocorrelation

Most of time sequences are the superposition results of cyclic variations and random fluctuations [8]. Generally, amplitudes of cyclic variations are larger than random fluctuations and cyclic variations in the time domain can be identified by virtue of correlation analysis. Hence, the autocorrelation [9] at lag τ for series $x(i)$ $(i=1,\cdots,N)$ is

$$C(\tau)=\frac{<x(i)-<x>><x(i-\tau)-<x>>}{\sigma^2}=\frac{\frac{1}{N}\sum(x(i)-mx)(x(i-\tau)-mx)}{\frac{1}{N}\sum(x(i)-mx)^2} \quad (1)$$

where the angular bracket $<\cdots>_n$ indicates the average over time and N denotes the total number of time series data point. Besides, σ^2 and mx indicate the variance of the time series and the means of the corresponding series, respectively. If a time series is periodic in time, then the autocorrelation function is also periodic in terms of the lag τ, and the relative maximum of $C(\tau)$ that yields the correlation coefficient for τ.

2.3. MF-DFA method

Detrended fluctuation analysis (DFA), first proposed by Peng et al [10], is a scaling analysis method for detection of long-range correlations embedded in data sequence and takes advantages of easy implementation and robust estimation. Based on the DFA method, multifractal detrended fluctuation analysis (MF-DFA) was proposed as an extended method to address the multifractal nature that embedded in time series [11]. The MF-DFA algorithm addresses much attention and contains the following steps:

Step 1. Reintegrate the new time series $Y(i)$ from the original time series $x(i)$,

$$Y(i) = \sum_{k=1}^{i} [x(k) - < x >], i = 1,2,\cdots N \tag{2}$$

where $< x >$ denotes the mean value of $x(i)$.

Step 2. Divide the profile $Y(i)$ by s and get $N_S \equiv \text{int}(N/s)$ segment of non-overlapping data. Note if the length N is not the integer times of time scale s, and for the sake of not disregarding the remaining part of the profile, the same procedure is repeated starting from the opposite end. Thus, $2N_S$ segments are obtained.

Step 3. For each segment v, we calculate the local linear trend y_v by the least-square fitting method and obtain the first N_S segments variances

$$F^2(v,s) = \frac{1}{s}\sum_{i=1}^{s}\{Y[(v-1)s+i] - y_v(i)\}^2, v = 1,2,\cdots N_S \tag{3}$$

while for the second half of $2N_S$ segments

$$F^2(v,s) = \frac{1}{s}\sum_{i=1}^{s}\{Y[N-(v-N_S)s+i] - y_v(i)\}^2, v = N_S+1,\cdots 2N_S \tag{4}$$

Step 4. Calculate the q^{th} order fluctuation by averaging over all segments

$$F_q(s) = \{\frac{1}{2N_S}\sum_{v=1}^{2N_S}[F^2(v,s)]\}^{1/q} \tag{5a}$$

If $q = 2$, the standard DFA procedure is regained. MF-DFA algorithm transforms into DFA. If $q = 0$, Eq. (4a) can be simplified into

$$\ln F_0(s) = \frac{1}{4N_S}\sum_{v=1}^{2N_S}\ln[F(v,s)]\} \tag{5b}$$

Step 5. Repeat the Step 4 for different s, a power-law relation for long-range correlated time series between the q^{th} order fluctuation function $F_q(s)$ and the timescale s is obtained, which reflect self-similar behaviours

$$F_q(s) \sim s^{h(q)} \tag{6}$$

where $h(q)$ is dubbed generalized Hurst exponent. For stationary time series s, $h(2)$ is identical to the well-known Hurst exponent. Then calculate the singularity spectrum $f(\alpha)$ and obtain the relation between singularity strength function α and multifractal spectrum $f(\alpha)$ via the Legendre transform

$$\alpha(q) = \frac{d\tau(q)}{dq} \tag{7}$$

$$f(q) = q\alpha - \tau(q) \tag{8}$$

If the scaling exponent function $\tau(q)$ is a nonlinear function of q, the time series presents multifractal nature. And the strength of multifractality can be characterized by the spans of singularity [6]

$$\Delta\alpha = \alpha_{\max} - \alpha_{\min} \tag{9}$$

According to the multifractal theory, the larger the $\Delta\alpha$, the stronger the multifractality does that describes the long-term persistence of concentration variations.

3. Results and Discussion

3.1. Correlation analysis

Based on the original data sets, Fig. 2 depicts the distinct periodicity that existing in RSP and FSP hourly concentration series from Causeway Bay station (Fig. 2(a) and (c)), while similar property could not be found in the time sequences from Tap Mun station (Fig. 2(b) and (s)) which indicated that the background concentration do not contain a notable periodicity, neither for RSP nor FSP. The periodic interval for Causeway Bay station was 24 hours which accorded with the daily (day and night) traffic cycle, and although the relevant correlation coefficients $C(\tau)$ varied in amplitudes, the road blockages hardly had impact on changing the embedded daily cycle of RSP and FSP. Note that during the protest period (Fig. 2(a) and (c)) when $\tau \in [72,144]$, most of the $C(\tau)$ had decayed to zero and persisted the trend as time extending for FSP, which indicated that the cumulative effect of FSP has been weaken on some particular days, while such behaviour was not shown obviously for RSP. This might imply that the road blockage would have more impact on crippling the ability of new finer particulates to mix with the cumulated ones from previous cycles.

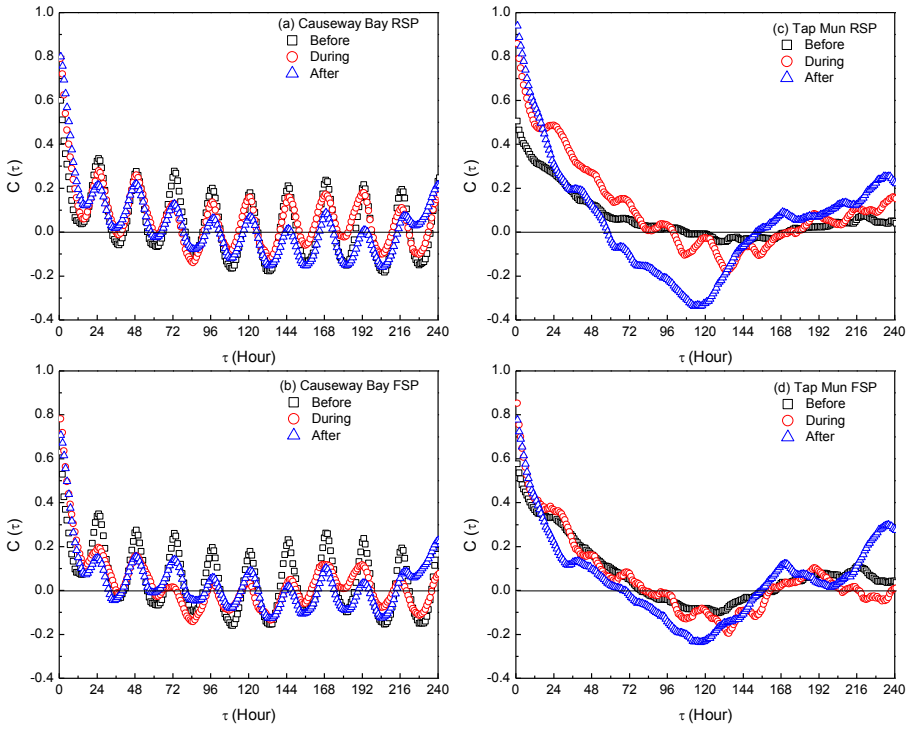

Fig. 2: Autocorrelation function of RSP and FSP in Causeway Bay and Tap Mun

3.2. Multifractal analysis

Fig. 3 reveals the dependence of the generalized Hurst exponents $h(q)$ on parameter q for all time sequences provided in Fig. 1. Basically, the MF-DFA analysis about the Tap Mun demonstrates that the background concentration series obtained before and after the protest, contained strong multifractal for both RSP and FSP due to $h(q)$ curves presented consistency and smooth changes at $q=0$, which is different from the data got during protest period that shown only weak multifractal by slight changes near $q=0$. Hence, the background multifractality of RSP and FSP experienced a first decline and then rise process in the research timeframe, which indicated the seasonal and meteorological change impact on the multifractality trend of RSP and FSP are limited. However, results displayed by the Causeway Bay station were different because monofractal ($h(q)$ curves seldom change before $q=0$) and weak multifractal were found in the data that obtained before and after the protest, while RSP and FSP shown strong multifractal feature during the protest period (Fig. 3(a) and (c)), which was an opposite process (first rise and then decline) compared to Tap Mun station. Supposed the topographical effect is homogeneous throughout the

year, therefore, it can be concluded that the road blockage happened in the protest period at Causeway Bay has caused the sudden strengthen change of the multifractality trend.

In order to quantify the change of the multifractality strength, Fig. 4 shows plots of multifractal spectrum $f(\alpha)$ against singularity strength function α for all data sets with corresponding $\Delta\alpha$ listed in Table 1. The results in Table 1 are agree with the above analysis about the change of multifractality trend, which implies that the road blockage has enhanced the long-term persistence of the concentration variations of RSP and FSP by strengthen the multifractality.

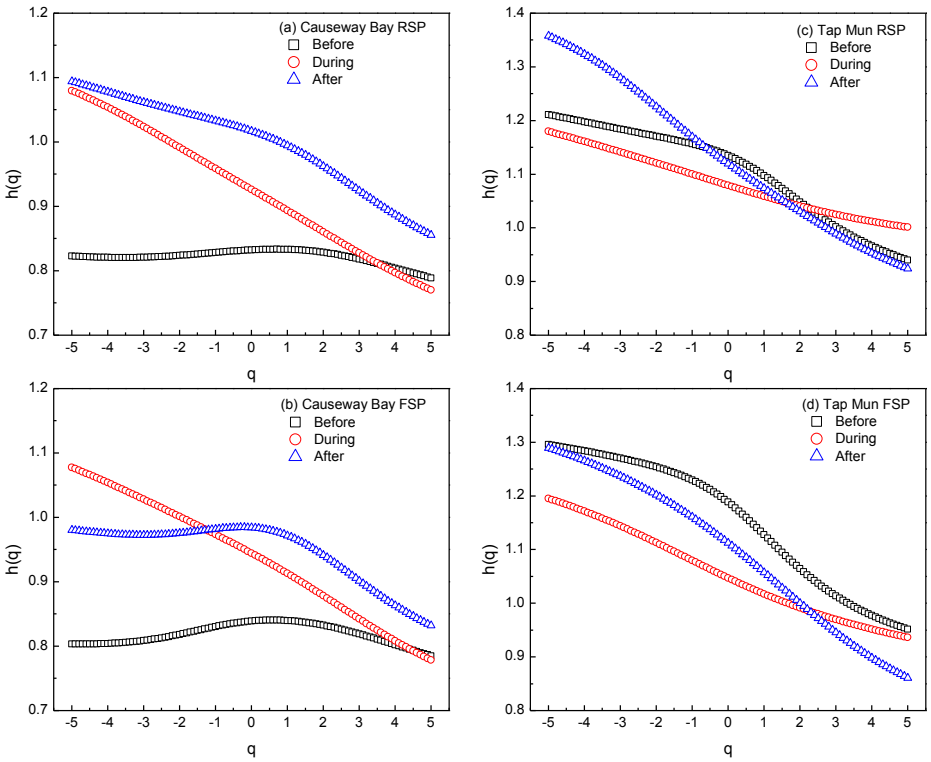

Fig. 3: The generalized Hurst exponent $h(q)$ vs. parameter q for RSP and FSP in Causeway Bay and Tap Mun

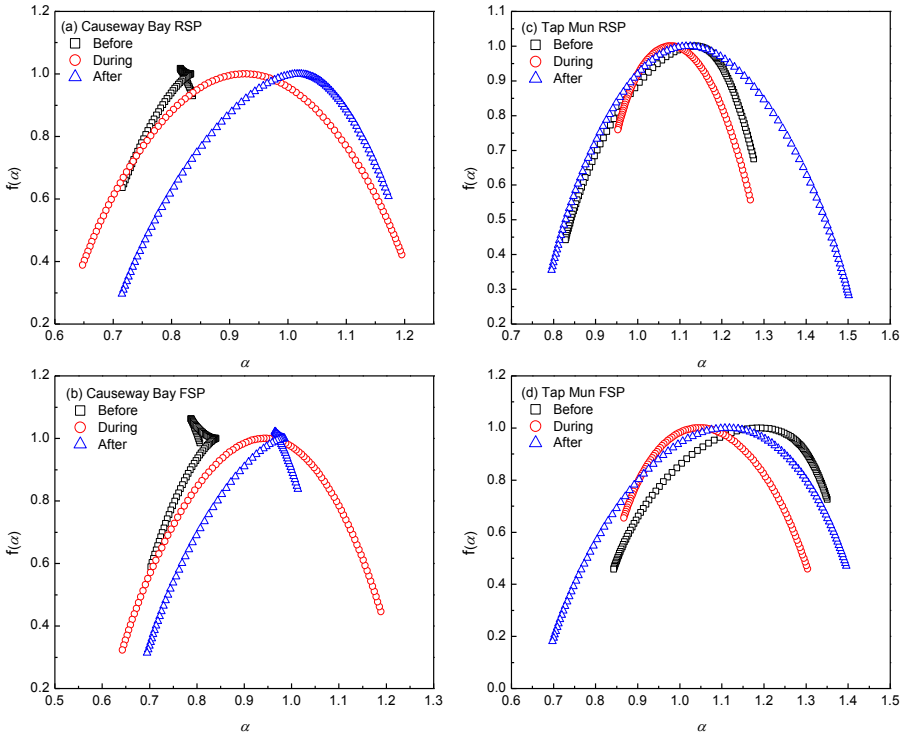

Fig. 4: Multifractal spectrum $f(\alpha)$ vs. singularity strength function α for RSP and FSP in Causeway Bay and Tap Mun

4. Conclusion

By analyzing the particulate matter data before, during and after the Hong Kong protest in Causeway Bay station, and compared with corresponding data at Tap Mun, which act as a background station, this paper assess the impact of road blockage on local PM Multifractality. Correlation analysis show that road blockage cannot change the daily cycle of RSP and FSP in urban area. Moreover, multifractal analysis demonstrates that road blockage can enhance the long-term persistence of the concentration variations of PMs by strengthen the multifractality.

5. Acknowledgements

The work was partially supported by Strategic Research Grant, City University of Hong Kong Grant (SRG-7004360), and National Natural Science Foundation of China (No. 11262003 & 11302125).

6. References

[1] P. Brimblecombe and Ning Z. Effect of road blockages on local air pollution during the Hong Kong protests and its implications for air quality management. Science of the Total Environment, 2015, 536, 443-448.

[2] Y. Xue, W. Pan, W.Z. Lu, and H.D. He. Multifractal nature of particulate matters (PMs) in Hong Kong urban air. Science of the Total Environment, 2015, 532, 744-751.

[3] C.K. Lee. Multifractal characteristics in air pollutant concentration time series. Water, Air, and Soil Pollution, 2002, 135(1-4), 389-409.

[4] A.B. Chelani. Statistical persistence analysis of hourly ground level ozone concentrations in Delhi. Atmospheric Research, 2009, 92(2), 244-250.

[5] A.M. Diosdado, G.G. Coyt, J.B. López, and J.L.D. Correa. Multifractal analysis of air pollutants time series. Rev Mex Fis, 2013, 59, 7-13.

[6] H.D. He, W. Pan, W.Z. Lu, Y. Xue, and G.H. Peng. Multifractal property and long-range cross-correlation behavior of particulate matters at urban traffic intersection in Shanghai. Stochastic Environmental Research and Risk Assessment, 2015, 1-11.

[7] HKEPD. Inquire and Download Air Quality Monitoring Data. http://epic.epd.gov.hk/EPICDI/air/station/. (accessed 20.12.2015)

[8] W.Z. Lu, Y. Xue, and H.D. He. Detrended fluctuation analysis of particle number concentrations on roadsides in Hong Kong. Building and Environment, 2014, 82, 580-587.

[9] R.N. Mantegna, and H.E. Stanley. An introduction to econophysics: correlations and complexity in finance. Cambridge University Press; 2000. pp. 14-25.

[10] C.K. Peng, S.V. Buldyrev, S. Havlin, M. Simons, H.E. Stanley, and A.L. Goldberger. Mosaic organization of DNA nucleotides. Physical Review E, 1994, 49(2), 1685.

[11] J.W. Kantelhardt, S.A. Zschiegner, E. Koscielny-Bunde, S. Havlin, A. Bunde, and H.E. Stanley. Multifractal detrended fluctuation analysis of nonstationary time series. Physica A: Statistical Mechanics and its Applications, 2002, 316(1), 87-114.

International Proceedings of Chemical, Biological and Environmental Engineering
Volume 94 of IPCBEE (2016)
DOI: 10.7763/IPCBEE. 2016. V94. 13

Current Developments in Anaerobic Digestion of Food Waste Coupled with Combined Heat and Power Generation of Electricity

Saidu, I.[1], Aminu, S. U. [2+], Aliyu, Y.[3] and Garba, B.[4]

[1]Sokoto State Polytechnic, Sokoto-Nigeria

[2] Jigawa State College of Education, P.M.B. 1002 Gumel, Nigeria

[3]Abdu-Gusau Polytechnic, Talata-Mafara, Zamfara-Nigeria

[4]Usmanu Danfodiyo University, Sokoto-Nigeria

Abstract. Anaerobic digestion is a series of process which breaks down organic matter into simple chemical components in the absence of oxygen. This process has long been used in treating various organic wastes and has been recognized as a form of energy production. Combine heat and generation of electricity is referred to as simultaneous usable heat and power within a single process. This paper aims to review the current trends in anaerobic digestion and the combined heat and power generation of electricity. The review covers the various stages in anaerobic digestion such as hydrolysis, acidogenesis, acetogenesis, and methanogenesis as well as codigestion of two or more feedstock, enhancement of pretreatment methods, inoculation of substances and temperature variation to reduce process time and enhance biogas production.

Keywords: Anaerobic Digestion, Biogas, Digestate, Co-digestion

1. Introduction

The amount municipal, agricultural and industrial waste being produced is increasing worldwide; therefore it is necessary to develop strategies for effective management of the generated waste [1]. Anaerobic digestion (AD) is one of the oldest means used in the waste treatment for the reduction of solids and pathogens destruction. The commercial use of AD starts in 1895 and the first digestion plant was built at a leper colony in Bombay, India. By the year 1895 AD stretched to England, biogas was trapped from sewage treatment facility and used as a fuel to lighting street lamps in Exeter [2]. The ability of biogas produce by AD to be utilized for electricity generation and other useful energy has steered researches and developing ways to improve gas production from anaerobic digestion [3].

AD has been principally used at larger wastewater treatment facilities treating sewage sludge and biogas production. In 1940 many sewage treatments plants in United State were already able to use anaerobic digestion (AD) and at the same time generate heat and electricity for the AD plant. This mark the beginning of sustainable waste management and pollution control [4]. However, Reference [3] noted that small scales AD were used typically for energy and sanitation purpose, although technical improvement and increasing energy prices have led to diversification of waste treated and large size AD plants.

2. Anaerobic Digestion

Anaerobic digestion (AD) is a series of processes in which microorganisms break down biodegradable material in the absence of oxygen, the end goal of the process is reduction in the waste substrate, organic content and at the same time generate a gaseous fuel called biogas, which can be burned in a boiler to

+ Corresponding author. Tel.: +2348061618366
E-mail address: yasurajringim@gmail.com

produce heat or into a combined heat and power (CHP) engine to produce heat and electricity. The biogas can further be subjected to secondary treatment to produce biomethane. This can be used as a natural gas fed into the national grid in the same way or used as fuel for vehicles [4, 5]. Beside waste minimization and biogas production, AD also produces a by-product called digestate which can be applied to the soil as nutrient supplement. The feedstock usually used in the digesters include sewage sludge, animal manure and slurry, industrial effluent and food wastes, though the potentials of using energy crops as feedstocks is increasing in popularity [5].

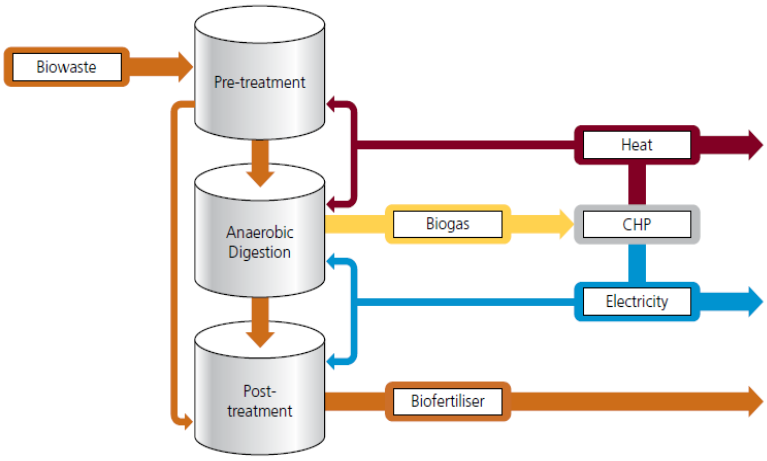

Fig. 1: Overview of an Anaerobic Digestion System [5]

Stages in AD process are divided into: pre-treatment, biological process (the digestion which is further divided into four steps leading to biogas production, the steps are; Hydrolysis, Acidogenesis, Acetogenesis, and Methanogenesis), gas upgrading and digestate treatment [3].

2.1. Pre-treatment stage

Pre-treatment stage is the first stage as shown in the Fig. 1. Which involves physical processes like screening, shredding and mixing with water for quick fermentation; it can also involve the use heat, mechanical, pressure, ultrasonic irradiation methods [6]. Screening is the process of separation and isolation of all non-digestible materials like plastics, glasses, stones and metallic objects and other harmful chemical products which can introduce pathogens or reactions in the biodigesters [7].

Shredding is aimed at reducing the size of the particles through the use of an industrial shredder calibrated to a certain size depending on the company choice and the type of the biodigesters used; because the particles size in relation to the type digester can determine the achievement of the process [8]. The reduction of particles size provides two benefits to the anaerobic digestion process. Firstly, it decreases the amount of residues produced at the end especially for substrates with high fibre content and it increases the amount of digester gas. Secondly, it decreases the time required for the digestion of substrates with low degradability [7].

2.2. Anaerobic digestion stage

Anaerobic digestion involves interactions between different microorganisms for the breakdown of organic matter in the absence of oxygen [7]. The process or the digester types can be classified into either wet system when it contains (< 10%) total solids or dry system when it contains (< 20%) total solids [9]. The digesters can also be either batch or continuous, batch is when the raw feedstock is loaded in the reactor vessel and the digestate is inoculated in another reactor which is left for decomposition to occur. While continuous digesters are continuously fed with digestate material and then the decomposed material is collected at the bottom of the reactor. The last types of digesters are single step or multi step, single step is a digester in which the digestion process occurs in a single reactor vessel; while a multi-step digester has separate steps for each digestion process [10]. The process is achieved in four stages namely Hydrolysis, Acidogenesis, Acetogenesis, and Methanogenesis.

2.2.1. Hydrolysis

Hydrolysis is also known as liquefaction, is a process where starch, lignocellulose materials, proteins and fats are broken down and converted to sugars, amino and fatty acids. The aim of this is to facilitate their transport through the cell membrane of the microorganism [11].

The mechanism of the process involves the conversion of insoluble complex organic matter into soluble molecules by the action of fermentative bacteria; proteolytic microbes secretes protease for the conversion of proteins to amino acids, cellulytic microbes secretes celluloses to convert cellulose to glucose while lipolytic microbes secretes lipases for the conversion of lipids into glycerol and fatty acids. This can also be enhanced by addition of chemicals to shorten the time of digestion and boost the methane production [11].

2.2.2. Acidogenesis

Acidogenesis involves the conversion of products formed during the hydrolysis stage; the facultative bacteria convert sugars amino acids, and fatty acid to acetates, hydrogen, carbon dioxide, acetic acids, alcohols and volatile fatty acids. The following equations show how glucose is being converted to different products by the action of the facultative bacteria [11]:

Glucose to acetate $C_6H_{12}O_6 + 2H_2O \rightarrow 2CH_3COOH + 2CO_2 + 4H_2$

Glucose to ethanol $C_6H_{12}O_6 \rightarrow 2CH_3CH_2OH + 2CO_2$

Glucose to propionic acid $C_6H_{12}O_6 + 2H_2 \rightarrow 2CH_3CH_2COOH + 2H_2O$

2.2.3. Acetogenesis

This stage comes after the acidogenesis stage; it involves the action of acetogenic bacteria otherwise known as acid formers in the conversion of fermentation products into acetate and hydrogen. Examples of acid formers includes S*ytrophomonos wolfei* known for decomposition of butyric acid, S*yntrophobacter wolinii* known for propionic decomposition, others include *Actinomyces, Peptococcus anerobus and lactobacillus and* [7]. The stage can be presented in the following equation below.

$$C_6H_{12}O_6 \rightarrow 2C_2H_5OH + 2CO_2$$

2.2.4. Methanogenesis

The final stage of the process involves the formation of the methane by the bacteria called methanogens. The methanogens make use of the intermediate products from the acetogenesis stage and then convert them to methane, water and carbon dioxide which are the major constituents of biogas. And the remaining organic materials which the methanogenic bacteria cannot feed on will combine with the residues of dead bacteria and form the solid digestate. Normal pH for Methanogenesis is 6.5 to 8.0, because any slight change in pH can affect the digesters performance because it is pH sensitive [12].

The four stages marked the end of the anaerobic stage and are important in the entire anaerobic process as they affect the performance of the digester. The hydrolysis stage plays a role in controlling the level at which Chemical Oxygen Demand (COD) is converted to methane during the anaerobic digestion of organic solids, while Methanogenesis is a rate limiting stage [12].

2.3. Post treatment stage

The basic products of food waste anaerobic digestion are biogas, and a digestate which can be in form of liquor or fibre. Post treatment stage involves processes of purifying the biogas from toxic or unwanted substances; and the pasteurization which is done kill any pathogens that might be harmful in the final product which depends on the purpose of the product.

2.3.1. Biogas

The biogas produced from the anaerobic digestion of food waste is mainly 60% of methane (CH_4), 40% carbon dioxide (CO_2) and a mixture of other compounds like hydrogen sulphide (H_2S), Hydrogen and Ammonia (NH_3). But the gas should ideally contain about 98% methane, and all other compounds should be

removed because high levels of CO_2 reduces the biogas' energy content, H_2S is corrosive and toxic, while NH_3 produces Nitrogen Oxides (NO_X) during combustion of biogas which are also greenhouse gases. However, a mixture of CO_2, H_2S, NH_3 and water can lead to corrosion of pipes [13]. So the post-treatment of biogas involves the removal of the toxic substances and excess water using different techniques as shown in Table 1 so as to get a 98% biogas.

Table 1: Biogas purification and improvement techniques [13]

Biogas compound	Technique
Elimination of Water	Demister, Cyclone separator, Condensation, Drying and Adsorption onto silica
Elimination of H_2S	Aerobic biological oxidation, Adding FeCl3 to the digester, Adsorption onto Fe2O3, Absorption (NaOH), Absorption (iron solution), Membrane separation, Biological filters, Activated carbon and Molecular sieves
Elimination of CO_2	Pressure swing Adsorption (PSA), Techniques based on physical absorption, Membrane separation, Techniques based on chemical absorption, Propane adding and Cryogenisation

When the biogas is purified and improved it can be utilized for various purposes which include heat and steam production, fuel oil when upgraded, used in production of chemicals, used in fuel cells as fuel, injection to national gas grid and as a source of energy for generation electricity and cooling (Naja *et al*, 2011) [13].

2.3.2. Digestate

Digestate is the remaining liquid or solid substance which cannot be used or decomposed by the microorganisms during the anaerobic digestion; it is composed of the bacteria that died during digestion and small traces of glasses, plastic and fibre. It is used as a fertilizer to provide soil nutrients to boost food production [14].

2.3.3. Combined heat and power generation of electricity

Combined heat and power (CHP) otherwise known as Cogeneration involves the generation of heat and power from the anaerobic digestion of food waste or other waste streams [15]. Fig. 2 showed a schematic diagram of how heat and power can be generated from biogas, and this happens based on the principle of cogeneration, where the combined heat and power unit burns the biogas in a combustion engine and the resultant pressure will power the generator and subsequently produce heat and electricity, the electricity can be connected to the national grid while the heat is mainly used back to heat the digester contents [16]. CHP power is in form of electricity which can be used on-site or connected to the national grid or power small housing unit; it can also be used mechanically for fans, compressors and pumps [15]. The type of engines used in CHP usually operates at 1,500 revolutions per minute (RPM).

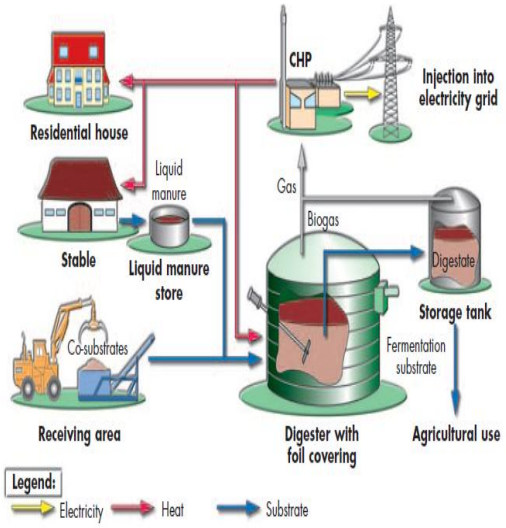

Fig. 2: Conversion of biogas to heat and power [16]

3. Current Trends in Anaerobic Digestion

The current trends in anaerobic digestion which includes combined heat and power generation of electricity are geared towards increasing biogas production through codigestion of two or more feedstock, enhancement of pretreatment methods, inoculation of substances and temperature variation to reduce process time and enhance biogas production. Some trends are explained as follows:

3.1. Co-digestion

Anaerobic co-digestion refers to the instantaneous digestion of two or more feedstock aimed at improving the effectiveness of anaerobic digestion. The importance of co-digestion over a single digestion process includes increment in biogas production, dilution of toxic compounds, and improvement in the buffer capacity, nutrients balance which includes supply of carbon to nitrogen ratio, micro and macro nutrients; and stabilization of pH [17].

Reference [18] evaluated the possibility of increasing methane production through co-digestion of food waste and brown water (faeces without urine). The results indicates an increase in the production of methane from the co-digestion of brown water and food waste than in the digestion of single substrate of brown water or food waste. This is similar to what Reference [19] reported when they carried out an anaerobic co-digestion of food waste and cattle manure aimed at finding out the parameters leading to increase in the biogas production. The study discovered that cattle manure improved the buffer capacity and there was in increased biogas production which was attributed to high biodegradation of lipid and carbon to nitrogen ratio.

3.2. Pretreatment

Pretreatment is an important method in anaerobic digestion which results to a decreased time of digestion due to decrease in the particles' size [6]. A study was carried by [20] in an effort to examine possibility of increase methane production and the efficiency of two physical pretreatment processes which are screwpress and dispergation technologies which employ the use of milling equipments for the treatment of household organic waste. The study finds out a decrease in the nutrients and biodegradable materials from screwpress technology over dispersion technology, which indicates a possible increase in the methane production. However, in an effort to study how waste activated sludge can be used in improving the effectiveness of anaerobic digestion, Reference [21] investigated the effects of chemical, thermal, ultrasonic and thermochemical pretreatment methods on the production of biogas. The study finds a significant increase in the methane production from thermochemical pretreatment compared to other methods as shown in Fig. 3. The study concluded that, thermochemical pretreatment can have impact on the rate limiting step for its increased biogas production.

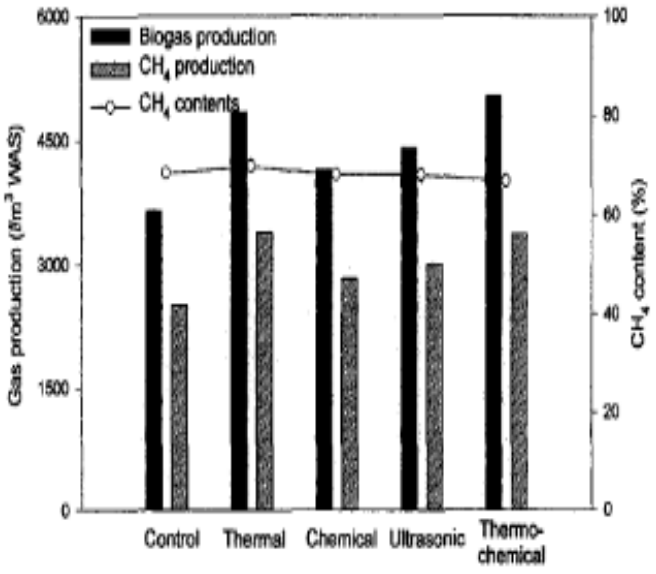

Fig. 3: How pretreatment methods improves biogas production [21]

3.3. Temperature

The activities of microorganisms in the biodigesters and the production of biogas are controlled by many factors temperature included. Lower temperatures during anaerobic digestion can lead to a decrease in the growth of microbial organisms, production of biogas and utilization rates of substrate; it can also lead to lysis or the leakage of intracellular substance and the exhausting of cellular energy. And on the other hand if the temperature is higher it can also reduce the production of biogas as a result of high volatile gases like ammonia which will hinder the action of methanogens [22].

Reference [23] developed a system which consists of hydrolysis, Acidogenesis and Methanogenesis for the digestion of food waste with an aim to check the effect of hydraulic retention time and temperature on the Methanogenesis. They adjusted the temperature from 30 ℃ to 55 ℃ with a retention time of 8 to 12 days.

The study finds out an increase in the production of biogas especially at 45 ℃ and 50 ℃, but there was a decrease in the soluble chemical demand (sCOD) but when digestion was carried below 45 ℃ or above 50 ℃, there will be need for stabilization period. And the study suggested the dependence of methanogenic bacteria on temperature which finally concluded that, thermophilic temperature (<55 ℃) is more effective than mesophilic temperature for biogas production as reported by reference [24] that "thermophilic operations are a reliable and acceptable option for digestion of organic urban wastes".

4. Conclusion

Anaerobic digestion is a current technology which is employed in the treatment of organic municipal solid waste aimed diverting waste sent to the landfills so as to avoid emission of harmful gases that are released into the atmosphere as well as recovering value from waste. The most important products recovered from the anaerobic digestion include biogas which is burnt and converted to heat and power and then used as a source of electricity for homes, industry and even injected to the national gas grid while the digestate is used as a soil conditioner.

5. References

[1] Athanasoulia, A., Melidis, P. and Aivasidis, A. Optimization of Biogas Production from Waste Activated Sludge through Serial Digestion: *Proceedings of the 12th International Conference on Environmental Science and Technology* [online]. Cemocritus University of Thrace, Rhodes, Greece 8-10 September, 2011. Available athttp://www.srcosmos.gr/srcosmos/showpub.aspx?aa=14983

[2] Abbasi, T., Tauseef, S., M., and Abbasi, S. A. Biogas Energy [online]. New York: Springer-Verlag. 2011. Available at http://www.waterstones.com/waterstonesweb

[3] Monnet, F. An Introduction to Anaerobic Digestion of Organic Waste Waters: A Survey of Recent Literature. *Environment Research* vol, 78 no. 29, 2003

[4] Maioli, A., Pulfer, J. And Mitjans, F. Generating electricity during peak hours in Asuncion, Paraguay, through anaerobic digestion of cultivated water hyacinths *revista ingenier á e investigaci ón,* vol.31 no. 2, pp. 66-70, 2011.

[5] Department for Environment, Food and Rural Affairs (DEFRA) (2011) Anaerobic Digestion Strategy and Action Plan: A commitment to increasing energy from waste through Anaerobic Digestion [Online]. Available at: https://www.gov.uk/government/uploads/system/uploads/attachment_data/file/69400/anaerobic-digestion-strat-action-plan.pdf.

[6] Izumi, K., Okishio, Y., Nagao, N., Niwa, C., Yamamoto, S. and Toda, T. Effects of particle size on anaerobic digestion of food waste. *International Biodeterioration & Biodegradation*, vol, 64 no. 7, pp. 601-608, 2010.

[7] Verma, S. (2002) Anaerobic Digestion of Biodegradable Organics in Municipal Solid Wastes, M.Sc. Thesis, Columbia University [Accessed 12 June 2013] Available at: http://www.seas.columbia.edu/earth/vermathesis.pdf

[8] Zhang, Y. and Banks, C.J. Impact of different particle size distributions on anaerobic digestion of the organic fraction of municipal solid waste. *Journal of Waste management* (New York, N.Y.), vol, 33, no. 2, pp. 297, 2013.

[9] Zeshan, Karthikeyan, O.P. and Visvanathan, C. Effect of C/N ratio and ammonia-N accumulation in a pilot-scale thermophilic dry anaerobic digester. *Bioresource technology*, vol. 113, pp. 294 2012.

[10] Regional Information Service Center for South East Asia on Appropriate Technology (RISE-AT) (1998) *Review of*

Current Status of Anaerobic Digestion Technology for Treatment of Municipal Solid Waste [Online]. Available at: <http://www.ist.cmu.ac.th/riseat/documents/adreview.pdf>

[11] Kangle, K. M. Kore, S. V. Kore, V. S. Kulkarni, G. S. Recent Trends in Anaerobic Codigestion: A Review, *Journal of Environmental Research and Technology*, vol, 2, no. 4, pp. 210-219, 2012.

[12] Lee, I., Parameswaran, P. and Rittmann, B.E. Effects of solids retention time on methanogenesis in anaerobic digestion of thickened mixed sludge. *Bioresource technology*, vol. 102. No. 22, pp. 10266, 2011.

[13] Naja, G.M., Modelon, H., Moletta-Denat, M., Ramalho, O., Rousselle, C., Wenisch, S., Zdanevitch, I., Alary, R., Bajeat, P., Bellenfant, G., Godon, J., Jaeg, J., Keck, G., Lattes, A. and Leroux, C. Assessment of biogas potential hazards. *Renewable Energy*, vol. 36, no**.** 12, pp. 3445-3451, 2011.

[14] Zhang, Y., Banks, C.J. and Heaven, S. Anaerobic digestion of two biodegradable municipal waste streams. *Journal of environmental management*, vol.104, pp. 166, 2012.

[15] Li, H., Marechal, F. and Favrat, D. Power and cogeneration technology environomic performance typification in the context of CO 2 abatement part II: Combined heat and power cogeneration. *Energy*, vol. 35 no. 9, pp. 3517-3523, 2010.

[16] Federal Ministry of Food, Agriculture and Consumer Production (BMELV) (2009). *Biogas - an Introduction* [Online]. Available at: http://www.bioenergyfarm.eu/media/default.aspx/emma/org/10727564/2009_FNR_Biogas_an_introduction.pdf

[17] Wang, L., Wang, Q., Cai, W. and Sun, X. Influence of mixing proportion on the solid-state anaerobic co-digestion of distiller's grains and food waste. *Biosystems Engineering*, vol. 112, no. 2, pp. 130, 2012.

[18] Rajagopal, R., Lim, J., Mao, Y., Chen, C. and Wang, J. Anaerobic co-digestion of source segregated brown water (faeces-without-urine) and food waste: For Singapore context. *Science of the total Environment*, vol 443 pp. 877-886, 2013.

[19] Zhang, C., Xiao, G., Peng, L., Su, H. and Tan, T. The anaerobic co-digestion of food waste and cattle manure. *Bioresource technology*, vol. 129, pp. 170-176, 2013.

[20] Bernstad, A., Malmquist, L., Truedsson, C. and la Cour Jansen, J. Need for improvements in physical pretreatment of source-separated household food waste. *Journal of Waste management* (New York, N.Y.), **33**(3), pp. 746, 2013.

[21] Kim, J., and C. Park. Effects of various pretreatments for enhanced anaerobic digestion with waste activated sludge. *J. Bioscience. Bioengineering*, vol. 95, no. 3, pp. 271-275, 2003.

[22] Fezzani, B. and Ben Cheikh, R. Two-phase anaerobic co-digestion of olive mill wastes in semi-continuous digesters at mesophilic temperature. *Bioresource technology*, vol. 101, no. 6, pp. 1628-1634, 2010.

[23] Kim, S.W., Kim, J.K., Oh, B.R. and Chun, Y.N. Effects of temperature and hydraulic retention time on anaerobic digestion of food waste. *Journal of Bioscience and Bioengineering*, vol. 102, no. 4, pp. 328-332, 2006.

[24] Forster-Carneiro, T., Pérez, M. and Romero, L.I. Anaerobic digestion of municipal solid wastes: dry thermophilic performance. *Bioresource technology*, vol. 99, no. 17, pp. 8180-8184, 2008.

International Proceedings of Chemical, Biological and Environmental Engineering
Volume 94 of IPCBEE (2016)
DOI: 10.7763/IPCBEE. 2016. V94. 14

Using Sewage Sludge as Alternative Fuel and Raw Material to Produce Cement Clinker

ZhenzhouYang[1], Yingyi Zhang[1], Lili Liu[1], Xidong Wang[1] and Zuotai Zhang[2+]

[1]Beijing Key Laboratory for Solid Waste Utilization and Management and Department of Energy and Resource Engineering, College of Engineering, Peking University, Beijing 100871, P.R. China

[2]School of Environmental Science and Engineering, South University of Science and Technology of China, Shenzhen, 518055, P.R. China

Abstract. In the present study, we proposed a method that using sewage sludge (SS) as alternative fuel and raw material to produce cement clinker. It was found that the increasing amount of SS can favor for the formation of tricalcium silicate (C3S) but the excessive amount can cause the impediment effect. Furthermore, SS contains high contents of trace elements, especially for zinc and manganese. The thermodynamic equilibrium calculation of Zn and Mn are also conducted to further understand their transformation behaviors and the results show that zine is predicted as a volatile element while manganese shows great condensed potential during the cement clinker calcination process.

Keywords: Sewage Sludge, Cement Clinker, Trace Element, Thermodynamic Equilibrium

1. Introduction

With the rapid development of urbanization and industrialization, a large quantity of wastes are produced. Amongst these wastes, sewage sludge (SS) is a kind of waste that derive from sewage treatment plant [1, 2]. According to the statistic, more than 8 million tons of dried SS is produced in China every year with the increasing rate of 10% annually [3]. How to deal with such a large number of SS has become a severe environmental issue that needs to be timely resolved. In China, the common ways for the SS treatment are agriculture, landfill and incineration, but the shortage of available of land and the increasing concern about of environment from public limit these methods application [4-6]. Utilization of SS in the cement kiln seems to be a promising method, which can completely destroy the hazardous substances due to the high temperature and long residual time that cement kiln involves [7]. Besides, due to SS contains significant heat value and the main component of its ash are SiO_2, Al_2O_3, CaO and Fe_2O_3, which are the main component of cement raw meals [8]. Therefore, SS can be used as alternative fuel and raw materials to produce cement clinker.

The utilization of SS in the cement kiln presents multiple advantages but also can exist some problems, such as trace element problem. Trace element has attracted more and more attention due to their hazardous effect on human health and ecosystem [9]. A better understanding of the trace elements transformation behaviors during cement clinker calcinations process can efficiently prevent its secondary pollution. However, this is still unclear. Besides, the transformation behaviors of trace elements can be influenced by various conditions, such as their thermodynamic properties, the combustion temperature and the characteristics of raw materials. Thermodynamic equilibrium calculation is widely used to study the trace elements behaviors under different conditions. To the best knowledge of present author, no thermodynamic

+ Corresponding author, Tel.: +86 10 6275 6623; Fax: 62754427
E-mail address: zgkdyzz@126.com

equilibrium study has been conducted on the trace elements behaviors during cement clinker calcination process.

The object of this study is to understand the effect on the cement clinker with different amounts of SS addition. Additionally, the trace elements transformation behaviors during cement clinker calcinations process are also studied using FactSage 6.4.

2. Materials and Method

The dried sewage sludge (SS) pellet was collected from a municipal wastewater treatment plant located in Beijing, China. The chemical composition of SS was determined by X-ray fluorescence spectrometer (XRF, S4-Explorer, Bruker), as shown in Table 1. It can be seen that major component of SS are SiO_2, Al_2O_3, Fe_2O_3, CaO, which are the essential component for the cement clinker manufacture and the mineralogical composition of SS was determined by X-ray diffraction (XRD, D/Max 2500, Rigaku).

The raw materials were prepared by the reagent of $CaCO_3$, SiO_2, Al_2O_3, Fe_2O_3 and various amount of SS. The raw materials were pressed to $\phi 20 \times 5$mm slices with the pressure of 10Mpa and then put into the electrically heated tube furnace. The temperature was set from room temperature to 1450 ^oC at the rate of 10 ℃/min.

The trace elements in the SS were measured by inductively coupled plasma-atomic emission spectroscopy (ICP-AES, Prodigy XP, Leeman) and the thermodynamic equilibrium calculation is conducted using FactSage 6.4.

Table 1: The chemical composition of sewage sludge

Chemical composition	Content (wt. %)
SiO_2	25.19
Al_2O_3	5.63
Fe_2O_3	4.15
CaO	6.35
MgO	1.54
K_2O	1.18
P_2O	4.85

3. Results and Discussion

3.1. Mineralogical characterization of the eco-cement clinker

The XRD pattern of eco-cement clinker with different amounts of SS addition are shown in the Fig. 1. It can be seen that the mainly crystalline composition in the blank sample are C_3S (Ca_3SiO_5), C_2S (Ca_2SiO_4), C_3A [$Ca_3Al_2O_6$ and $Ca_3(Al,Fe)_2O_6$] and C_4AF ($Ca_4Fe_2Al_2O_{10}$), which is similar with that in the commercial use cement clinker. The most important characteristic peak of C_3S appeared at 2θ about 32°, which is the major component of Portland cement clinker that determines its quality, as shown in Fig. 2. The intensity of it can indicate the relative content of C_3S in the clinker to some extent [10, 11]. It can be seen that the characteristic peak of C_3S shows no obvious change as SS addition up to 10wt. %. However, it obviously increase with 15wt. % SS addition. With the addition of SS further increase, the phase of C_3S disappears and the phase of f-CaO, C_2S-$0.05C_3P$ are formed, which might be attributed to the high content of phosphorus in SS, as shown in Table 1. During the cement clinker calcinations, the excessive phosphorus can decompose the C_3S into C_2S and f-CaO, and then causing the formation of phosphorus in C_2S solid solution (C_2S-$0.05C_3P$). This indicates that the high intake of SS can cause the undesirable effect on the C_3S formation. Therefore, the addition of SS should be strictly controlled.

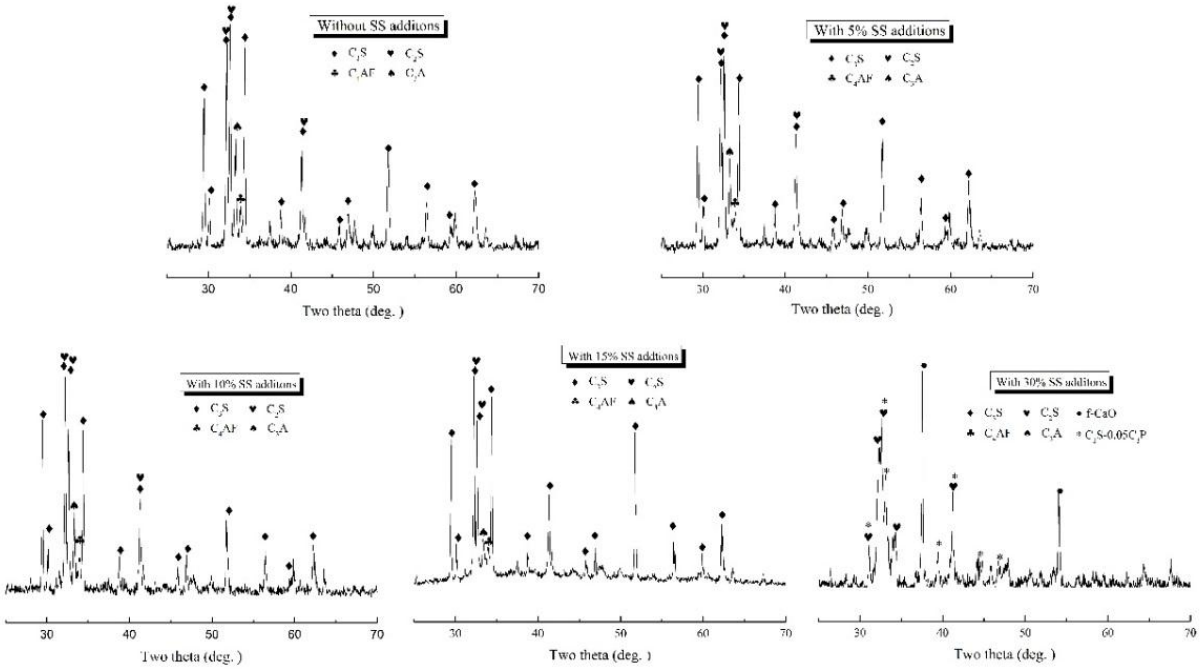

Fig. 1: The XRD pattern of cement clinker with different amount of SS addition

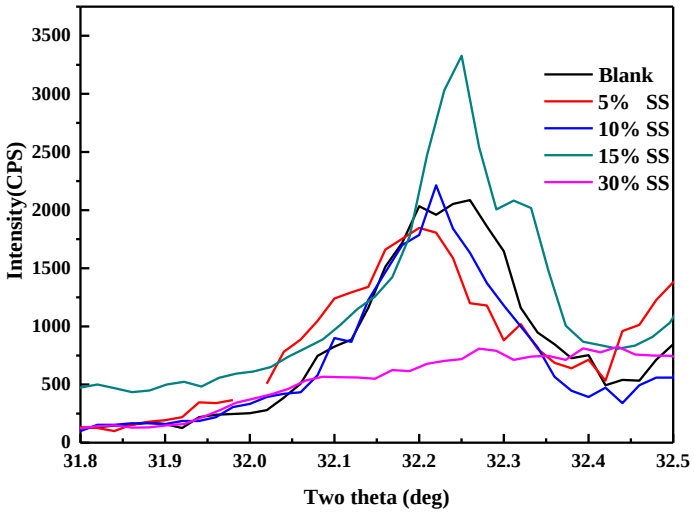

Fig. 2: The characteristic peak of C3S

3.2. Micrographs observation

The C_3S in the cement clinker is commonly produced by the reaction between C_2S and CaO in liquid phase. The liquid phase in the clinker can be observed by SEM, which is shown in Fig. 3. It can be seen that the big crystal grains are close to each other and are stacked together with distinct contours and boundary in the blank sample. With the SS addition, the outline of the crystal grains became more blurred. As the addition of SS reaches 15 wt. %, the boundary lines of the crystalline grains get mixed with the interphase and cannot be clearly identified. Furthermore, the crystal grains exhibit independent existence and are connected directly to the liquid phase as the amount of SS addition increases to 15 and 30 wt. %. Therefore, the addition of SS can raise the amount of liquid phase. As for the crystal size, the present results show that SS addition has no obvious influence on the growth of the crystalline grains until the amount of SS reached 15 wt. %. In addition, a large amount of pores were observed to be distributed in the blank sample. The pores were found to decrease with the SS addition and the crystalline grains were connected to each other. These

results differ from those reported by Lin et al [12], which might be due to the increasing liquid phase with SS addition, resulting in a more compact cement clinker with decreased porosity.

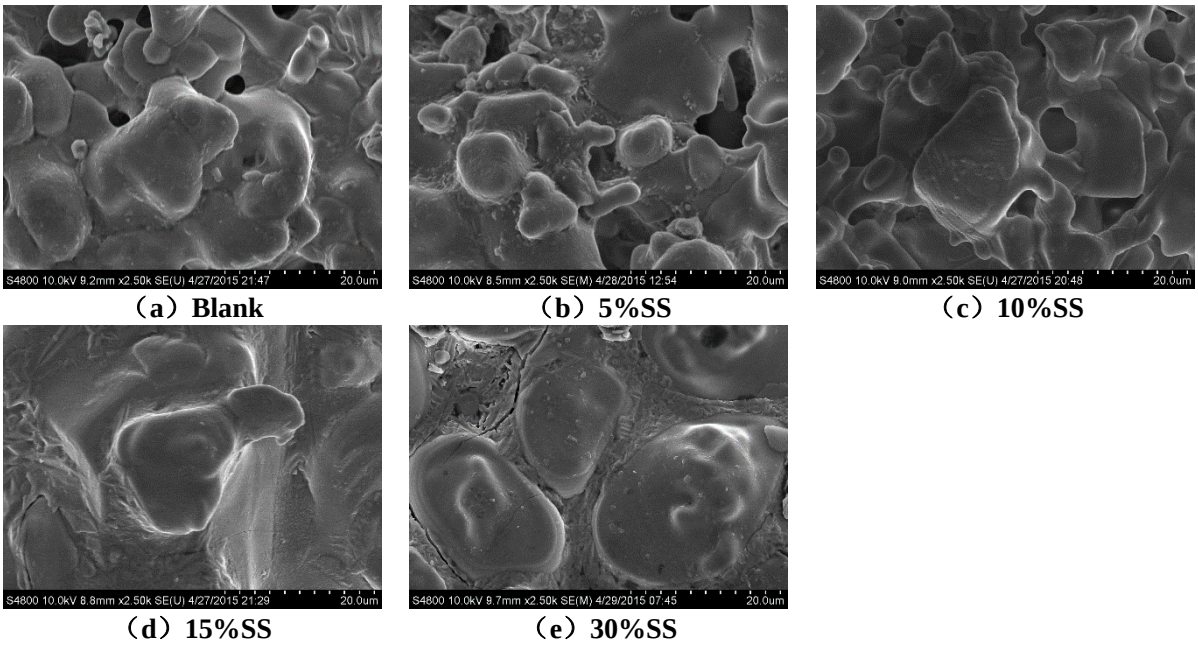

（a）Blank **（b）5%SS** **（c）10%SS**

（d）15%SS **（e）30%SS**

Fig. 3: SEM micrographs of the eco-cement clinkers with different amounts SS

3.3. The transformation of trace element during cement clinker calcinations

It is known that equilibrium calculations have limitations due to its neglect on kinetic effects, nonuniform distribution as well as the mode of occurrence of the elements [13]. However, from the current study, it can be seen that equilibrium calculation helps to understand the general disciplines of the elements behavior under different variables. To further understand the influence of different process variables and chemical compositions on trace elements behavior, thermodynamic equilibrium calculations were conducted using FactSage 6.4 assuming a closed environment and 1 kg of raw materials is used as input data. Several calculation condition is considered: The system only containing C, H, N, S is calculation as basic system. The introduction of Cl in the system is considered to identify the possible impact. The mineral contents are added into the system to examine the possible interaction. The calculations is performed at the range of temperature 1000 - 2000K and this range of temperature includes the clinker calcinations at 1723K.

The trace element content in the SS are shown in the Table 2. It can be seen that the trace element in SS is notably high, especially zinc and manganese. Thus, the elements of zinc and manganese are selected for the thermodynamic equilibrium study and the results are shown in Fig. 4 and Fig. 5. It can be seen that, the equilibrium composition for zine mainly depends on the temperature. ZnO(s) in only stable species in the equilibrium at the temperature between 1000~1400K. With temperature further increase, the proportion of ZnO(s) sharply decrease with the increase of Zn(g). All of the zinc exists as vapor phase when the temperature above 1800K. The presence of choline can lead to the formation of $ZnCl_2$(g) but in a small proportion. Furthermore, it can be seen that zinc shows no interaction behavior with mineral phase. The average temperature in cement kiln is about 1723K. Therefore, zine is predicted as a volatile element in cement kiln according to the simulated result. As for manganese, it can be seen that manganese shows great condensed potential during cement clinker manufacturing process. When the temperature is under 1500K, almost of manganese is in the form of Mn_2O_3(s2). With the temperature further increase, MnO(s) becomes the most stable species. The introduction of choline and mineral phase have no obvious influence on the species of manganese.

Table 2: The trace elements content in SS (mg/kg)

	As	Ba	Cd	Co	Cr	Cu	Mn	Ni	Pb	Zn
SS	80	256	2	11	124	358	543	41	48	1084

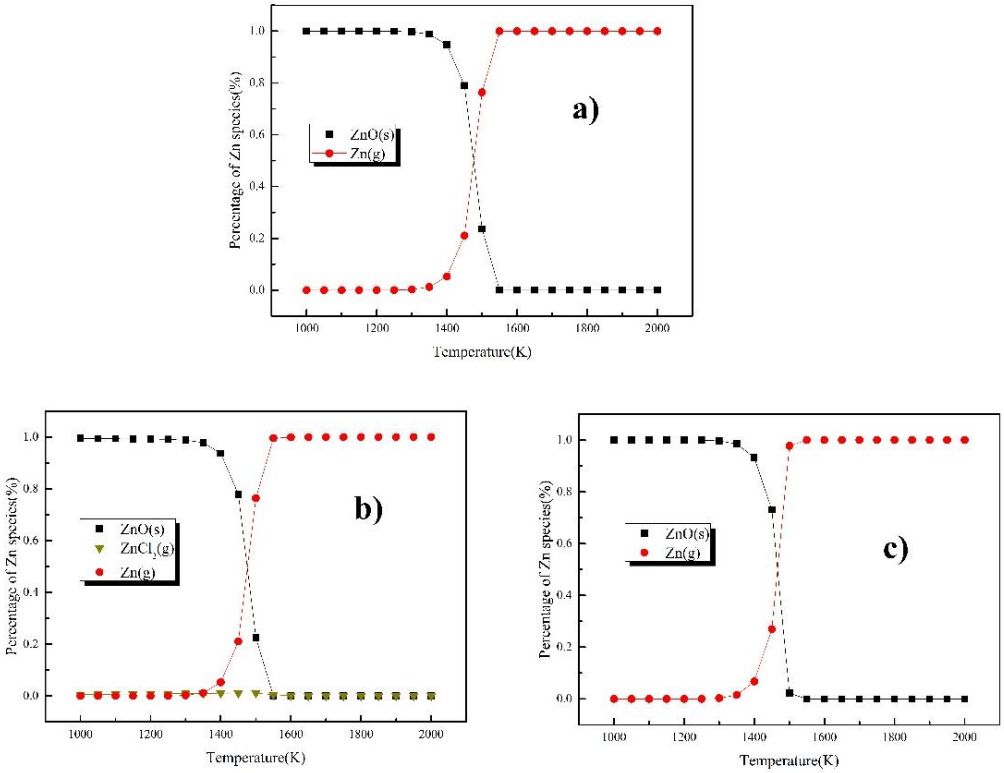

Fig. 4: The influence of different parameters on speciation of Zinc: a) Basic system: C, H, N, S, O; b) +Cl, a=1.2; c) Basic system + Cl + mineral contents.

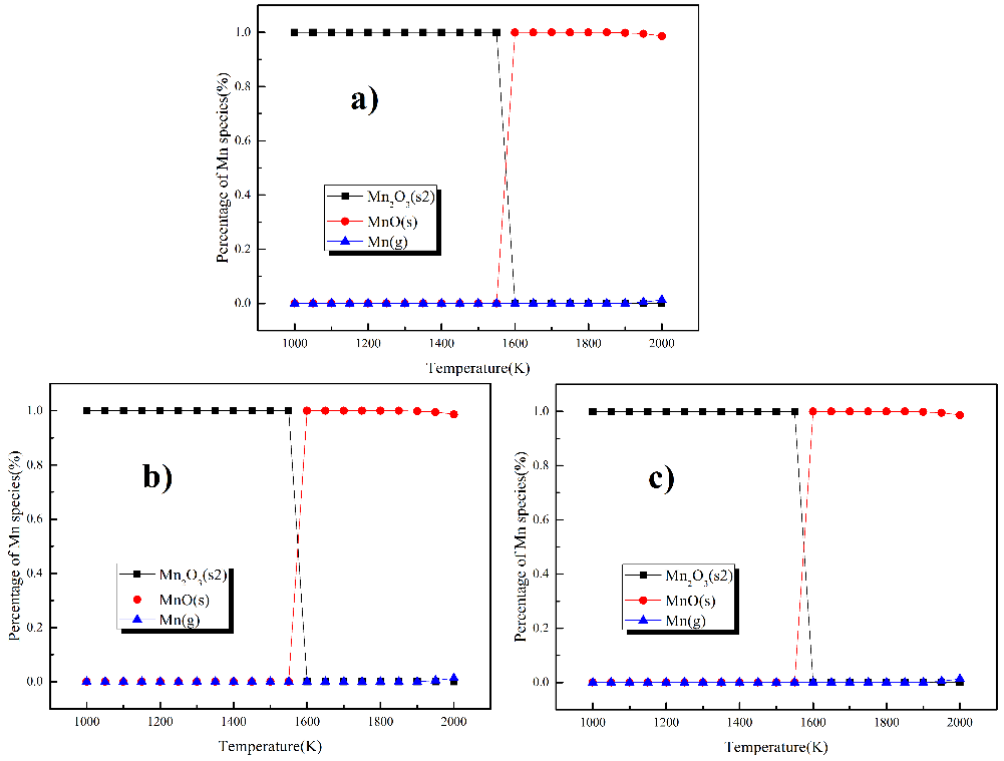

Fig. 5: The influence of different parameters on speciation of Manganese: a) Basic system: C, H, N, S, O; b) +Cl, a=1.2; c) Basic system + Cl + mineral contents.

4. Conclusion

From our present study, we can draw the conclusion that the appropriate amount of SS additions can favor for the C_3S formation, while the excessive amount can cause the impediment effect. Besides, the addition of SS can effectively increase the liquid phase content during the cement clinker calcination process. SS contains high contents of trace elements, especially for zinc and manganese. According to the thermodynamic equilibrium calculation, zinc tends to exist as vapor phase, while manganese shows the great condensed potential during the cement clinker calcinations process.

5. Acknowledgements

Zuotai Zhang and Zhenzhou Yang designed the experiments; Zhenzhou Yang conducted the experiments, analyzed the data, and wrote the manuscript; Yingyi Zhang, Lili Liu, Xidong Wang advised the experiments and helped editing the manuscript.

6. References

[1] Jiang, L., et al., Co-pelletization of sewage sludge and biomass: The density and hardness of pellet. *Bioresource Technology*, 2014. 166: 435-443.

[2] Singh, R.P. and M. Agrawal, Potential benefits and risks of land application of sewage sludge. *Waste Management*, 2008. 28(2): 347-358.

[3] Hong, J.M., et al., Life cycle assessment of sewage sludge co-incineration in a coal-based power station. *Waste Management*, 2013. 33(9): 1843-1852.

[4] Folgueras, M.B., M. Alonso, and R.M. Diaz, Influence of sewage sludge treatment on pyrolysis and combustion of dry sludge. *Energy*, 2013. 55: 426-435.

[5] Murakami, T., et al., Combustion characteristics of sewage sludge in an incineration plant for energy recovery. *Fuel Processing Technology*, 2009. 90(6): 778-783.

[6] Zhou, H.B., et al., Application of a recyclable plastic bulking agent for sewage sludge composting. *Bioresource Technology*, 2014. 152: 329-336.

[7] Conesa, J.A., et al., Pollutant Formation and Emissions from Cement Kiln Stack Using a Solid Recovered Fuel from Municipal Solid Waste. *Environmental Science & Technology*, 2011. 45(13): 5878-5884.

[8] Zabaniotou, A. and C. Theofilou, Green energy at cement kiln in Cyprus - Use of sewage sludge as a conventional fuel substitute. *Renewable & Sustainable Energy Reviews*, 2008. 12(2): 531-541.

[9] Zhang, Y.Y., et al., Trace element partitioning behavior of coal gangue-fired CFB plant: experimental and equilibrium calculation. *Environmental Science And Pollution Research*, 2015. 22(20): 15469-15478.

[10] Xu, W., et al., The utilization of lime-dried sludge as resource for producing cement. *Journal Of Cleaner Production*, 2014. 83: 286-293.

[11] Li, H.X., et al., Preparation of Portland cement with sugar filter mud as lime-based raw material. Journal Of Cleaner Production, 2014. 66: 107-112.

[12] Lin, Y.M., et al., Utilization of municipal sewage sludge as additives for the production of eco-cement. *Journal Of Hazardous Materials*, 2012. 213: 457-465.

[13] Miller, B.B., R. Kandiyoti, and D.R. Dugwell, Trace element behavior during co-combustion of sewage sludge with polish coal. *Energy & Fuels*, 2004. 18(4): 1093-1103.

International Proceedings of Chemical, Biological and Environmental Engineering
Volume 94 of IPCBEE (2016)
DOI: 10.7763/IPCBEE. 2016. V94. 15

Analysis of Air Pollution through Geographical Information Systems (GIS): Sampling of Kutahya Province in Turkey

Hatice Canan Gungor [1+] and Gulgun Ozkan [2]

[1] University of Necmettin Erbakan , Konya/Turkey
[2] University of Selcuk Konya/Turkey

Abstract. Environment that contains information on geographical functions is one of the most intensive application areas of Geographical Information Systems (GIS). Availability of decisions related to the environment, identify the factors that affect the environment, spatial analysis and detection and monitoring of environmental changes, environmental factors are measured with GIS mapping.
In our country, one of the most important environmental problems appears through rapid population growth, unplanned urbanization and industrialization is air pollution. A geographic information system (GIS) is a computer-based tool for mapping and analyzing geographic phenomenon that exist and events that occur on Earth. GIS technology integrates common database operations such as query and statistical analysis with the unique visualization and geographic analysis benefits offered by maps. In general, a GIS provides facilities for data capture, data management, data manipulation and analysis, and the presentation of results in both graphic and report form, with a particular emphasis upon preserving and utilizing inherent characteristics of spatial data. The ability to incorporate spatial data, manage it, analyze it, and answer spatial questions is the distinctive characteristic of geographic information systems. So, to use GIS as a tool in solving and to realizing problems of air pollutions has been right solution.
In this study, between 2000-2008, air pollution that consists of Particulate Matter (PM) and Sulfur Dioxide (SO2) is examined in Kutahya and the values of the density of the city center are created as thematic maps using GIS. In parallel with an increase in natural gas usage since 2006 has been observed improvements in values of PM and SO2. Thematic maps generated are compared.

Keywords: Air Pollution, Gis, Kutahya Province, Thematic Maps

1. Introduction

Today, the borders of scientific branches are expanding continually; therefore, interdisciplinary common subjects exist that can be solved efficiently together. In this perspective, with many developing technologies in their structure which is improving and developing continuously, Geographical Information Systems (GIS) serve a wide range of subjects.

GIS is an information system that works with spatial or geographic coordinate data [1]. The use of GIS spatial data in the interpretation of air pollution is a new development. [2, 3]. Maps of spatial distributions of SO2 in Istanbul metropolitan were created by Tayanç [4].by using kriging method and he identified the problematic areas.

Mapping urban air pollution nevertheless faces many problems. The complex geography of emission sources and the equal complexity of dispersion processes in an urban environment mean that levels of air pollution typically vary over extremely short distances, often no more than a few tens of meters [5]. On the other hand, data on both emission sources and pollution levels are often sparse. As a result, maps of urban air pollution tend to be highly generalized, and estimates of exposure to air pollutants subject to serious misclassification. The spatial analysis and overlay techniques available in GIS also provide powerful tools

[+] Corresponding author. Tel.: +905362129941.
E-mail address: cnngungor@gmail.com

for pollution mapping. [6] Because GIS monitors parameters of pollution consistently and allows spatial analysis for questioning, it is seen as the most effective technological tools.

In this study, in Kutahya, sulfur dioxide (SO_2) and particulate matter (PM) values that denote air quality values were used and maps of air pollution were formed for the years 2006-2007 by analyzing with GIS. Pollution levels changes over time were examined and the results were compare with air quality standards of Turkish Air Quality Control Regulations, AB, WHO and US EPA.

1.1. Climate and air pollution sources

Atmosphere pollution consists of joining with meteorological factors and negative topographer structure. The geographical embodiments which prevent air circulation are effective pollution[7]. Atmospheric dirts spread from right resources to the environment allow horizontal and vertical movements which are the meteorological factors [8].

Examined the topography of the province, the apparent character of the region's surface in terms of figures where is on the threshold of Interior western Anatolia consists of plateaus and plains. Both series of mountain and hill and the pit fields extend the northwest - southeast direction in accordance with the general character of the threshold. The two steps can be distinguished by the different altitudes in plateaus of Kutahya. 1000-1250 meters corresponds to low plateaus and 1250-1450 meters corresponds to high plateaus.

When meteorological information is analyzed, the characteristics of each type of climate among Aegean, Marmara and Central Anatolia are possible to see. The climate is a type of transition between the dry climate and humid climate.

Table. 1: Long-years averages and extreme meteorological data in Kutahya

Mean temperature (℃)	33 years	10,7	Highest temperature	29.07.2000
	5 years	11,3		39,5
Total rainfall (mm)	33 years	544,4	Lowest temperature	21.02.1985
	5 years	489,0		-21,5
The mean maximum temperature (℃)	33 years	17,0	Highest snow cover (cm)	26.01.2006
	5 years	17,5		60
The mean minimum temperature (℃)	33 years	5,0	Wind direction	WNW
	5 years	5,7		
The average relative humidity (%)	33 years	64	Average duration of sunshine (hour)	05:48
	5 years	65		
Snow days	33 years	31,5	Highest rated wind speed (km/hour)	05.02.2003
	5 years	22,5		99,4

Source: Provincial Directorate of Meteorology of Kutahya

As shown in Table 1, in Kutahya, the average temperature is 10,7 (℃), total rainfall is 544,4 (mm), the average relative humidity is 64%, wind direction is north-northwest and average duration of sunshine 5 hours and 48 minutes.

Reaching important levels of air pollution in our province, especially in the winter months, as well as plant and animal life in the human health is threatened. In our province, warm-up period is approximately 6 months and fuels used for heating during the winter months as the air pollution plays an important role.

Listed as the most important causes of air pollution in Kutahya:

Topographic structure of the city

1. Meteorological conditions,
2. Unplanned urbanization,
3. The use of poor quality fuel,
4. Incorrect combustion techniques,
5. Activities of Industry and Industrial Plants,
6. Central heating boilers and stoves lack of appropriate design and failure to their periodic maintenance,
7. Increase in per capita energy consumption,
8. More than motor vehicles,
9. Deficiencies in isolation and construction quality.

2. Materials and Methods

2.1. Research areas

The research area was chosen Kutahya province in Aegean Region with its location between 38° 70’ and 39° 80’ northern latitude and 29° 00’ and 30° 30’ southern longitude (Fig. 1) in Turkey. The altitude of the city centre is about 969m. above the sea. According to the year 2007 ETF (Recording Household Number), the population of the central district is 228,956. Its area is 11890 km2 with central district population density 88 people/km2.

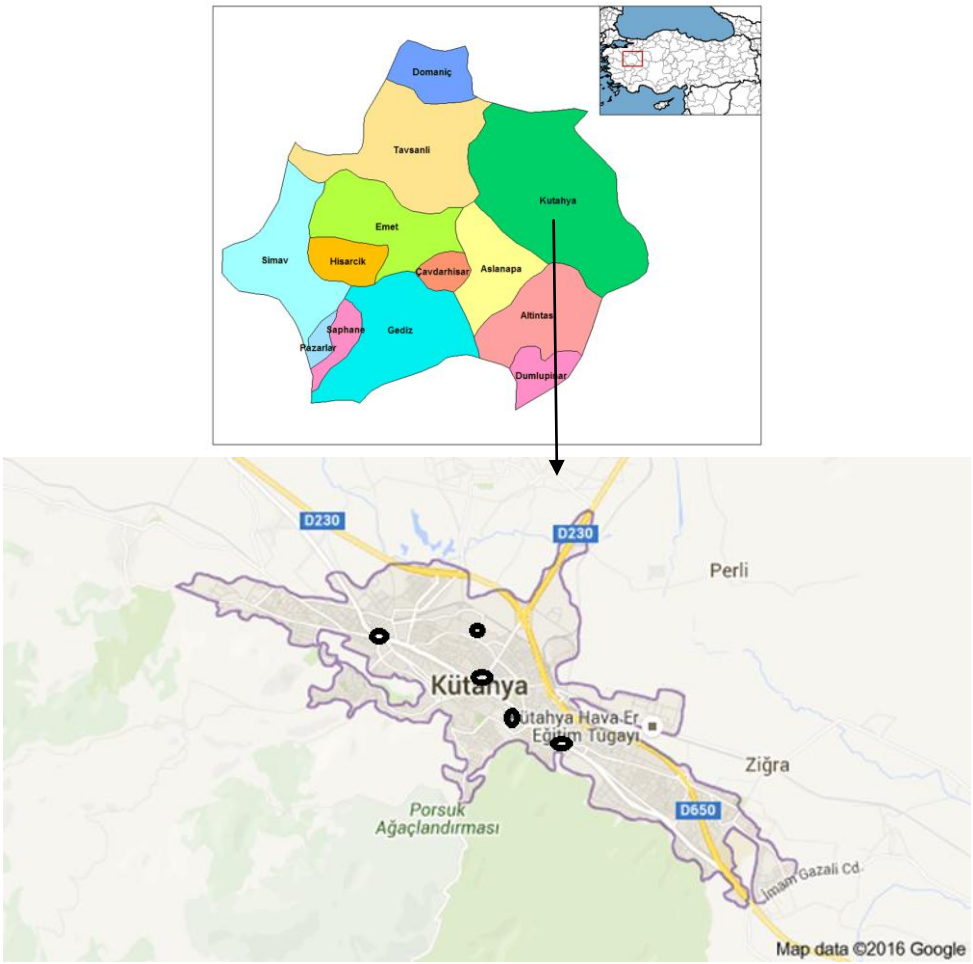

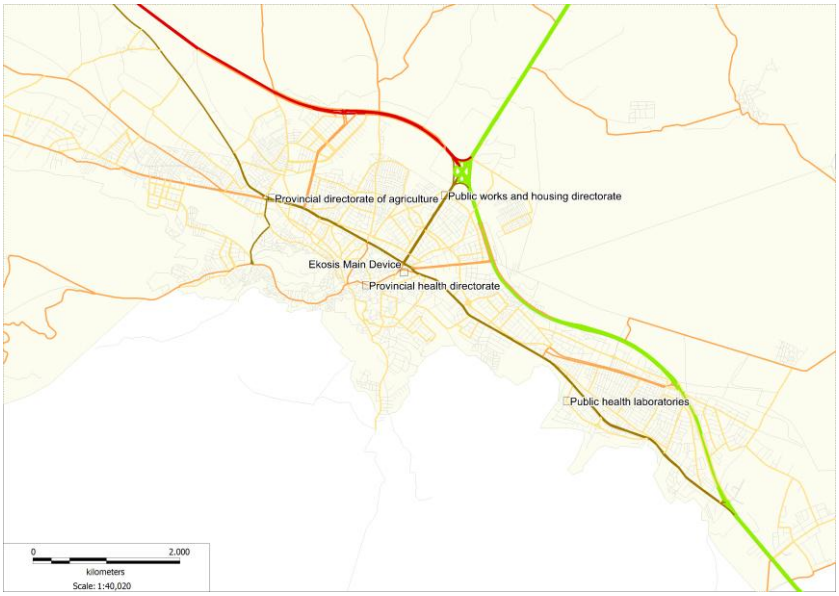

Fig. 1: Research area

It is shown research area in Fig. 1.

2.2 Application

The study area was chosen as the center of the city of Kutahya. Kutahya province's air pollutions ratio had got high values in average of the other provinces in Turkey. For thus Kutahya was chosen research area. In Fig. 2 show that thematic map which was created for all cities in Turkey by software to export Google Earth.

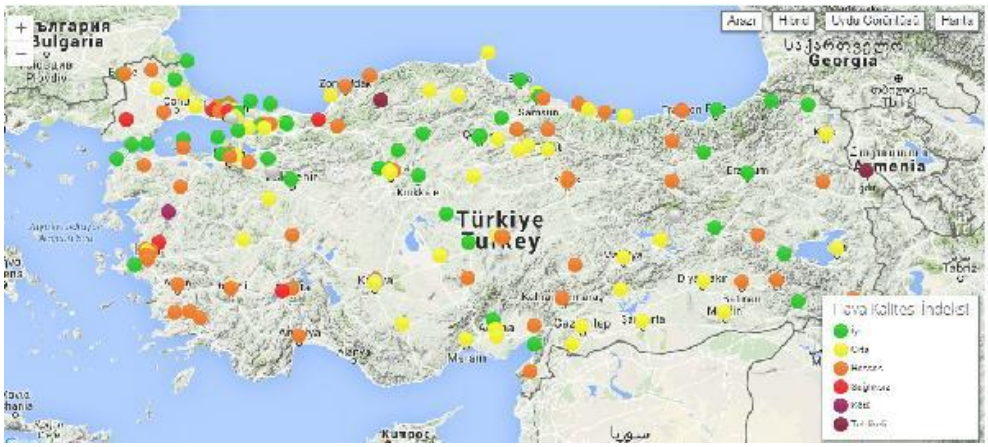

Fig. 2: Air quality data [9]

Measurement Monitoring Stations in 2000-2006 was 8 at the point of measurement. As of 2006, measurements continued to 5 points. To create thematic maps, coordinates the creation of centers Measurement monitoring station has been geocode by city map, Table 2 shows the coordinates.

Table 2: Measurement monitoring station locations and coordinates

Device Location	**X-COORDINATE**	**Y-COORDINATE**
Provincial health directorate	498312	4365024
Provincial directorate of agriculture	497051	4366170
Public health laboratories	498938	4366011
Provincial directorate of public works	499361	4366197
Provincial directorate of environment and forestry*	498820	4365170

*** Automatic Measurement System**

Source: Provincial Directorate of Environment and Forestry (Director of Environmental Management)

Measurement monitoring station locations was shown in Fig. 1. Which neighbourhoods could be covered by the measurements of pollution in the values of these stations, interviews with experts and the province of Kutahya in wind direction and development have been identified with the state. Accordingly, the measurement values of five monitoring stations in all the thematic center of goods and density maps were created using MapInfo software. Firstly, SO_2 and PM values which were created as a excel format entered to the program for every years. Built in the neighborhood polygon layer is created in the program of province boundaries. Measurement monitoring stations were geocode coordinates of the point layer by their names. Associated with the station numbers in the colon is a common link was the creation of thematic maps.

Table 3: The average values of SO2 and PM (µg/m3) (2000-2007 years)

Months	2000_SO2	2001_SO2	2002_SO2	2003_SO2	2004_SO2	2005_SO2	2006_SO2	2007_SO2
january	416	266	521	177	270	275	175	163
february	385	257	426	179	245	170	170	106
march	334	168	197	192	185	148	108	69
april	89	135	138	134	158	110	83	51
may	54	97	37	51	101	63	73	42
june	27	36	17	42	63	40	28	11
july	32	27	16	40	50	37	22	20
august	29	27	14	40	51	33	44	14
september	39	55	23	49	58	43	11	20
october	114	177	102	107	153	78	34	29
november	350	290	328	293	291	105	164	36
december	360	246	288	275	332	157	224	59
Average	186	148	176	132	163	105	95	52

(µg m3): (micrograms/ cubic meters)

Months	2000_PM	2001_PM	2002_PM	2003_PM	2004_PM	2005_PM	2006_PM	2007_PM
january	125	146	253	112	170	214	163	213
february	113	143	267	105	139	118	154	179
march	96	84	135	120	114	108	83	122
april	66	70	102	91	93	83	66	103
may	51	54	41	34	49	51	57	100
june	34	24	26	30	32	31	19	49
july	32	23	22	25	27	28	18	100
august	33	30	27	29	31	23	137	97
september	45	44	33	40	41	34	65	99
october	107	121	123	67	119	70	178	104
november	274	134	237	250	232	97	273	118
december	202	114	195	183	265	149	326	165
Average	98	82	122	90	109	84	129	121

(µg m3): (micrograms/ cubic meters)

Table 3 at the average of the values is understood that the rate of pollution in the winter months, this rate is higher in the summer watching the fall. We also observed a decrease in the average rate each year of SO2 pollution. As can be seen here in the great cause of pollution is considered to be the use of heating fuel and coal of poor quality. Heating fuel in the province since 2005 is quite reduced the rate of pollution increase in the use of natural gas. However, the average values of PM does not show much difference. Powder is also called as the ratio of PM values, the city's topography and structures, thought to be stable unless there is a change. The creation of thematic maps for the years 2006-2007 and the 2008 monthly average values of SO_2 and PM are used. Table 4a, 4b and Table 5a, 5b also shows the values in 2006-2007.

SO_2 and PM10 measured values has been compared with the limit values set by the long-term limit of the Turkish Air Quality Control Regulations (HKKY, SO2; 150 μg/m3, PM10; 150 μg/m3), the European Union (AB, SO_2; 20 μg/m3, PM10; 40 μg/m3), the World Health Organization (WHO, SO2; 50 μg/m3), the U.S. Environmental Protection Agency (US EPA, SO2; 80 μg/m3, PM10; 50μg/m3). The central values of Kutahya are seen more than the standard values. MapInfo software has been entered SO_2 and PM10 values to the database and maps are created with the help of the thematic map module.

Table: 4a 2005 values of PM

Measurement locations and PM values	Public works and housing directorate	Provincial health directorate	Provincial directorate of agriculture	Public health laboratories	Ekosis Main Device
PM_1	157	171	157	168	217
PM_2	149	161	148	159	189
PM_3	85	92	85	91	163
PM_4	64	Fault	65	67	127
PM_5	58	Fault	60	63	130
PM_6	27	Fault	27	25	99
PM_7	20	Fault	17	19	83
PM_8	22	Fault	22	24	137
PM_9	32	Fault	32	34	142
PM_10	57	Fault	50	55	178
PM_11	136	Fault	133	133	273
PM_12	218	219	218	222	249
PM_aver.	85,42	160,75	84,5	88,33	165,58

Table: 4b 2006 values of PM

Measurement locations and PM values	Public works and housing directorate	Provincial health directorate	Provincial directorate of agriculture	Public health laboratories	Ekosis Main Device
PM_1	176	183	175	179	213
PM_2	112	127	108	118	179
PM_3	58	66	56	63	122
PM_4	37	40	34	40	51
PM_5	20	22	19	22	100
PM_6	19	21	19	29	118
PM_7	21	24	20	23	107
PM_8	22	24	19	24	94
PM_9	30	32	29	31	99
PM_10	56	60	55	59	227
PM_11	76	83	68	71	127
PM_12	88	94	98	109	165
PM_aver.	59,58	64,67	58,33	64	133,5

As shown in Fig. 3a and Fig. 3b, dust ratio is higher in the center of the city. This supports the prevailing wind direction is north-northwest and the middle sections of the city's topography is low-height. Between 2006 and 2007 years, the data sheet in the map window shows measurement of the monthly averages for each station. We also learn about the station information by using info tool module on map.

Table: 5a 2005 values of SO2

Measurement locations and SO_2 values	Public works and housing directorate	Provincial health directorate	Provincial directorate of agriculture	Public health laboratories	Ekosis Main Device
SO_2_1	168	181	169	181	92
SO_2_2	164	178	163	175	87
SO_2_3	105	112	105	112	79
SO_2_4	80	Fault	83	87	87
SO_2_5	74	Fault	76	78	44
SO_2_6	39	Fault	39	39	92
SO_2_7	25	Fault	23	23	25
SO_2_8	24	Fault	22	24	44
SO_2_9	36	Fault	36	37	14
SO_2_10	63	Fault	57	62	34
SO_2_11	140	Fault	137	139	164
SO_2_12	227	226	224	228	224
SO_2_aver.	95.42	174.25	94.5	98.75	77.17

Table: 5b values of SO2

Measurement locations and SO_2 values	Public works and housing directorate	Provincial health directorate	Provincial directorate of agriculture	Public health laboratories	Ekosis Main Device
SO_2_1	195	202	193	199	163
SO_2_2	141	164	138	150	106
SO_2_3	78	88	74	85	69
SO_2_4	48	53	45	51	51
SO_2_5	25	29	24	28	42
SO_2_6	21	23	19	23	26
SO_2_7	22	25	21	24	20
SO_2_8	23	26	21	26	14
SO_2_9	30	33	29	32	20
SO_2_10	49	55	47	54	41
SO_2_11	70	74	68	71	36
SO_2_12	100	111	98	109	59
SO_2_aver.	66.83	73.58	64.75	71	53.92

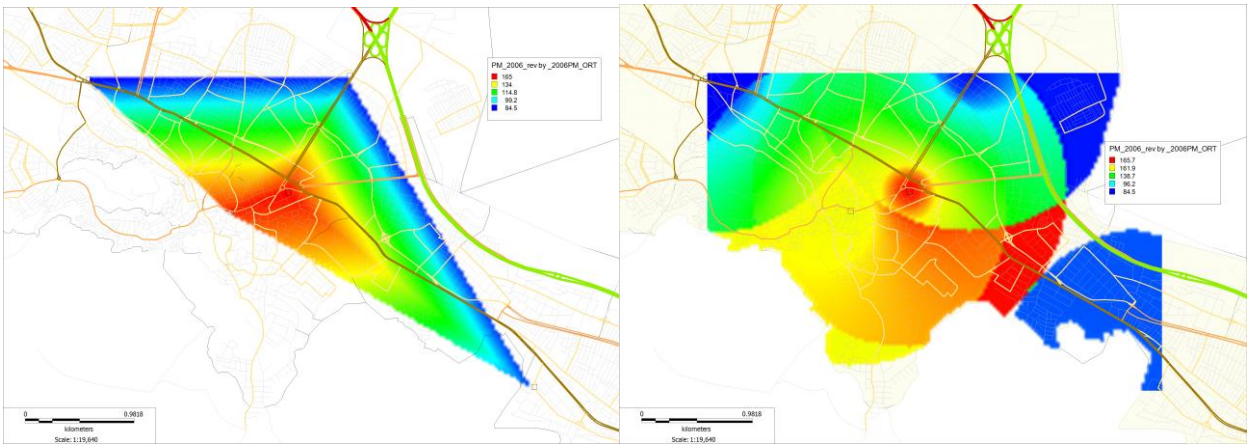

Fig.3a: Rates of 2006 PMs (TIN And IDW enterpoation)

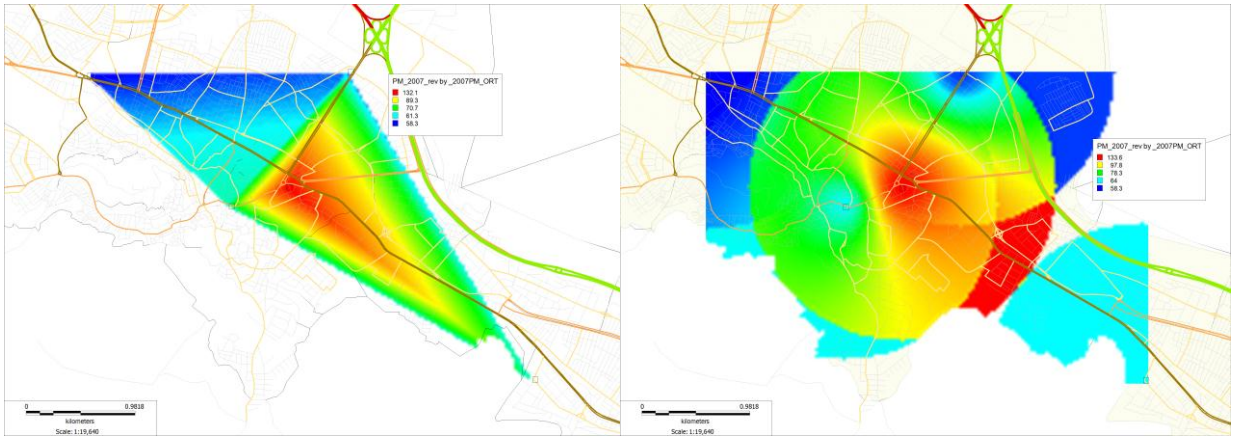

Fig.3b: Rates of 2007 PMs

As shown in Fig. 4a and Fig. 4b, rate of pollution is lower in the city center. Using natural gas which is heating fuel has been early a greater number of houses in the center. Away from the center, especially in the eastern sectors use coal as fuel for heating homes, increases the rate of pollution. Because there are more less housing in the north-east side, pollution is observed to be low.

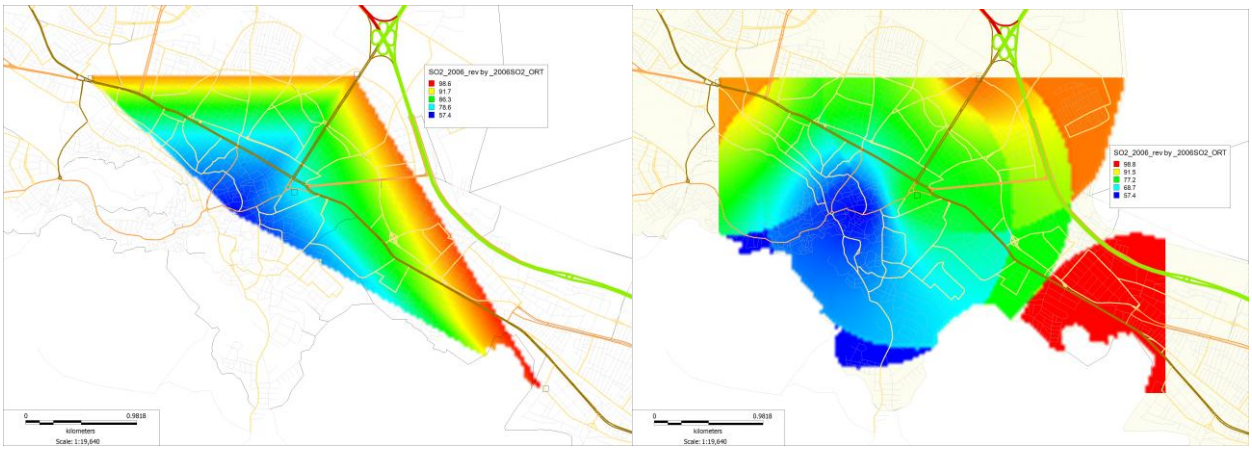

Fig.4a: Rates of 2006 SO2s (TIN AND IDW)

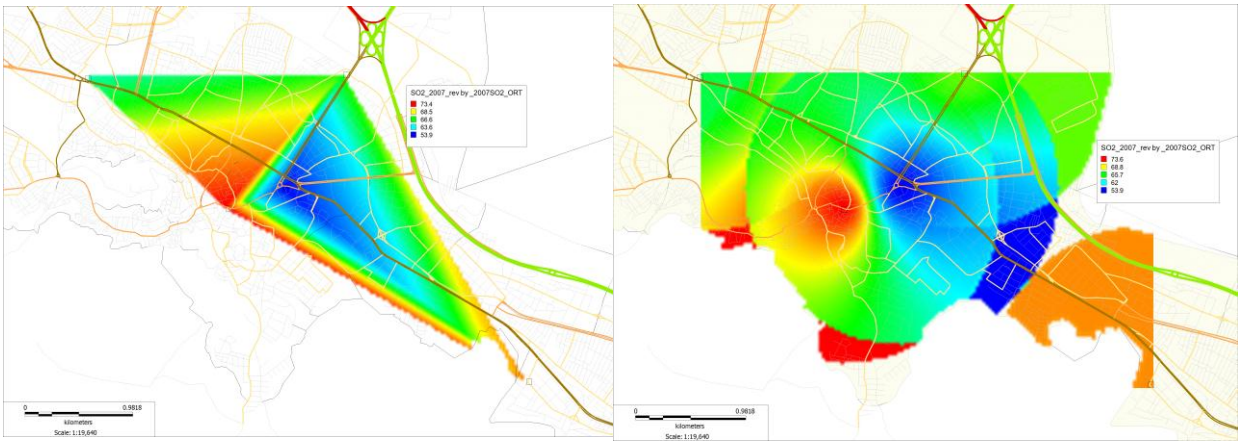

Fig. 4b: Rates of 2007 SO_2s (TIN And IDW enterpoation)

3. Conclusions

As the results for Kutahya Province show in this study Kutahya city is one of the leading cities by air pollution in Turkey. Air pollution's reasons are which used the wrong fuel consumption, the city's topography and wrong urbanization.

Make use of geographical information systems to emphasize the importance of this pollution, to reduce pollution in the common institutions will work fast, accurate and timely availability of data will provide support for decision-making process by providing a common base.

Visualization has always showed and recognized us to understand events. Finally this study and further research will help local authorities to air pollution prevention and monitor.

4. References

[1] Star, J. ve Estes, J., 1990, Geographic Information Systems, Prentice Hall, Inc., New Jersey.

[2] Richards, M., Ghanem, M., Osmond, M Guo, Y., and Hassard J. 2006, Grid-based analysis of air pollution data, Ecological Modelling, 194: 274-286.

[3] Puliafito, E., Guevara, M., Pand uliafito, C. 2003, Characterization of urban air quality using GIS as a management system, Environmental Pollution. 122, 105–117.

[4] Tayanç M. 2000, An assessment of spatial and temporal variation of sulfur dioxide levels over Istanbul, Turkey, Environmental Pollution.107: 61-69.

[5] Hewitt, C. N., 1991, Spatial variations in nitrogen dioxide concentration in an urban area. Atmospheric Environment, 25B, 429 ± 34.

[6] Briggs, D. J., Collins, S., Elliott, P., Fisher, P., Kinham, S., Lebret, E., Pryl, K., Reeuwıjk, H., Smalbone, K., and Veen, A. 1997, Mapping urban air pollution using GIS: a regression-based approach", Geographical Information Science. 11: 699-718.

[7] Güler, M. and Kara, T., 2007, Alansal Dağılım Özelliği Gösteren İklim Parametrelerinin Coğrafi Bilgi Sistemleri İle Belirlenmesi Ve Kullanım Alanları; Genel Bir Bakış, Ondokuz Mayıs Üniversitesi Ziraat Fakültesi Dergisi, S. 323-328, Samsun.

[8] Erbas O., and Kose R. ,2003, Bazı Meteorolojik Faktörlerin Kutahya'daki Hava Kirliliğine Etkisi, Dumlupınar University Journal of Science. Kutahya Volume:4,September 2003

[9] Türkiye Çevresel Veri Değisim Ağının Kurulması için Teknik Yardım (TEIEN). MAPINFO ile hava kirliliği analizlerinin yapılması eğitim notları, 2010.

International Proceedings of Chemical, Biological and Environmental Engineering
Volume 94 of IPCBEE (2016)
DOI: 10.7763/IPCBEE. 2016. V94. 16

The Strengthening of Geological Infrastructure, Research and Data Acquisition - Using Gis in Ivory Coast Gold Mines

Kouame Joseph Arthur Kouame [+], Fuxing Jiang, Yu Feng and Sitao Zhu

School of Civil and Environmental Engineering, University of Science and Technology Beijing, Beijing China

Abstract. The artisanal gold mining in Ivory Coast has become a key problem in the mining sector. A diverse group of people in Ivory Coast, including the young and the old, are all engaged in these activities that are reportedly better than agricultural inputs. . However, it is still a high-risk activity that leads to pollution, environmental degradation and the loss of human life. About ten people die each year in the gold mines. This paper focuses on gold mine safety by using the Geographic Information System (GIS) as a major solution to solve the artisanal gold mines problem, and also seeks to promote the mining industry in Ivory Coast.

Key words: Artisanal Gold Mine, Safety; Ivory Coast, Gis

Acronyms and Abbreviations: SODEMI-State Society for Development of the Mining Industry (Société pour le Développement Minier de la Côte d'Ivoire); UN-United Nations; MDA-Ministry Departments Agencies; NGO-Non-governmental Organization; GIS Geographic Information System

1. Introduction

1.1. Definition of artisanal mining

The term Artisanal and Small-scale mining broadly refers to a mining practiced by individuals, groups, or communities, often occurring informally in developing nations. A common definition of this sector has not been adopted yet as a legal status, and local definitions vary from country to country. Due to this reason, it is difficult to estimate the extent of artisanal mining in developing contexts due to the lack of a common definition, its use of seasonal workers, and the lack of official statistics [1] (Hilson,G. ,2002).

Artisanal mining is a thorny issue for both governments and large-scale mining areas in developing countries due to the various associated benefits and risks. In the last ten to fifteen years, the introduction of technology that has made this mining process more efficient. The problem however is that artisanal mining is not all that risk free. This paper focuses on artisanal mining in the Ivory Coast.

2.1. Artisanal mining in the Ivory Coast

Ivory Coast in the western part of Africa has a high fertility rate that is expected to reach nearly 80% in 2018. The increasing poverty rate of the population is mainly due to the presence of the youth, men, and women in the artisanal gold mines. Many children who became orphans during the rebellion in 2002 and the post electoral crisis; view working in the artisanal gold mines as the perfect job to provide for their daily bread and to support their relatives. A majority of the breadwinners of a family in Africa are children. ([2, 3])(African Economic Outlook, 2013 and Carisch, 2012). The country has a large portion of the Birimian

[+] Corresponding author. Tel.: +15210952596
E-mail address: josepharthurkk.ustb@yahoo.com.

geological formations that make West Africa a mining region par excellence. In the case of the Ivory Coast, the issue of mining became rampant during the period of turmoil between 2003 and 2011, mainly due to the absence of a state authority, particularly in the north that was occupied by rebels at the time. Many efforts have been made to the promotion and transfer of artisanal mining in the so-called "small scale" mine by West African states, through projects and multi-sectorial funding programs that aim at optimizing national investment and promoting socio-economic welfare through the fight against poverty, assistance in communities settlement, protection of the environment, and quality of life improvement, among others [4] (Sogal, 2012).

Recent research has shown that artisanal miners have increased in number, and artisanal mining activities have become a privileged destination for local people and foreigners in the western part of Africa such as Ivory Coast, Guinea, Mali, and Ghana. This is mainly due to their changed livelihood standards, as a result of this activity ([5-7]) (Hilson et al., 2013, Bryceson and Jonsson 2009, Nyame et al, 2010).

According to SODEMI, the unique national company in Ivory Coast 24 out of 31 regions in the country are being illegally exploited by more than 500,000 miners which are mostly foreigners and indigenous people [8] (Assie, 2009). But we cannot determine the real number of the people who venture into illegal gold mine activities in the country, due to the fact that local people sometimes connive with foreigners for these activities. Despite the current government of Ivory Coast taking a decision to close several illegal mines around some cities like Ity , Djekenou Zanzan region, Zouan-Hounien, and other regions, illegal miners always back to the gold exploitation on the same sites after few months ([9-11] (Randgold Resources Ltd., 2012, Economie, 2015, AZUBUIKE.OKEH, 2014).

The vast majority of artisanal mining is illegal. Miners usually have to apply for a license to mine from the local authorities before they start digging, but the local industry estimates that 95% of all the artisanal mining goes ahead without such regulations. Regulation, rather than banning artisanal mining altogether is the only sustainable solution.

In the 1990's, the liberalization of the gold mining industry meant a downward shift in terms of environmental, human rights as well as transparency standards in many of the West African states. This is the case because the goal at the time was to lure foreign investors. However, governments at present need to come together and to harmonize the standards upwards. There has been some progress in this regard, due to the efforts of regional bodies such s the Economic Community of West African States (ECOWAS), which is working on a new mining code to apply to all its members. It is expected that this law would be deliberated on and passed in the following years, after heads of state within the region passed a directive on high level commitment to mining. With artisanal mining growing steadily and industrial scale mining set to significantly increase between now and 2020, networks and industries need to work hard and keep tabs on the industry at all levels.

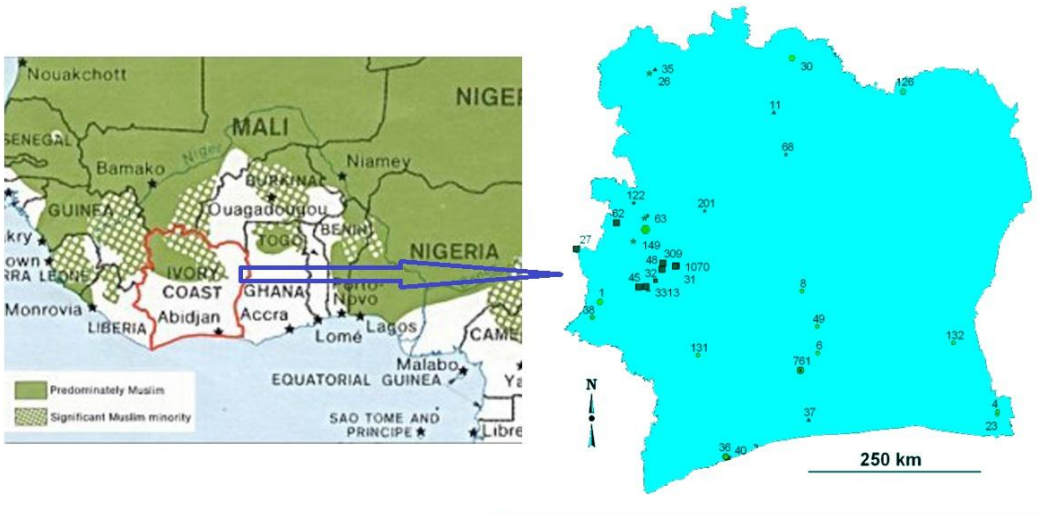

Fig. 1: Legend and ore deposit name in Ivory Coast

However, Ivory Coast is now becoming a trustful country in the world after 10 years of political unrest. The current government attaches a great importance to the safety of persons and property. The poverty rate averages slightly, and the country's GDP grew from 7% in 2011 to 13% in 2013. The country can borrow funds from the World Bank and also from other financial institutions such as the Inter-American Development Bank (IDB) to acquire new technologies and invest fully in the mining sector. This is the case because recent research has shown satisfactory results that have discovered a huge mining potential in many parts of the national territory. (Fig. 1).

In the gold mine or coal mine production process, safety is a very important part of the disaster prevention in terms of mine gas disasters, coal dust hazards, and fire hazards. Unfortunately, Ivory Coast at present has a lot of artisanal gold mines such that the safety information management level is still relatively backward and has not completely desorbed from the traditional manual operation. The presence of low work efficiency, staff duplication, difficult data found in long series of problems in the information transfer cycle, and untimely safety information and accident reporting treatment, leads to vicious consequences of property damage and casualties. Therefore, carrying out a research of mining safety information on the safety management of gold production in Ivory Coast is of important significance.

The geospatial information technologies (GIS) and geospatial integrated information technology (IT) are increasingly used in the field of the mining industry. This new technology continues to improve the views of all their utilities in management of mining resources, planning and good management infrastructure in localisation and assessments of mining sites. These modern advanced technologies are also important in the health field of education and administration.

The majority of the mining deposit in Ivory Coast is mainly found in a gold mine that is located in the northern, western, central and eastern part of the country, as the most explored targets for gold deposits. The gold deposit in Ivory Coast has been previously interpreted since the independence, but today young gold has been discovered in Angovia and bonikro. Today several foreign mining companies are heading to the country for further deep explorations and exploitations for those already had the exploration permits. This is due to the fact that the government of the Ivory Coast has begun to take an interest in the mining sector in order to diversify its economy that is primarily based on agriculture. However some mining investors have met with problems such conflict over land and insecurity due to the presence of thousands of artisanal gold miners. For this reason, this paper is mainly focussed on offering GIS as a tool to establish a real predictive model for mapping gold mineralization in all the regions in the country to preventing such outcomes.

2. System Design

2.1. Functions of GIS system

The geographic information system (GIS) will exist to elaborate the map information management and to deal with monitoring information system management in Ivory Coast (Fig. 2).

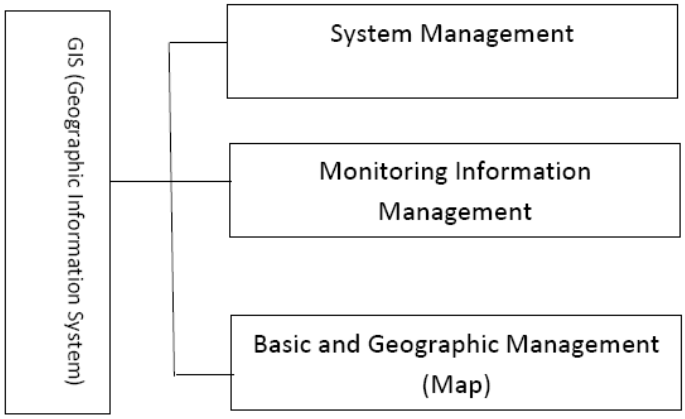

Fig. 2: System functional

2.2. Elaboration of the map information management

GIS-based graphics leads to achieve the map to zoom, pan, layer control and other editing functions. At the same time, it realizes maps and attributes peer review. Ivory Coast is today a privilege destination for artisanal miners. Thousands foreigners and citizens are involved in artisanal and small-scale mining (ASM) in Ivory Coast due to the high rate of poverty and unemployment, which are the direct consequences of the political unrest from 1999 to 2011 [12] (UN, 2014).

The adoption of the new technology will play a major role in the Ivory Coast mining industry, by elaborating maps which will locate all the mining sites of the national territory first, and then identify all the artisans involved in the artisanal gold mining sector who illegally exploit the natural resources of countries. The Government of Ivory Coast will as such be able to control the quasi totality of the mining sector and take necessary steps towards better management of natural resources. This is the case because the lower system operating environment requirements provides a friendly user interface, which is easy for non-GIS personnel to operate the application.

2.3. Monitoring information system management

The real development of the mining sector in the Ivory Coast necessitates the understanding of knowledge of the mineral potential of each region and locality of the country. The new advanced technologies will be useful in obtaining accurate information on natural resources in Ivory Coast. Data based information will be acquired, processed and analyzed according to the geographical information of each locality and area of the Ivory Coast. Due to the dynamics of new advanced techniques and also their capacity expansion, the advanced technologies can collect geological data, resulting in many problems such as soil degradation and restoration of the environment being resolved. Land used jointly by mining, communities and epidemiology will be evaluated. Additionally, the deaths and flooding of the mine site will also be attenuated. As a result, the possibility to record all mineral production from the Ivory Coast and provide transparent and based information to the mining administration through the use of new technologies will be a great asset to the country's economy. Ivory Coast will experience a rapid economic development, epidemiologically secures evaluation, and disaster recovery. This is due the fact that the mine safety monitoring system with real-time data exchange, data exchange files for safety monitoring system, in accordance with a given data format specification, development of the data read and display algorithm, can read data files in real-time monitoring systems, the underground monitoring basic information and its operational status information about the device is displayed on the map.

3. The Main Function

The GIS system will be important in the mining industry in Ivory Coast in the following way:

(1) The introduction of the GIS in Ivory Coast mining operation will lead to the safety of local people and miners due to the medical system management in the operational mining areas. Numerous diseases such as lungs, heart and skin diseases, and also the spreading of HIV / AIDS are very often recorded on mining sites.

It is clear that GIS is now an important element in the medical service. The medical sector actors use GIS to invest in the geographical effects on humans. The Ivory Coast must be endowed with GIS for environmental preservation. Thus the risk of epidemic and infectious diseases proliferation will be greatly reduced on mining sites, and the local population will be free from diseases. In our advanced case, the use of GIS is essential because it can detect danger on future mining operation sites. The government of Ivory Coast will certainly invest huge funds for the acquisition of new geologic technologies, but the rewarding of that will greatly benefit the reduction of the WHO liabilities, which include the construction of hospitals and treatment of those suffering from HIV / AIDS and, tuberculosis. The proceeds will be used to solve some immediate problems of the population such as unemployment, securities, and poverty.

(2) GIS is a system which has good interactive capabilities, automatic connection and a two-way electronic map and database queries, and functions according to the need for thematic map output. Compared to the previous cut graphics and data established mutual monitoring software, this system has successfully realized the data and graphics correspondence and sync output. Many mining sites in Ivory Coast remain

undiscovered or undeveloped, and some exploited sites even have often been abandoned by their operators due to the political unrest or land conflict between the mining companies and local people. The existence of many undeveloped mining sites is thus due to the lack of the high technology in the mining sector in Ivory Coast. Some of the major strengths of a Geographic Information System (GIS) include its ability to plan a reclamation activity. Additionally, potential problems in operation can be remotely monitored and diagnosed by experts, who can propose effective solutions and provide technical support directly through online consultation

The active use of GIS applications will lead to the restoration of most of the abandoned mining sites in Ivory Coast. The minerals (gold, diamond, iron..) which are currently exploited by illegal miners in the northern, western, central and even in the southern part of the country can be controlled by the government and attributed to some reliable foreign investors such as Amara mining, the British mining company; which is expected to run the biggest gold mine deposit in 2017. The mining industry will be the second largest sector of the country's economy beside cocoa ([13-15]) (United Nations. Resolution 1528 (2011); United Nations. Resolution 2045 (2011); Ogwang Tom, 2011).

4. Conclusions

GIS-based integrated safety management is a system that holds a great and high level of visual, interactive and good man-machine interface coordination. This will assist in creating a real stable and fast response, with a strong security comprehension due to the smart work of GIS and its applications. The system plays an impressive role in safety management, as well as controlling and reducing the mine disasters during the operation. A good use of GIS leads to the development of the mining sector and enhances better management levels. Besides the technical support of GIS system in the advance sustainable development of gold mine production safety, GIS will play an increasingly large role in the mining industry in Ivory Coast. As such, the development of GIS – based graphic safety technology with an integrated visual information management system, which aims at enhancing the level of mine safety management in the Ivory Coast, is essential.

5. References

[1] Hilson, G. (2002, February). Small‐scale mining and its socio‐economic impact in developing countries. *In Natural Resources Forum* (Vol. 26, No. 1, pp. 3-13). Blackwell Publishing Ltd.

[2] African Economic Outlook (2013).Promoting youth employment in Africa. Why an African economic outlook on youth employment.

[3] Carisch, E. (2012). Conflict gold to criminal gold: The new face of artisanal gold mining in Congo. South Africa: Southern Africa Resource Watch.

[4] Sogah, S. G. (2012). *The effects of differences in agro-ecosystems on the diversity and distribution of avifauna in selected areas in the Eastern Region of Ghana* (Doctoral dissertation).

[5] Hilson, G., & Garforth, C. (2013). Everyone now is concentrating on the mining: drivers and implications of rural economic transition in the eastern region of Ghana. Journal of Development Studies, 49(3), 348–364.

[6] Jønsson, J. B., & Bryceson, D. F. (2009).Rushing for Gold: Mobility and Small‐Scale Mining in East Africa. Development and Change, 40(2), 249-279.

[7] Nyame, F. K., & Blocher, J. (2010). Influence of land tenure practices on artisanal mining activity in Ghana. Resources Policy, 35(1), 47-53.

[8] ASSIE, K.E. 2009. Lode gold mineralization in the Paleoproterozoic (Birimian) volco-sedimentary sequence of Afema gold district, southeastern Cote d'Ivoire, PhD thesis, Technical University of Clausthal, Germany

[9] Randgold resources Ltd., 2012, 2011 annual report: London, United Kingdom, Randgold resources Ltd., 185 p.

[10] Economie. (2015, Decembre 21). *Centre-Ouest ivoirien: La mine d'or de Gamina exploitée illégalement un mois après sa fermeture (REPORTAGE)*. Retrieved Decembre 24, 2015, from Abidjan.net: http://news.abidjan.net/h/576676.html

[11] AZUBUIKE.OKEH. (2014, October 23). *Cote d'Ivoire closes 150 illegal gold mines*. Retrieved November 12,

2014, from NEWS AGENCY OF NIFERIA: http://nannewsnigeria.com/cote-d%E2%80%99ivoire-closes-150-illegal-gold-mines

[12] United Nations Security Council, 2011a, Letter dated 17 October 2011 from the Chair of the Security Council Committee established pursuant to resolution 1572 (2004) concerning Côte d'Ivoire addressed to the President of the Security Council: United Nations Security Council report S/2011/642, 34 p.

[13] UN Security Council Security Council members unanimously adopt resolution 2153 (2014), 2014 Reed, Jared, 29.04.2014 http://www.dw.de/un-lifts-diamond-export-embargo-for-ivory-coast/a-17601628

[14] United Nations Security Council, 2011b, Letter dated 20 April 2011 from the Chair of the Security Council Committee established pursuant to resolution 1572 (2004) concerning Cȏte d'Ivoire addressed to the President of the Security Council: United Nations Security Council report S/2011/272, 80 p.

[15] Ogwang, T. (2011). The root causes of the conflict in Ivory Coast. *Backgrounder*, (5), 1.

Author Index